Contributions of *fli1a* and *hox13* during Zebrafish Pectoral Fin Development and Implications for Ewing Sarcoma

Mustafa Issa Hamid

Thesis submitted to the University of Ottawa in partial fulfilments of the requirements of the Master of Science in Biology Degree

Department of Biology
Faculty of Science
University of Ottawa

ABSTRACT

The zebrafish embryonic pectoral fin is comprised of the endoskeletal disc (ED) and the pectoral fin fold (PFF). Throughout larval development, the ED will give rise to the endoskeleton, consisting of proximal and distal radials, while the PFF will contribute to the formation of exoskeletal fin rays. The development of the pectoral fin is dependent on the coordinated activity of various transcription factors including Hox13 which are essential for patterning of the pectoral fin. Another transcription factor, Fli1a, is well-characterized in blood vessels, however, its role in the ED remains elusive. Using transgenic reporter lines, our laboratory has demonstrated a complementary pattern between *fli1a* and *hox13* domains of expression, suggesting a regulatory relationship between these genes during pectoral fin development. Using time-course analysis, we discover that *hox13*-expressing cells in the pectoral fin emerge from *fli1a*-negative chondrocytes of the ED. Furthermore, we show that a brighter *fli1a*-expressing cell population gives rise to distal radials, while *hox13*-expressing cells localize with presumptive fin rays, concomitant with blood vessel remodeling in the PFF. Surprisingly, our analyses reveal that *fli1a* and *hox13* domains of activity remain complementary throughout larval development. This pattern was also present during fin regeneration and recapitulated in the mouse autopod. In support of the regulatory relationship between *fli1a* and *hox13*, studies in Ewing sarcoma, an aggressive bone and soft tissue cancer, describe that FLI1 dysregulation is associated with an increase in *HOXA13* and *HOXD13* expression. To examine this regulation in zebrafish, we have induced ectopic *fli1a* expression in the *hox13* domain. The mis-expression of *fli1a* was associated with an increase in *hox13* expression during larval development and long-lasting aberrations in the morphology and migration of *hox13*-expressing cells, leading to defects in the adult pectoral fin. The ectopic *fli1a* anomalies also

recapitulated some Ewing sarcoma phenotypes. Taken together, our results confirm the coordinated participation of *fli1a* and *hox13* during pectoral fin development and provide important insights into fin fold cell migration, distal radial formation, fin ray morphogenesis, and blood vessel remodeling. Understanding the regulation between *fli1a* and *hox13* could not only elucidate the development of the paired appendages but also shed light on the roles of *FLI1* and *HOX13* in the pathology of Ewing sarcoma.

ACKNOWLEDGMENTS

First and foremost, I would like to express my sincere gratitude to my supervisor Dr. Marie-Andrée Akimenko for giving me the opportunity to pursue a master's degree in her laboratory and for providing continuous support, guidance, and encouragement during my graduate studies. I would also like to thank my thesis advisory committee members Dr. Marc Ekker and Dr. Iain McKinnell for their valuable input and suggestions to improve my research project.

Furthermore, I would like to acknowledge Dr. Robert Lalonde and laboratory technician Jing Zhang for being excellent mentors and providing immense support in the form of training and troubleshooting.

I would like to thank my all colleagues: Dr. Qingming Qu, Hannah Nicholas, Reeham Kadhom, Shea Keil, Bidemi Keshinro, Hailey Quigley, and Joshua Ivare for being supportive and creating a collaborative, productive, and entertaining work environment. I am also grateful to NSERC, Honours, and high school students for their contributions throughout my graduate studies.

In addition, I would like to thank Simon Monis for helping me with qRT-PCR analysis, and for working on future research directions along with Reeham Kadhom and Caroline Grela.

Moreover, I would like to thank the Animal Care and Veterinary Service (ACVS) team at the University of Ottawa for maintaining the aquatic facility and providing care to zebrafish, including Vishal Saxena for performing microinjections of zebrafish embryos.

Lastly, I would like to thank my mother, grandparents, siblings, significant other, and friends for their tremendous support and motivation throughout my thesis.

Funding for this research was provided by the Natural Science and Engineering Council of Canada (NSERC) and Canadian Institutes of Health Research (CIHR) to Dr. Marie-Andrée Akimenko.

TABLE OF CONTENTS

LIST OF FIGURES & TABLES

CHAPTER 1: INTRODUCTION

CHAPTER 2: MATERIALS & METHODS

CHAPTER 3: RESULTS

CHAPTER 4: DISCUSSION

LIST OF ABBREVIATIONS

A-P – anterior-posterior
Actino – actinotrichia
AER – apical ectodermal ridge
AF – apical fold
B.p (bp) – base pairs
cDNA – complementary deoxyribonucleic acid
ChiP – chromatin immunoprecipitation assay
Cryaa – crystallin Alpha A
CSZ – cartilage subdivision zone
D-V – dorsal-ventral
dpa – days post amputation
dpf – days post fertilization
DsRed – red fluorescent protein isolated from *Discosma*
E13.5 – embryonic day 13.5
ED – endoskeletal disc
eGFP – enhanced green fluorescent protein
EMT – epithelial-to-mesenchymal transition
FF – fin fold
Fgf – fibroblast growth factor
FISH – fluorescent *in situ* hybridization
Fli1a – friend leukemia integration 1a transcription factor
Fw – forward primer
GLI1 – Glioma-associated Oncogene proteins
HBB –human beta-globin minimal promoter (β-globin)
Hox – homeobox-containing gene
hox13 – *hoxa13a*, *hoxa13b*, and *hoxd13a* genes
hpf – hours post fertilization
IHC – immunohistochemistry
ISH – *in situ* hybridization
kbp – kilobase pairs
KR19 – killerRed 19
m-Inta11 – enhancer identified in mouse intron of homeobox A11 gene
m-Prrx1 – mouse paired related homeobox 1
mbv – marginal blood vessel
mCherry – monomeric red fluorescent protein
Mes – mesenchyme
MFF – median fin fold
mRNA - messenger ribonucleic acid
NTC – notochord
P-D – proximal-distal
PAC – P1-derived artificial chromosome
PTCH1 – patched 1 receptor
PcG – polycomb proteins
PCR – polymerase chain reaction

PFF – pectoral fin fold
PHHS3 – phosphohistone H3
PRP – precoracoid process
PZ – progress zone
RA – retinoic acid
Rev – reverse primer
RT – room temperature
SHH – sonic hedgehog
TcG – trithorax proteins
Tg – transgenic
TUNEL – terminal deoxynucleotidyl transferase dUTP nick end labeling
UTR – untranslated region
WT – wildtype
ZPA – zone of polarizing activity

NOMENCLATURE

Zebrafish

Gene: *fli1a*
Protein: Fli1a

Mouse

Gene: *Fli1*
Protein: FLI1

Human/Chicken

Gene: *FLI1*
Protein: FLI1

CHAPTER 1: INTRODUCTION

1.0 General Introduction

The development of the vertebrate appendage is contingent on the coordinated activity of multiple gene regulatory networks. In this dissertation, we will discuss the contributions of two transcription factor families during zebrafish pectoral fin development. Our analysis will focus on *fli1a* and *hox13* genes, as well as examine their regulatory relationship during embryonic and larval development. In addition, we will investigate the dysregulation of *fli1a* and *hox13* genes in pectoral fin tissue and explore their implications for the pathology of Ewing sarcoma.

Zebrafish have long been used to study the development and diversification of the vertebrate appendage. This teleost fish possesses three unpaired fins, known as the dorsal, caudal, and anal fins, as well as two sets of paired fins, known as the pelvic and pectoral fins (Figure 1.0B). The embryonic fins of zebrafish are comprised of the median fin fold and the paired pectoral fin buds (Figure 1.0A). The median fin fold surrounds the trunk of the zebrafish embryo along the midline and is partially resorbed during larval development to give rise to the dorsal, anal, and caudal fins (van den Boogaart, Muller, & Osse, 2012). Meanwhile, the pectoral fin buds are located above the yolk sac of the embryo on both sides of the trunk and lead to the formation of the adult pectoral fins. The pelvic fins, however, do not emerge from an embryonic structure but rather arise from the ventrolateral body wall of the fish during later stages of larval development (Parichy, Elizondo, Mills, Gordon, & Engeszer, 2009). The next section will describe in more detail the development of the pectoral fin.

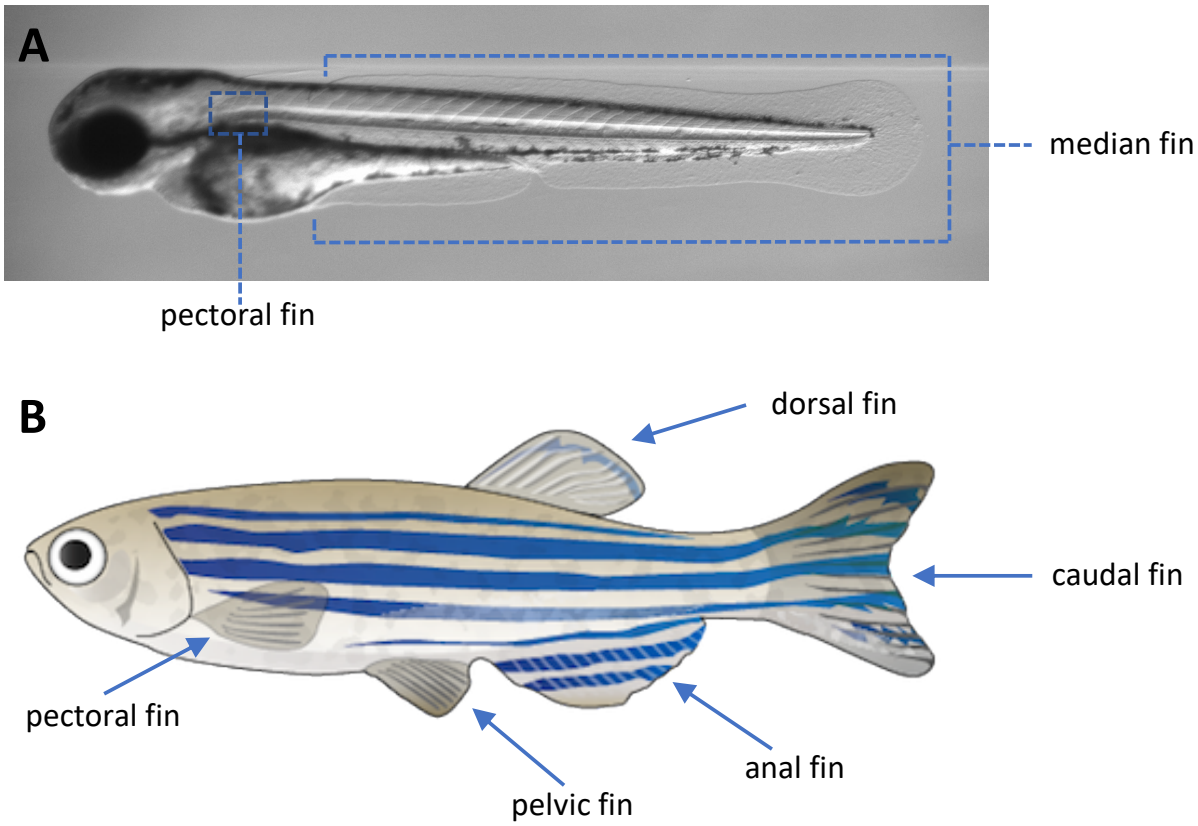

Figure 1.0: **Zebrafish fins during embryonic development and adulthood**. (A) Zebrafish embryo at 3 days post fertilization (dpf), showing the median fin fold and the paired pectoral fin buds. Image captured by Robert A. Lalonde (B) Schematic of adult zebrafish, showing the three unpaired fins: the dorsal, caudal and anal fins, and the two sets of paired fins: the pectoral and pelvic fins. Schematic created by Togo Picture Gallery and obtained from Database Centre for Life Sciences (DCLS) CC BY 3.0 (https://creativecommons.org/licenses/by/3.0/deed.en)

1.1 Overview of Zebrafish Pectoral Fin Development

1.1.1 Embryonic Development

The development of the zebrafish pectoral fins is comprised of the embryonic and the larval stage, which have been previously described by Grandel & Schulte-Merker, 1998. The first stage begins a day after fertilization when the somatopleure, at the level of somites 1-4, contributes to the formation of the paired fin buds (Wyngaarden et al., 2010) The pectoral fin buds are comprised of mesenchymal cells that are surrounded by a basement membrane, which is covered by an ectoderm, and a periderm being the outer-most layer (Wood & Thorogood, 1984). During the early stages of development, mesenchymal cells begin to arrange their orientation relative to the basement membrane. As the anlagen continue to grow by proliferation, an apical thickening derived from the basal epithelial layer becomes visible at 31 hours post fertilization (hpf). This transient layer borders the fin bud along its anterior-posterior axis and will later establish the apical fold. After about 6 hours, mesenchymal cells rearrange and form a unique chondrogenic condensation that is flanked by a population of ventral and dorsal myogenic mesenchyme at 48 hpf (Figure 1.1A). These myogenic regions will give rise to fin musculature accordingly. The proximal chondrogenic condensation will form the rudiments of the girdle, scapulocoracoid, and postcoracoid process at 52 hpf (not shown in Figure 1.1 but see Figure 1.2). The distal chondrogenic condensation, however, will go on to develop the cartilaginous endoskeletal disc (ED) at 57 hpf. Around the same time, mesenchymal cells begin to migrate distally towards the fold. This migration coincides with the appearance of rigid actinotrichia fibrils, which consist of collagenous components (i.e. collagen type I and type II) and non-collagenous material including actinodin proteins (Durán, Marí-Beffa, Santamaría, Becerra, & Santos-Ruiz, 2011; Zhang et al., 2010). Apart from providing structural support to the fold, actinotrichia serve as a scaffold for the

migration of mesenchymal cells into the pectoral fin fold (PFF) starting at 60 hpf (Figure 1.1 B) (Wood & Thorogood, 1984). A similar process involving actinotrichia formation and mesenchymal invasion results in the generation of the median fin fold (MFF), which becomes visible at 18 hpf (Kimmel, Ballard, Kimmel, Ullmann, & Schilling, 1995). The larval stage of pectoral fin development is reached as soon as the marginal blood vessel (mbv) is formed (Grandel & Schulte-Merker, 1998)(Figure 1.1C). Over the next couple of weeks, the scapulocoracoid (sco) fuses to the cleithrum, and chondrocytes within the disc divide and expand (Figure 1.2A) (Grandel & Schulte-Merker, 1998).

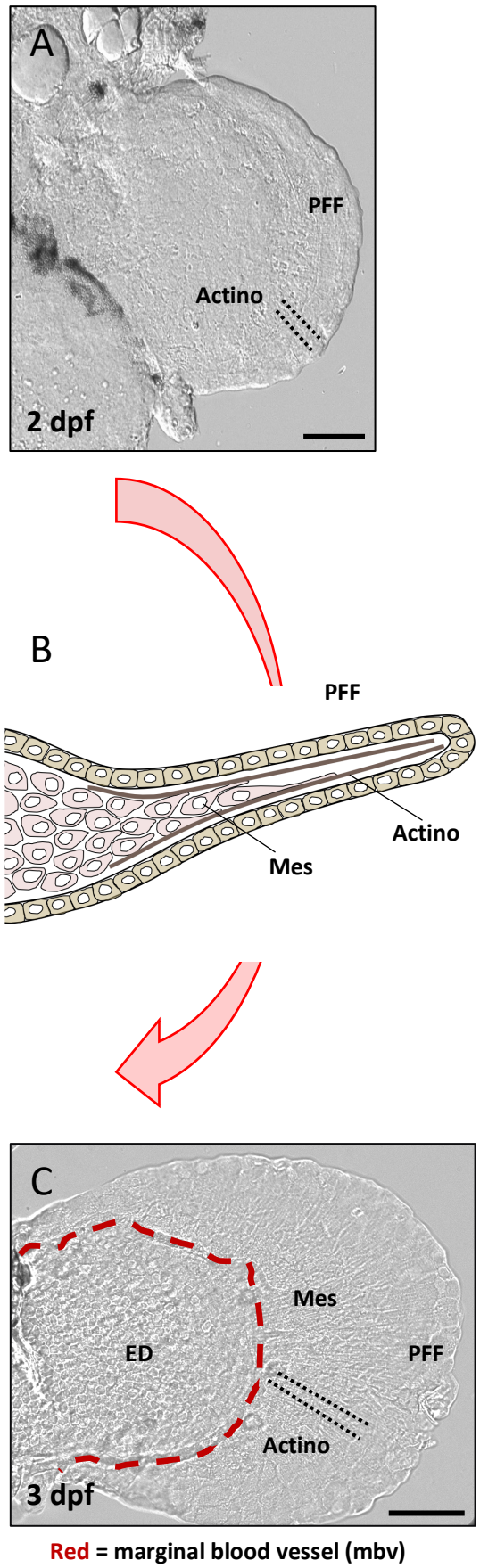

Figure 1.1: The embryonic development of zebrafish pectoral fins. (A) The formation of the fin fold coincides with the appearance of actinotrichia. (B) Actinotrichia support the elongation of the fin fold and guide the invasion of migrating mesenchymal cells (C) The embryonic stage is considered complete as soon as the marginal blood vessel is formed. PFF = pectoral fin fold, Actino= actinotrichia, Mes = mesenchyme, ED = endoskeletal disc, mbv = marginal blood vessel. Scale bars: A = 30 µm, C = 50 µm. Panel A and C were captured by R. L. Lalonde.

1.1.2 Late Larval Development

The second stage begins during the third week of development (Grandel & Schulte-Merker, 1998). This section will briefly describe the development of the girdle but will focus on the fate of the endoskeletal disc (ED) and the distal region of the larval fin. During larval development, the postcoracoid process (pop) gradually regresses and eventually vanishes (Grandel & Schulte-Merker, 1998). Meanwhile, the precoracoid process, which is situated beneath the cleithrum expands in the rostral direction (not shown). It will later contribute to the structural support of the adult pectoral girdle. In the following days, the disc undergoes reorganization leading to the formation of proximal and distal radials. This process varies in developing larvae and has been shown to occur between 20- and 25-days post fertilization (dpf) (Grandel and Schulte-Merker, 1998). Some of the changes that take place during the development of the ED include three major rounds of cell division that coincide with the formation of cartilage subdivision zones (CSZ) (Dewit, Witten, & Huysseune, 2011). The first set of divisions is synchronous with the growth and expansion of the ED in the proximal-distal axis. The second-round results in a thicker ED and corresponds with the appearance of two sequential cartilage subdivision zones, CSZ0 and CSZ1 (Figure 1.2 B). The CSZ0 is responsible for separating the scapulocoracoid from the ED, whereas the SCZ1 divides the disc into an anterior and a posterior half (Figure 1.2B). This round is characterized by the elongation of the precoracoid process (not shown). The third round shows no preference in the orientation of division and precedes the formation of CSZ2 and CSZ3 (Figure 1.2C). The appearance of CSZ1, CSZ2, and CSZ3 corresponds with the formation of the four proximal radials (Figure 1.2 C). Once proximal radial condensations are defined, bones of the presumptive fin rays known as lepidotrichia appear in the anterior part of the fin at 23 dpf and distal rim mesenchyme is reorganized (Figure 1.2B). Subsequently, new cartilaginous

condensations, precursors to the distal radials, appear adjacent to the disc (Figure 1.2B). The first distal radial to form attaches to the most anterior presumptive fin ray and subsequently articulates with the developing scapula. The formation of distal radials progresses in an anterior to posterior direction and is concomitant with the articulation of distal radials to presumptive fin rays. In the anterior region, distal radials articulate with presumptive fin rays in a one-to-one manner. In the posterior region, each distal radial can support several presumptive fin rays (Grandel & Schulte-Merker, 1998). While articulation proceeds to posterior radials, the fin skeleton undergoes a rotation against the girdle bone process. This stage is marked by further differentiation and ossification leading to the adult fins. While the endoskeleton, including 4 proximal radials and 6-8 distal radials, is formed through endochondral ossification, the exoskeleton, corresponding to 10-12 exoskeletal fin rays is formed via intramembranous ossification (Grandel & Schulte-Merker, 1998; T. Yano, Abe, Yokoyama, Kawakami, & Tamura, 2012).

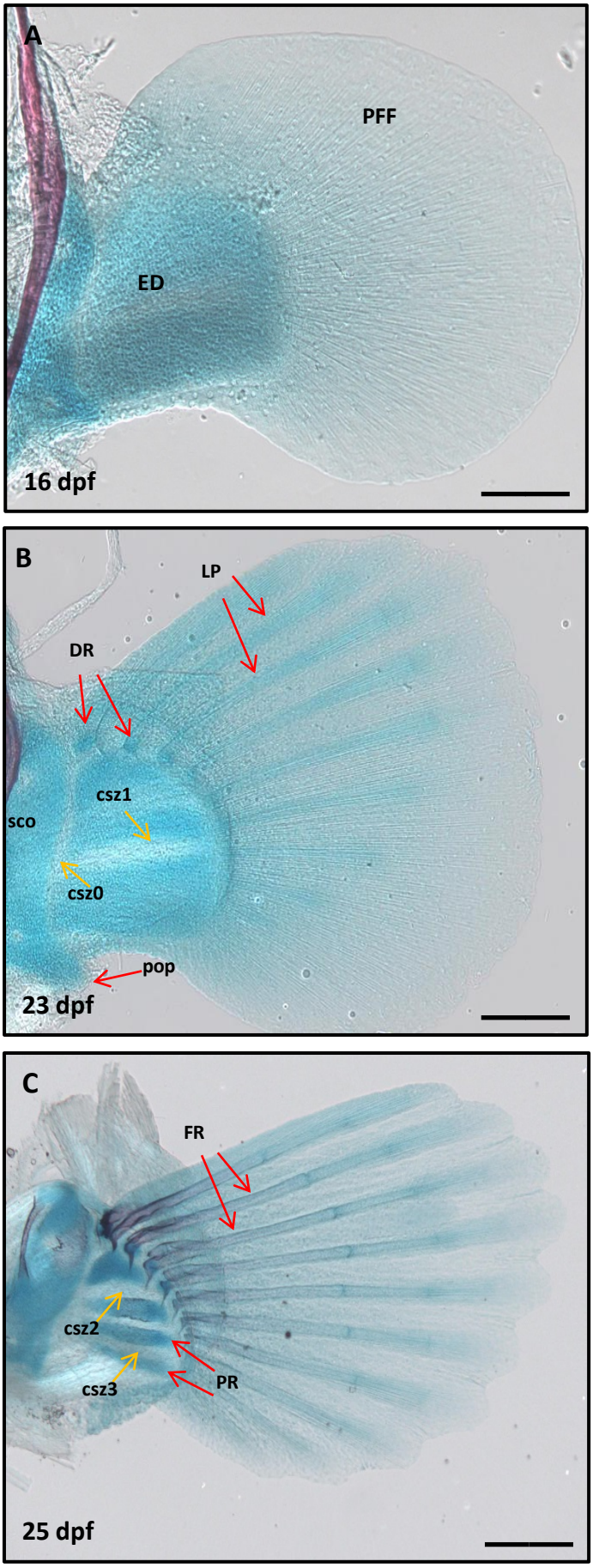

Figure 1.2: The larval development of zebrafish pectoral fins. (A) The endoskeletal disc and fin fold are well-defined at 16 dpf and continue to expand. (B) The pectoral fin tissue is reorganized leading to the formation of distal radials at 23 dpf. (C) The distal radials serve as an attachment point to fin rays which begin to ossify in the proximal-to-distal axis at 25 dpf. PFF = pectoral fin fold, ED = endoskeletal disc. LP = lepidotrichia, DR = distal radials, sco = scapulocoracoid, pop = postcoracoid process, FR = fin rays, PR = proximal radials, csz = cartilage subdivision zones. Scale bars: A, B = 200 µm, C = 400 µm. Bone and cartilage staining was performed by R. L. Lalonde.

1.2 Overview of Blood Vessel Development

The acquisition of vasculature during embryonic development is highly conserved between vertebrates. In tetrapods, precursors including hematopoietic and endothelial cells develop from blood islands that reside in the extraembryonic yolk sac tissue (Gore, Monzo, Cha, Pan, & Weinstein, 2012). In zebrafish, precursor cells emerge from the intermediate cell mass of the ventral mesoderm at 12 hpf (Gore et al., 2012; Wingert & Zon, 2006). During early embryogenesis, primitive blood vessels form through vasculogenesis (Gore et al., 2012). This mechanism is characterized by the fusion of angioblast cells and is required for establishing major blood vessels. The formation of blood vessels can also occur through angiogenesis (Gore et al., 2012). This process involves the emergence of *de novo* blood vessels as sprouts that protrude from pre-existing vessels. These sprouts engage in pathfinding filopodia-like activity until they make contact with a target vessel (Lawson & Weinstein, 2002). In fact, angiogenesis is utilized during later stages of development and accounts for most of the arborization within the vasculature (Gore et al., 2012). Nonetheless, both mechanisms are necessary for the proper formation of nascent blood vessel networks that progressively become more elaborated and invade surrounding tissue. In the embryonic pectoral fin, two blood vessels have been shown to invade the anlage from the anterior and posterior border (T. Yano et al., 2012). The two vessels continue to extend until they meet in the posterior region at 48 hpf and result in the formation of the marginal blood vessel which surrounds the endoskeletal disc (T. Yano et al., 2012) (Figure 1.1C). While this process is well-defined, little is known about the molecular mechanisms that guide vascular invasion and remodeling during zebrafish development (Ellertsdóttir et al., 2010). Previous work has identified several factors including *scl* and *vegfr2* that are necessary for the maintenance of hematopoietic and endothelial progenitors (Habeck et al., 2002; Kabrun et al., 1997). In addition, many members

of the ETS transcription factor family (i.e. *fli1a*, *fli1b*, *ets1*, *etv2*) are involved in the specification and differentiation of newly formed blood vessels (Craig et al., 2015). The *etv2* member initiates early vasculogenesis by stimulating the expression of *fli1a*, *fli1b*, *kdrl*, and *scl* genes. The Etv2 and Fli1b factors are functional during the later stages of vasculogenesis and activate a unique genetic program that promotes early angiogenic sprouting (Craig et al., 2015). The role of *fli1a* outside the context of vascular development will be the subject of later discussions (see section 1.4.4).

1.3 Overview of Developmental and Molecular Mechanisms in Fins and Limbs

1.3.1 The Apical Ectodermal Ridge

In light of their evolutionary origin, tetrapods including amphibians, reptiles, mammals, and birds have many embryological similarities with fish (Wolpert, Tickle, & Martinez Arias, 2015). This is pronounced at the pharyngula stage where embryos essentially resemble one another. In fact, at this stage both fin- and limb-buds are considered homologous structures with parallel mechanisms of patterning yet distinct morphology during development (Yano & Tamura, 2013). Limb and fin buds have organizing centers that pattern the appendage along the three major axes (Grandel & Schulte-Merker, 1998; Tohru Yano & Tamura, 2013). The apical ectodermal ridge (AER) is a thickening of columnar epithelial cells situated at the distal tip of the bud (Figure 1.3). It sits at the dorsoventral boundary and above a highly proliferative region of mesenchymal cells known as the progress zone (PZ). The AER in mice secretes several fibroblast growth factor (FGF) proteins including FGF2, FGF4, FGF8, and FGF9 that interact with adjacent tissue to define structures along the proximal-distal (P-D) axis (Mariani, Ahn, & Martin, 2008). FGF8 signals are directed to cells of the PZ, which secrete FGF10 proteins that, in turn, target the AER. This reciprocal

interaction maintains the activity of the AER and supports the proliferation of the PZ during bud outgrowth. The cells of the PZ remain undifferentiated until they leave this region, and positional information is thought to be conferred by the time limb bud cells spend under the influence of the PZ (Towers, Tickle, & Capecchi, 2009). The ectodermal layers that flank the AER will eventually express specific factors to form the dorsal-ventral (D-V) axis. Other FGF signals oppose retinoic acid (RA) emanating from the proximal end in a gradient-dependent fashion. This results in differential expression of homeotic factors including homeobox (Hox) transcription factors. In tetrapods, this antagonism restricts homeotic *Meis1* expression to the proximal bud, *Hoxa11* to the medial portion (see section 1.4.2), and *Hoxa13* to the distal bud. These transcription factors interpret signaling gradients and internal timing mechanisms to give rise to the stylopod, zeugopod, and autopod bone-composing regions, respectively (Saiz-Lopez, Chinnaiya, Towers, & Ros, 2017). In contrast to tetrapods, the zebrafish *hoxa11*b and *hoxa13b* domains overlap and never become mutually exclusive (Kherdjemil et al., 2016; Yano & Tamura, 2013).

In tetrapods, the AER stimulates the proliferation and expansion of the underlying mesenchyme until they express skeletal factors (Masselink et al., 2016; Zhang et al., 2010). Once the mesenchymal cells become specified, the AER undergoes programmed cell death leaving behind a thin layer of epithelium (Lu, Yu, Perdue, & Werb, 2008; Masselink et al., 2016). In zebrafish, the AER is functional for a shorter period of time. Using a time-lapse analysis, a subpopulation of somite-derived cells has been shown to leave the mesenchymal region and migrate to the AER by 37 hpf (Masselink et al., 2016). These cells will contribute to the induction of AF, which later transforms into a PFF (Masselink et al., 2016). In fact, the transition from the AER to the AF is considered inhibitory for the growth and elaboration of the distal endoskeleton (Tohru Yano &

Tamura, 2013). This AER-AF transition is absent in tetrapods and results in sustained AER activity (Masselink et al., 2016). Moreover, the length of the time the AER is active has been proposed to correspond to the extent of distal endochondral expansion (Thorogood, 1991). Accordingly, teleost fish have AER signaling for a shorter period of time compared to tetrapods, leading to fewer and less elaborated distal endochondral bones (Thorogood, 1991; Yano et al., 2012).

1.3.2 The Zone of Polarizing Activity

The zone of polarizing activity (ZPA) is another organizing center that exists in fish and tetrapods. This section will use studies in tetrapods to explain the role of the aforementioned signaling center. The ZPA is established at the posterior mesenchymal portion of the bud as a result of FGF4 signaling from the AER (Figure 1.3)(Wolpert et al., 2015). It secretes sonic hedgehog (SHH) – a diffusible ligand that is responsible for patterning the anterior-posterior (A-P) axis (Towers et al., 2009). The signaling cascade is initiated by the binding of SHH to the patched 1(PTCH1) receptor, which inhibits the action of PTCH1 and facilities the translocation of Glioma-associated Oncogene (GLI) transcription factors into the nucleus. In the absence of SHH, GLI proteins are modified into transcriptional repressors that prevent the activation of downstream targets (Towers et al., 2009; B. Wang, Fallon, & Beachy, 2000). SHH signaling and downstream effectors are particularly important for specifying digit identity and promoting digit outgrowth during limb development (Suzuki, 2013). This morphogen forms a concentration-gradient such that different thresholds provide cells with unique positional information to specify digit identity. Accordingly, cells with the highest exposure to SHH signaling become specified to form the most posterior digit, whereas cells with the least exposure acquire the fate of the most anterior digit (Suzuki, 2013). Interestingly, the activity of the ZPA and AER become maintained by a positive feedback mechanism, allowing

their respective signals to regulate the expression of downstream genes. This includes late-phase 5'HoxA/D gene expression which is critical for the proper formation of the vertebrate appendage.

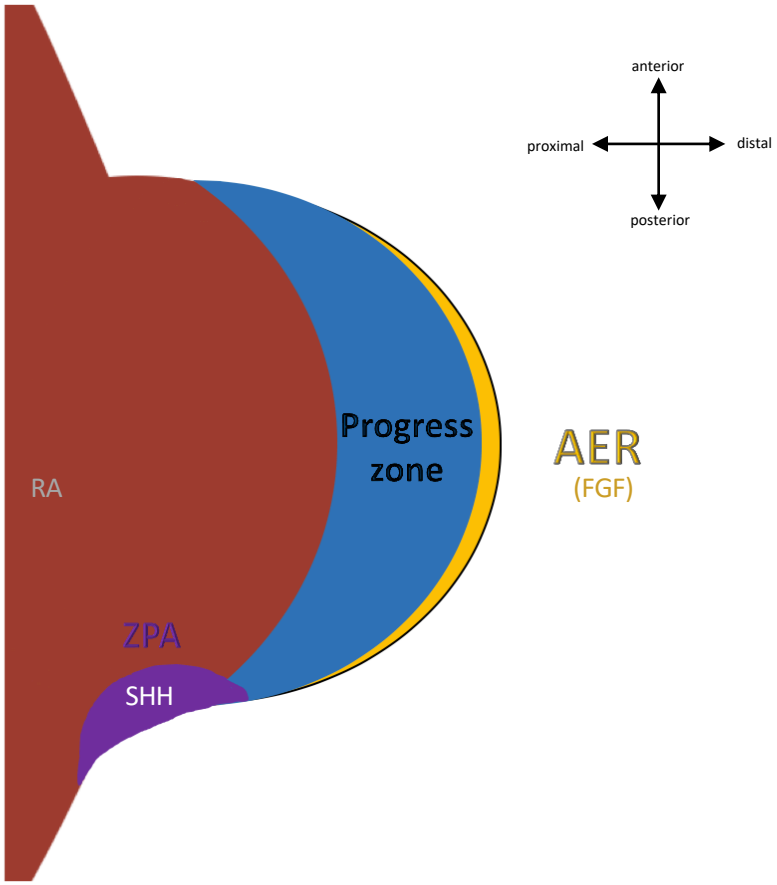

Figure 1.3: The Apical ectodermal ridge (AER) is instrumental in the development and patterning of the vertebrate appendage. It secretes FGF signals which antagonize retinoic acid (RA) from the proximal end to define the proximal-distal axis. The AER interacts with the zone of polarizing activity (ZPA), which secretes SHH and establishes the anterior-posterior axis.

1.4 Contributions of *m-Inta11* and *fli1a* during development

1.4.1 *Hox* genes

Hox genes encode transcription factors that are essential for establishing the body plan of an embryo including the position of limb and fin buds. These genes are instrumental in appendicular patterning and provide cells with specific positional identities during development (Ahn & Ho, 2008; Lalonde & Akimenko, 2018a). The spatial and temporal regulation of *Hox* genes guides cell differentiation and tissue morphogenesis along the P-D axis. In addition, Hox genes are arranged in clusters and display collinear expression, such that their spatiotemporal activity corresponds to their 3' to 5' position within a gene complex of a chromosome (Zakany & Duboule, 2007). Accordingly, genes closer to the 5' end of a cluster are expressed at later time points and have more distal domains of expression. The most posterior genes of the HoxA/D cluster, the 5' HoxA/D genes (i.e. *Hox9-13*) dictate appendicular patterning of distal elements (Ahn & Ho, 2008; Krumlauf, 1994; Lalonde & Akimenko, 2018a; Nelson et al., 1996; Sordino, van der Hoeven, & Duboule, 1995; Spence, Gerlach, Lawrence, & Smith, 2007; Woltering, Noordermeer, Leleu, & Duboule, 2014).

In tetrapods, *Hoxd13* and *Hoxa13* are two genes that are crucial for the specification and patterning of distal endoskeletal structures including digits (Kherdjemil et al., 2016; Nakamura, Gehrke, Lemberg, Szymaszek, & Shubin, 2016). During development, expression of *Hoxd13* is primarily restricted to the posterior region but later extends anteriorly to occupy the entire distal aspect of the bud (Freitas, Gómez-Marín, Wilson, Casares, & Gómez-Skarmeta, 2012a). Moreover, distal mesenchyme that expresses *Hoxa13* is associated with the patterning of the presumptive autopod region (Ahn and Ho, 2008). Furthermore, mutant mice that are homozygous for the deletion of

Hoxa13 alleles exhibit severe defects in skeletal elements of the autopod region (Fromental-Ramain et al., 1996; Stadler, Higgins, & Capecchi, 2001). In fact, the loss-of-function of both *Hoxa13* and *Hoxd13* results in a phenotype where skeletal elements of the autopod region (i.e. digits, wrist) fail to form (Fromental-Ramain et al., 1996; Stadler et al., 2001). The exact mechanism of action encoded by the HOXA13/HOXD13 transcription factors is yet to be elucidated. More recently, HOXA13 as well as HOXD13 transcription factors, have been shown to inhibit chondrogenic differentiation in chicken micro-mass culture of primary mesenchymal limb progenitor cells (Jerković et al., 2017). Previous studies have demonstrated a role for *Hoxa13* in cell adhesion, cell sorting, and delineating the boundaries between different tissue (Saiz-Lopez et al., 2017; Stadler et al., 2001). The downstream effectors of *Hoxa13* include ephrin receptors which are necessary for the formation of tarsals, carpals, and phalanges (Perez, Weller, Shou, & Stadler, 2010; Stadler et al., 2001). Phenotypic analyses of mutant *Hoxa13* homozygous mice show deformed chondrogenic condensations, missing or truncated skeletal elements, and fusion of the interdigit tissue (Fromental-Ramain et al., 1996; Perez et al., 2010). Other studies in chick limb buds demonstrate that misexpression of *HOXA13* in the zeugopod region at Hamburger Hamilton stage 22 induces pre-cartilaginous condensations that are consistent with the formation of autopodial skeletal elements (Fromental-Ramain et al., 1996; Yokouchi et al., 1995).

Hoxa13 is also implicated in the patterning of blood vessels during mammalian development (Shaut, Keene, Sorensen, Li, & Stadler, 2008; Shaut et al., 2007; Stadler et al., 2001). Gene expression studies show that *Hoxa13* is active in the cells that make up the wall of the uterine arteries, the vascular endothelia of the genital tubercle, and the labyrinth of the placenta (Shaut et al., 2008; Shaut et al., 2007; Stadler et al., 2001). Mutant mice that lack *Hoxa13* display narrowing

of the umbilical arteries, disorganized epithelial and mesenchymal cells, and no cell layer stratification (Stadler et al., 2001). In addition, homozygous *Hoxa13* mutants present with enlarged genital tubercle vessels, aberrant organization of the labyrinth endothelia, and diminished integrity of the placental vasculature (Shaut et al., 2008; Shaut et al., 2007). This phenotype produces edema in the blood vessels of the placenta leading to gestational lethality (Shaut et al., 2008; Shaut et al., 2007).

Zebrafish have two clusters of *hoxA* genes (i.e. *hoxAa*, *hoxAb*) due to a whole-genome duplication event that occurred in teleost fish after diversification from more primitive ray-finned fishes (Amores et al., 1998). The same is not true for *hoxD* because while one cluster (i.e. *hoxDa*) was retained, the other (i.e. *hoxDb*) was lost during evolution (Duboule, 2007). During embryonic development, *hoxd13a* is confined to the distal posterior region of the fin bud (Figure 1.4A) (Ahn & Ho, 2008; Sordino et al., 1995; Zhang et al., 2010). It first appears at 30 hpf and continues to expand until 60 hpf. Thereupon, the expression levels of *hoxd13a* drop and the pattern shows little polarization toward the distal anterior half of the fin bud (Ahn & Ho, 2008). Unlike *hoxd13a*, the expression of *hoxa13a* is first established at 42 hpf (Figure 1.4B). It later stabilizes in the distal mesenchyme and subsequently confines to the proximal fin blade region at 72hpf. In contrast, the expression of *hoxa13b* begins at 30 hpf, progressively increases, and encompasses a broad domain of expression by 60 hpf (Figure 1.4C) (Ahn & Ho, 2008).

Using fate-mapping approaches in zebrafish, late phase *hoxa* expression was localized in the actinotrichia at 20 dpf and later in fin rays at 90 dpf (Nakamura et al., 2016). In addition, the generation of single homozygous *hoxa13a* and *hoxa13b* mutants using CRISPR/Cas9 genome

editing result in the formation of shorter adult fin rays compared to the WT phenotype. Furthermore, double homozygous *hoxa13a hoxa13b* mutants, as well as mosaic triple homozygous *hoxa13a hoxa13b hoxd13a* mutants display an increase in the number of endochondral bones and fail to complete the formation of the adult fin rays (i.e. only form the first fin ray segments) (Nakamura et al., 2016). This data suggest that *hoxa13a*, *hoxa13b*, and *hoxd13a* are associated with the formation and patterning of the presumptive fin rays (Nakamura et al., 2016). In addition, these genes appear to be involved in specifying fin ray segment length by determining the position of the joint between the bone segments (McMillan et al., 2018). It is yet unclear whether *hoxa13a* or *hoxa13b* in zebrafish have similar functions to those described by *Hoxa13* in murine cell adhesion and blood vessel patterning.

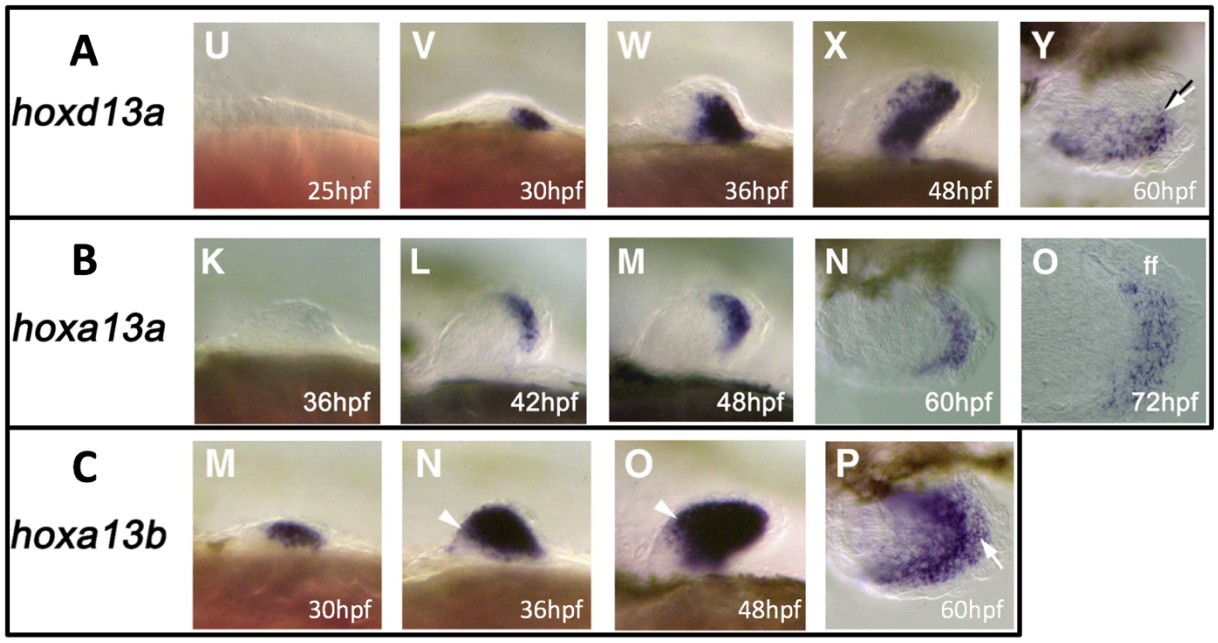

Figure 1.4: The expression of *hoxd13a*, *hoxa13a*, and *hoxd13b* in zebrafish pectoral fins during embryonic development. (A) The expression domain of *hoxd13a* at 25, 30, 36, 48, and 60 hpf is predominantly localized to the posterior region of the fin bud with some anterior

expansion (B) The expression domain of *hoxa13a* at 36, 42, 48, 60, and 72 hpf is restricted to the distal region of the fin bud (C) The expression domain of *hoxa13b* at 30, 36, 48, and 60 hpf is broadly extended through the fin bud. Permission granted by Elsevier and Copyright Clearance Centre through RightsLink® service to reuse data in thesis/dissertation on May 28th, 2019 (License number: 4597681210446). Figure adapted from Ahn & Ho, 2008.

1.4.2 The *m-Inta11 cis*-acting regulatory elements

Our collaborators have previously identified an enhancer known as *m-Inta11* within a unique intron of the mouse *Hoxa11* gene (Kherdjemil et al., 2016). This *cis*-acting regulatory element is instrumental to the separation of the *Hoxa11* and *Hoxa13* expression domains during tetrapod limb development. As mentioned in section 1.3.1, the activity of these genes is required for the patterning of the P-D axis. During limb-bud outgrowth, *Hoxa13* expression is restricted to the distal mesenchyme and does not overlap with the more proximal domain of *Hoxa11*. The *m-Inta11* enhancer has been shown to stimulate anti-sense transcription of RNA including the first exon of *Hoxa11* (*Hoxa11as-b*) in the presumptive autopod region (Kherdjemil et al., 2016). This activity is thought to block the binding of transcriptional factors to the sense strand and prevents *Hoxa11* expression in distal cells (Kherdjemil et al., 2016). Furthermore, deletion of this enhancer diminishes *Hoxa11as-b* transcription and results in ectopic expansion of *Hoxa11* to distal cells. Chromatin Immunoprecipitation-sequencing (ChIP-seq) analysis has revealed that the sequence of *m-Inta11* enhancer contains binding sites for HOXA13 and HOXD13 proteins (Kherdjemil et al., 2016). In addition, transfection assays in cell culture have demonstrated that HOXA13 is able to increase the activity of *m-Inta11* (Kherdjemil et al., 2016). The next section will examine the functionality of the *m-Inta11* enhancer in zebrafish.

1.4.3 *m-Inta11* functionality in zebrafish

The *m-Inta11*, as mentioned previously, is a distal enhancer found within a unique intron of *Hoxa11* that triggers *Hoxa11* antisense transcription (Kherdjemil et al., 2016). In zebrafish, intronic sequences of *hoxa11a* and *hoxa11b* were not capable of driving reporter expression in the fins of transgenic fish, suggesting the *hoxa11a* and *hoxa11b* introns do not contain a distal enhancer (Kherdjemil et al., 2016). A transgenic approach was used to test the functionality of *m-Inta11* in zebrafish. A human beta-globin minimal promoter (HBB) was subcloned downstream of this enhancer to drive the expression of reporter cDNA, leading to the creation of the transgenic (*m-Inta11:mCherry*) line (Kherdjemil et al., 2016). Accordingly, *m-Inta11* was capable of driving reporter monomeric red fluorescent (*mCherry*) expression in the migrating cells of the median fin fold and pectoral fin buds during embryonic development (Figure 1.5). This suggests that *m-Inta11* positive cells contain the necessary transcription factors to induce *m-Inta11* enhancer activity. Furthermore, the activity of *m-Inta11* correlates with endogenous *hoxa13a* expression. This includes the distal median fin fold, the pectoral fin buds, and the urogenital pore region during embryonic and early larval development, as well as the joints of the rays during adult fin regeneration (Lalonde & Akimenko, 2018a, 2018b; McMillan et al., 2018). In the pectoral fin buds, *m-Inta11* is active in cells where the expression of *hoxa13a*, *hoxa13b*, and *hoxd13a* overlap (Figure 1.6). This correlative evidence suggests that *hoxa13a*, *hoxa13b*, *hoxd13a* – collectively termed *hox13* genes, either in unison or independent of one another, are involved in the activation of *m-Inta11*. Due to the proximity of the *m-Inta11* positive cells to the marginal blood vessel in the pectoral fin, it was postulated that the source of migrating *m-Inta11* positive cells may originate from the marginal blood vessel (Figure 1.5 B). Accordingly, the transgenic *Tg*(*m-Inta11:mCherry*)

line was crossed with a another transgenic line, known as *Tg(fli1a:eGFP)*, that allows us to visualize blood vessels.

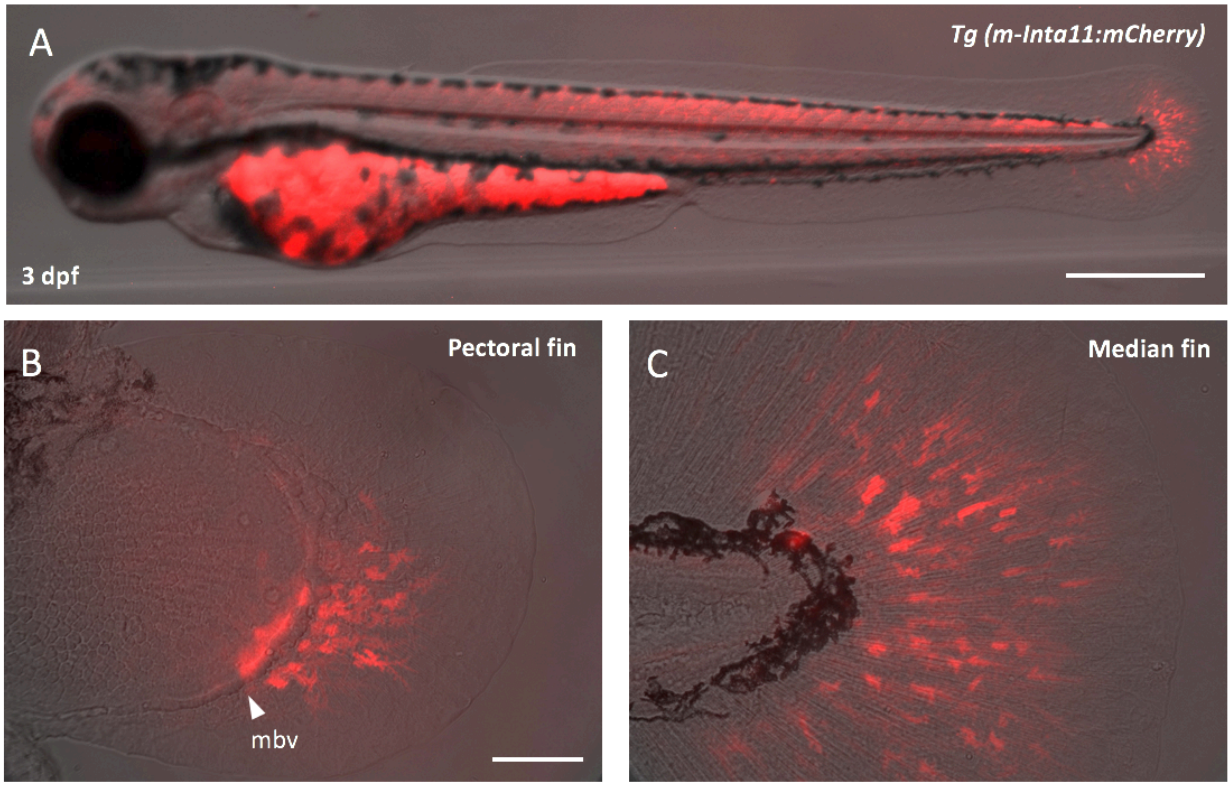

Figure 1.5: The transgenic (*m-Inta11:mCherry*) line drives reporter *mCherry* expression in the migrating cells of the median and pectoral fins during development. (A) zebrafish larva at 3 dpf showing reporter mCherry expression in the median fin fold. Note: Autofluorescence can be observed in the head, yolk sac, and trunk. (B) The pectoral fin bud showing migrating cells of the pectoral fin fold. Note the proximity of *m-Inta11* positive cells to the marginal blood vessel (mbv). (C) The median fin fold showing distal cell migration. mbv = marginal blood vessel. Scale bars of A = 500 µm, B-C = 50 µm. Images were captured by R. L. Lalonde.

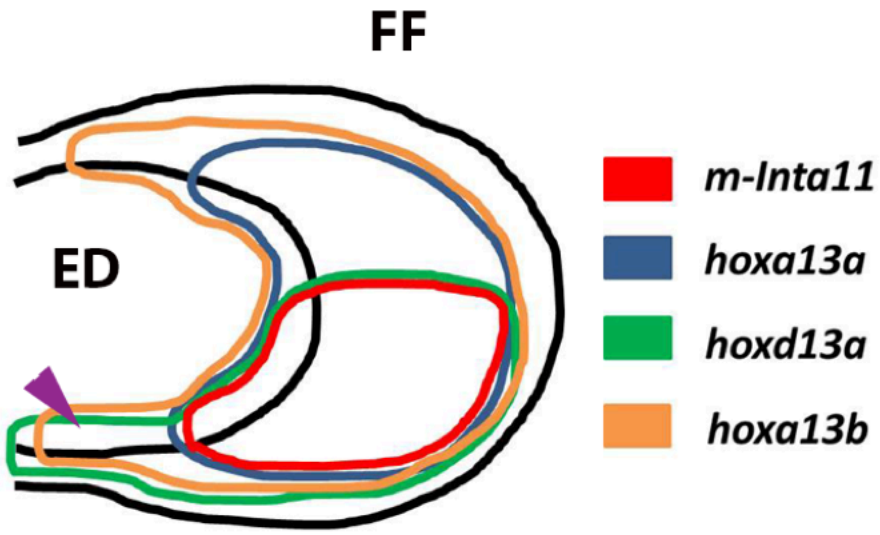

Figure 1.6: *m-Inta11* positive cells express *hoxa13a*, *hoxa13b*, and *hoxd13a* genes during pectoral fin development. *m-Inta11* is active in a cell population where the domains of *hoxa13a*, *hoxa13b*, and *hoxd13a* intersect. The *hoxa13a, hoxa13b,* and *hoxd13a* genes are collectively known as *hox13*. ED = endoskeletal disc. FF = fin fold. (Lalonde & Akimenko, 2018a).

1.4.4 The *fli1a cis*-acting regulatory elements

The zebrafish *Tg*(*fli1a:eGFP)* transgenic line recapitulates the activity of the friend leukemia integration 1 transcription factor (Fli1a) in endothelial cells. This member of the ETS family is one of the first markers of endothelial cell differentiation during embryonic development. It encodes a transcription factor that participates in establishing vasculogenic networks and facilitate the sprouting of new blood vessels (Craig et al., 2015). *fli1a* is also a proto-oncogene and its human ortholog *Fli1* has been implicated in various malignancies, which will be discussed in further detail

in section 1.4.6 (Li, Luo, Liu, Zacksenhaus, & Ben-David, 2015). *fli1b*, the paralog of *fli1a*, is also a transcription factor that is associated with embryonic vascularization. *fli1b* and *fli1a* have comparable domains of expression between the 10- and 14-somite stage, suggesting a redundant function in vascularization (Craig et al., 2015). In fact, transposon-mediated gene trap studies support a genetic redundancy between *fli1a* and *fli1b*, since single and double homozygous *fli1a* and *fli1b* mutants did not exhibit defects in vascular patterning (Craig et al., 2015). The transgenic line reporting endogenous *fli1a* was created using a P-1 artificial library (PAC) library (Lawson & Weinstein, 2002). Accordingly, a 15-kilobase region around the promoter and the first exon of the *fli1* locus was cloned into a plasmid. An enhanced green fluorescent protein (*eGFP*) reporter cDNA was then cloned in the 5' untranslated region (UTR) upstream of the start codon and *cis*-acting regulatory elements were able to drive *eGFP* expression in endothelial cells of the blood vessels throughout development and into adulthood (Figure 1.7A) (Lawson & Weinstein, 2002). By examining the pectoral fin bud, *fli1a* expression can be observed in the marginal blood vessel as would be expected. However, *fli1a* is also expressed in the chondrocytes of the endoskeletal disc. The expression is first concentrated in the anterior portion of the disc at 48 hpf and progressively extends to the posterior portion at later time points. Surprisingly, we show there is no *eGFP* reporter expression in the distal posterior chondrocytes of the disc (Figure 1.7B). It is still unclear how *fli1a* expression in the ED contributes to pectoral fin development. Nonetheless, gene expression analysis in mouse limbs shows that *Fli1* is active in chondrogenic condensations, suggesting a role in endochondral bone formation (Vlaeminck-Guillem et al., 2000).

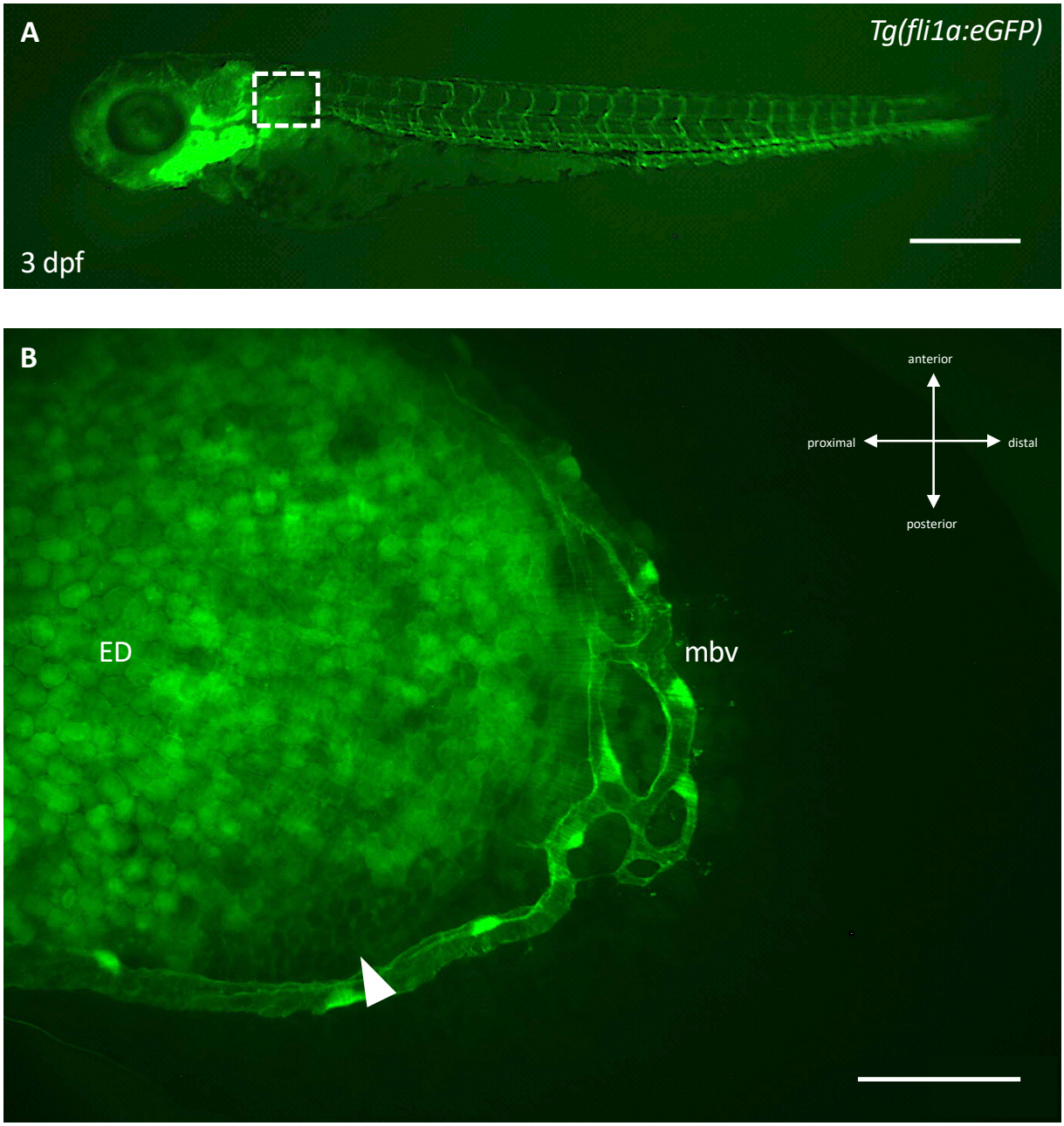

Figure 1.7: The transgenic reporter line *Tg(fli1a:eGFP)* recapitulates endogenous *fli1a*. (A) It drives reporter *eGFP* expression in endothelial cells of the blood vessels of zebrafish embryos and larvae (here 3dpf larva). (B) In the pectoral fin bud, *fli1a* is expressed in the marginal blood vessel and the major part of the endoskeletal disc with the exception of the distal posterior chondrocytes (arrowhead). ED = endoskeletal disc, mbv = marginal blood vessel. Scale bars: A = 500 µm, B = 50 µm.

1.4.5 Complementary pattern

In the double transgenic *Tg(m-Inta11:mCherry; fli1a: eGFP)* line, the domain of initiation of *m-Inta11* activity at 3 dpf correlates with the domain where an absence of *fli1a* reporter expression in the distal endoskeletal disc (ED) is observed. In fact, the domains of *m-Inta11* and *fli1a* enhancer activity appear complementary, as evidenced by the lack of overlap between mCherry and eGFP reporter proteins (Figure 1.8D). This suggests that there may be a regulation between *fli1a* and *hox13* genes. In fact, there is some evidence in Ewing sarcoma studies to support this regulation.

1.4.6 The role of *Fli1* and *Hox13* in Ewing sarcoma

Ewing sarcoma is an aggressive bone and soft tissue cancer that predominantly affects children and young adolescents with frequent manifestations in the long bones and the pelvis (Balamuth & Womer, 2010). It is comprised of malignant cells that remain poorly differentiated and presumably have a neural crest or mesenchymal origin (Svoboda et al., 2014). The pathogenesis of Ewing sarcoma is most commonly caused by a chromosome translocation between *EWSR1* of chromosome 22 and *FLI1* of chromosome 11, resulting in the *EWSRI-FLI1* gene coding for the EWS-FLI1 chimeric fusion protein (Richter et al., 2009). Under normal circumstances, the *EWSR1* gene encoding the EWS RNA-binding protein regulates transcription, RNA splicing, cell division, cell cycle arrest, and cell differentiation (Leemann-Zakaryan et al., 2009). As mentioned previously, the FLI1 transcription factor is essential for the progression of vasculogenesis and angiogenesis during early embryonic development (Li et al., 2015). In addition, FLI1 is involved in the maintenance of hematopoietic stem cells and the differentiation of various cell lineages including T-cells, B-cells, megakaryocytes, and myeloid precursor cells (Li et al., 2015). The processes that are mediated by *EWSR1*, *FLI1*, and their downstream effectors are severely

perturbed by the chromosomal translocation (Svoboda et al., 2014). The *EWS-FLI1* translocation accounts for 85% of all Ewing sarcoma family of tumors (Burchill, 2003). Other forms of Ewing sarcoma are the result of a translocation between *EWSR1* and other members of the ETS family such as *ERG* and make up to 10% of all Ewing sarcoma malignancies (Burchill, 2003; Jinawath et al., 2010). The EWS-FLI1 fusion protein contains the N-terminus of EWS including the transactivation domain, as well as the C-terminus of FLI1 containing the ETS DNA binding domain (Bernstein et al., 2006). It encodes an oncogenic transcription factor that is under the influence of putative *EWSR1* and *FLI1 cis*-acting regulatory elements, resulting in ectopic expression of the EWS-FLI1 fusion oncoprotein. In fact, this fusion protein has been shown to induce stronger activation of FLI1 targets and regulate genes that do not normally respond to FLI1 (Li et al., 2015; May et al., 1993). While EWS-FLI1 is a principal mediator that initiates the development of Ewing Sarcoma, other events and downstream effectors drive the progression of malignancy in bone and soft tissue. This includes cooperating mutations in various oncogenes (i.e. *RAS*), tumor suppressor genes (i.e. *p53*), and growth factors (i.e. *VEGF*) (Radig et al., 1998). The changes induced by EWS-FLI1 promote vasculogenesis, angiogenesis, cell survival, proliferation, and metastasis (Toomey, Schiffman, & Lessnick, 2010). In addition, expression of *EWS-FLI1* in cell culture of primary pediatric mesenchymal stem cells has been shown to dysregulate the transcriptional program during development and impair mechanism of stem cell renewal and differentiation (Riggi et al., 2014). Furthermore, Ewing sarcoma cells and EWS-FLI1 positive stem cells display perturbations to the activity of Trithorax (TcG) and Polycomb (PcG) family of proteins, as evidenced by the gain of TcG-dependent active methylation mark and loss of PcG-dependent repressive methylation mark at the posterior *HOXD* locus (Svoboda et al., 2014). These protein families remodel chromatin and modulate epigenetic changes during development, leading

to the activation and silencing of target genes, respectively (Svoboda et al., 2017, 2014; von Heyking et al., 2016). *HOX* genes are well-established targets of TcG and PcG proteins and the posterior *HOXD* locus, in particular, is critical for the transformation of the Ewing sarcoma phenotype (von Heyking et al., 2016). In fact, suppression of *HOXD10*, *HOXD11*, *HOXD13* using short-hairpin RNA reduces contact-independent growth, colony formation, proliferation, and invasiveness in Ewing sarcoma cell lines, as well as metastasis in mouse subjects (von Heyking et al., 2016). Moreover, two *TcG* genes, mixed lineage leukemia (*MLL1*) and menin (*MEN1*), are highly expressed in Ewing sarcoma tumors and form a protein-protein complex that renders the posterior *HOXD* locus (i.e. *HOXD10*, *HOXD11*, *HOXD13*) accessible to transcriptional machinery. In fact, short-hairpin RNA mediated knockdown of *MLL1* in Ewing sarcoma cell lines diminishes colony formation and downregulates *HOXD13* expression, as well as reduces tumor volume in xenograft studies (Svoboda et al., 2017). Similarly, *MEN1* knockdown decreases proliferation and *HOXD10* expression in Ewing sarcoma cell lines (Svoboda et al., 2017). Interestingly, inhibition of the MEN1-MLL1 protein complex by a pharmacological agent reduces proliferation and expansion of Ewing sarcoma cells, downregulates the expression of *HOX10*, *HOXD11*, and *HOXD13*, as well as stump xenograft tumor growth (Svoboda et al., 2017). The expression of these *HOX* genes is thus associated with promoting cell survival, proliferation, and tumorigenicity in Ewing sarcoma (Svoboda et al., 2017). The elevated expression of other *HOX* genes including *HOXA13* has been associated with promoting the epithelial to mesenchymal transition in esophageal squamous cell carcinoma (ESCC) cells (Shi et al., 2018). Other studies in transduced neural-crest-derived stem cells (NCSC) have demonstrated that the phenotype of EWS-FLI1 positive cells is linked to the dysregulation of multiple *HOX* genes. Most notably, there is a two-fold increase in *HOXA13* and *HOXD13* expression, which are thought to contribute to the

malignancy of Ewing sarcoma (Svoboda et al., 2017, 2014; von Heyking et al., 2016). Furthermore, Ewing sarcoma cell lines display changes in focal cell adhesion including alterations to the integrity of the extracellular matrix and the actin cytoskeleton, which are mediated by the EWS-FLI1 oncoprotein (Chaturvedi et al., 2014; Svoboda et al., 2014). These changes repress the transcription of various genes encoding integral cytoskeletal and adhesion-associated proteins, thus facilitating the growth of Ewing sarcoma tumors (Chaturvedi et al., 2014). The introduction of exogenous zyxin and α5 integrin proteins is capable of restoring cytoskeleton integrity and focal adhesion in Ewing sarcoma cells (Chaturvedi et al., 2014). The *EWS-FLI1* induced phenotypes in models of Ewing sarcoma (i.e. ectopic activation of FLI1 targets, dysregulation of *HOX13*, changes in cell adhesion) could inform our understanding of the roles of *Fli1* and *HOX13* during normal development.

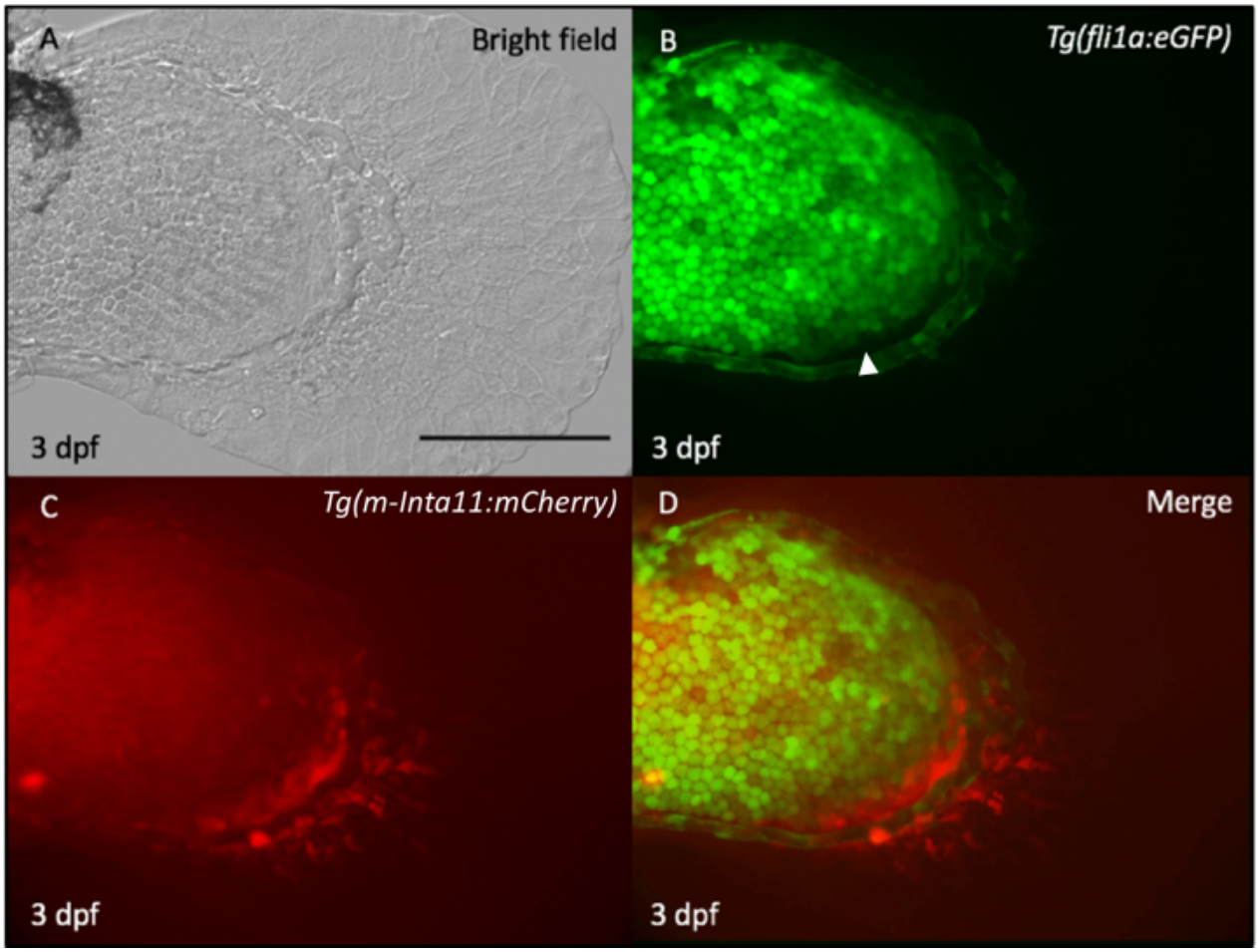

Figure 1.8: The absence of *fli1a* reporter expression in endoskeletal disc chondrocytes correlates with the beginning domain of *m-Inta11* enhancer activity in a complementary fashion. The pectoral fin of a double transgenic *Tg(fli1a:eGFP; m-Inta11: mCherry)* larva at 3 dpf, showing the absence of *fli1a* reporter expression (arrowhead) correlates with the beginning of *m-Inta11* reporter expression in the distal posterior chondrocytes. (A) brightfield. (B) eGFP channel. (C) mCherry channel. (D) Merge. Scale bars: A-D = 100 µm. Images were obtained by R. L. Lalonde.

1.5 Summary of Objectives

The main objectives discussed in this dissertation focus on further understanding the morphological changes and molecular mechanisms that underlie the formation of the pectoral fin during embryonic and larval development. Previous work in our lab has demonstrated that the *m-Inta11* enhancer is active in pectoral fin cells that express *hoxa13a*, *hoxa13b*, and *hoxd13a* genes. Interestingly, the activity of *m-Inta11* appears to be complementary with *fli1a* reporter expression during early development, suggesting there may be a regulation between *fli1a* and *hox13* genes. Accordingly, **we hypothesize that *fli1a* and *hox13* participate in tissue organization and remodeling during zebrafish pectoral fin development**.

Objective (1): The source of migrating *m-Inta11* positive cells in the pectoral fin is unknown. However, due to the proximity of these cells to the marginal blood vessel, it was postulated that the migrating cells of the pectoral fin fold may emerge from the marginal blood vessel. Accordingly, **we wish to determine the origin of the migrating *m-Inta11*-positive cells and examine their changes in cell morphology**. These cells may emerge from the marginal blood vessel, the endoskeletal disc, or elsewhere in the fin.

Objective (2): Some of the changes that occur during pectoral fin development have been previously characterized. However, several processes remain to be elucidated, including the reorganization of the ED, the formation of distal radials, and the remodeling of blood vessels. In fact, the formation of distal radials has only been described through mitotic indices and little is known about early development prior to the emergence of precursor condensations. In addition, no studies have explored vascular remodeling beyond the formation of the marginal blood vessel.

Using time-course analysis, **we wish to follow *m-Inta11* and *fli1a*-positive cells during development and determine their contributions to adult structures**. Furthermore, we would like to determine if *m-Inta11* and *fli1a* domains of activity remain complementary during later stages of development.

Objective (3): In Ewing sarcoma studies, the EWS-FLI1 fusion protein induces ectopic activation of *FLI1* and is evinced to upregulate the expression of *HOX13* genes. Despite this evidence, little is known about the relationship between FLI1 transcriptional activity and HOX13 genes during normal development. In zebrafish, it is unclear how *fli1a* and *hox13* genes influence the regulation of one another during fin development. **We wish to understand the regulation behind the complementary pattern**. Accordingly, we would like to undertake functional analysis of the effects of ectopic *fli1a* expression in the *m-Inta11* domain. The introduction of *fli1a* in *hox13*-expressing cells could provide insights into the regulation between *fli1a* and *hox13* genes during pectoral fin development and shed light on the pathology of Ewing sarcoma.

CHAPTER 2: MATERIALS & METHODS

2.1 Animal Care

All zebrafish husbandry was carried out in the D' Iorio fish facility at the University of Ottawa. The fish are regularly fed and the facility is maintained at 28 °C with a standard photoperiod consisting of 14 h of light and 10 h of darkness (Westerfield, 2007). Adult zebrafish males and females were placed in breeding tanks and separated by a divider. The divider was removed the next morning between the hours of 9:00 and 10:00 am when fish would naturally mate. To optimize reproductive performance, the water was changed, and breeding tanks were slanted at an angle less than or equal to 45°. Once breeding was complete, the fish were returned to their normal tanks. Collected embryos were transferred to Petri dishes containing 50 ml of E3 medium and subsequently stored in a 28 °C incubator. Each petri dish contained no more than 100 embryos. To raise into adulthood, developing embryos were sterilized between 10 – 28 hpf. Accordingly, embryos were placed in a 10-minute bleach wash (0.003% NaClO), 1-minute neutralization solution (0.05% $Na_2S_2O_3$), and two 5-minute consecutive washes in E3 medium. Embryos were stored in E3 medium at 28 °C until transfer to the nursery facility at 5 dpf. Fish facility personnel monitor developing larvae and provide diet regularly. All experiments and procedures were performed in accordance with the Canadian Council on Animal Care (CCAC) guidelines.

2.2 Median and Pectoral Fin Dissections

Zebrafish fin dissections were collected at various time points during embryonic and larval development. For each collection, 10 embryos or larvae were anesthetized using 0.17mg/ml tricaine (3-aminobenzoic acid ethyl ester) (Westerfield, 2007). Following anesthesia, embryos/larvae were immersed in 4% (w/v) paraformaldehyde (PFA) in Phosphate-buffered saline

(PBS: 137 mM NaCl, 2.7 mM KCl, 4.3 mM Na_2HPO_4, 1.47 mM KH_2PO_4, and adjusted to pH of 7.4) solution for 2 hours at room temperature or stored overnight at 4 °C. After fixation, fish underwent three 5-minute washes in 1X PBS with Tween® detergent (0.1% tween-20-from 20X stock) solution (PBST) at room temperature, followed by overnight storage at °C. Next, embryos or larvae were examined under a Leica MZ FLIII dissection microscope to ensure comparable morphology and fluorescence between collected fish at each timepoint. One or two fish were then selected for dissection. For larvae 12 dpf and older, the standard length (SL) was measured because age alone is not reliable for staging larvae. A surgical blade (Feather® Sterile Surgical Blade #10) was used to generate a median fin dissection, while two needles (329424 - 1 mL BD™ U-100 insulin syringe with 28 G x 1/2 in) were used to isolate pectoral fin tissue. Dissected tissue was then placed on a microscope slide, immersed with mounting medium (Aqua-Mount®), and covered with a coverslip. Median and pectoral fin tissue were imaged on a Zeiss Axioshop compound microscope using AxioCam HSM digital camera and AxioVision AC software (Carl Zeiss). For double fluorescent tissue, images were acquired under each filter separately and merged using Adobe Photoshop CS6 software. For higher resolution imaging, median and pectoral fin tissue were captured using a Nikon A1RsiMP Confocal Microscope and processed with NIS-Elements software.

2.3 Live Imaging of Zebrafish Embryos

Double transgenic embryos were anesthetized using 0.17mg/mL tricaine and transferred to a 1% agarose plate containing impressions from a microinjection and transplantation mold (Z-MOLD ET 21, K-Life Solutions) and E3 embryo medium. The impressions facilitate the orientation of anesthetized embryos to the lateral view and ensure no movement of the embryo. Once placed in a groove, embryonic pectoral fins were imaged every 30-minute interval for up to 8 hours using

the 25x water immersion objective lens of the Nikon A1RsiMP Confocal Microscope. All images were processed using NIS-Elements software.

2.4 Caudal Fin Regeneration

Adult transgenic fish were anesthetized using 0.17 mg/ml tricaine and positioned on a plastic bottom Petri dish. Using a surgical blade (Feather® Sterile Surgical Blade #10), the caudal fin amputation plane was generated two segments proximal to the first bifurcation point of the lepidotrichia, according to standard procedure. Fish were then returned to their housing tanks and allowed to recover. After 4 days of recovery, the fish were transferred to a 1% agarose plate containing 0.17 mg/ml tricaine in water. A slide hold-down (Warner Instruments catalog # 64-0248) was used to flatten the caudal fin regenerate and anchor the fish to the bottom of the plate. Caudal fin regenerates were imaged as previously described in section 2.3.

2.5 Whole-Mount Single Fluorescent *in situ* Hybridization of Zebrafish Embryos

In situ hybridization procedure was adapted from Stetsyuk et al., 2007 and modified by Jing Zhang (October 2016). Embryos were collected at various time points and fixed in 4% PFA for 2 hours at room temperature or overnight at 4 °C. Following fixation, embryos were washed in PBS (2 x 5 min), dehydrated (2 x 5 min) in 100% methanol (MeOH), and stored at -20 °C until further use. On day one, embryos were rehydrated incrementally into PBST environment (5 min in 75% MeOH/25% PBST solution, 5 min in 50% MeOH/50% PBST solution, 5 min in 25% MeOH/75% PBST, and 3x 5 min in PBST). Following rehydration, embryos were digested with Proteinase K (4 µl of 10 mg/ml Proteinase K stock in 4 ml PBST) for 30 minutes and washed (2 x 5 min) in PBST. Next, embryos were fixed (4% PFA in PBS) for 20 minutes and washed (5 x 5 min) in PBST. Subsequently, embryos were incubated in 700 µl of pre-hybridization solution (5 ml of

100% deionized formamide, 2.5 ml of 20X SSC, 12.5% of Tween® 20x stock, 200 µl of 1M Citric acid, 100 µl of 10 mg/ml yeast tRNA, 10 µl of 50 mg/ml heparin, and diethylpyrocarbonate (DEPC) water to a total of 10 ml) for 2-4 hours in a 70 °C water-bath. At this point, spare embryos were incubated in 1 ml of TBSTB (0.1 M Tris HCl pH 7.5, 0.15 M NaCl, 0.5% Tween®20, 0.5% Perkin-Elmer blocking powder) containing 4 µl of Anti-Digoxigenin-POD (Roche catalog # 1207733), gently rocked at room temperature for 2 hours, and subsequently stored at 4 °C overnight. Thereupon, embryos in water-bath had 700 µl of pre-hybridization solution replaced with 200 ul of the pre-hybridization solution containing 200 ng of 1ng/µl RNA probe. Hybridization was allowed to proceed in a 70 °C water-bath overnight. On day two, embryos were washed with 5X, 2X, and 0.2X SSC solutions (5 min in 5X SSC, 5 min in 3:1 5X:2X, 5 min in 1:1 5X:2X, 5 min in 1:3 5X:2X, 5 min in 2X, 3 x 20 min in 0.2X SSC) at 70 °C, followed by washes (2 x 10 min) in PBST. Next, embryos were incubated in PBST solution containing 2% H_2O_2 to inhibit endogenous Horseradish peroxidase and washed (4 x 5 min) in TNT (0.1 M Tris HCl pH 7.5, 0.15 M NaCl, 0.5% Tween® 20) solution. Embryos were then immersed in TBSTB solution for 2-4 hours with gentle shaking. Subsequently, the embryos were incubated in a solution containing 1 ml of pre-absorbed anti-DIG-POD and 4 ml of TBSTB at 4 °C overnight. On day three, embryos were washed (2 x 5 min, 2 x 10 min, 20 min, 30 min, and 40 min) in TNT solution. To prepare for staining, embryos were immersed in 50 µl of Perkin Elmer Amplification Diluent solution for 5min. At this point, embryos were kept in dark and incubated with 100 µl Amplification Diluent solution containing 1:100 Tyr-fluorescein (Perkin-Elmer Manufacturers protocols of TSA™ Plus Cyanine 3/Fluorescein System, Perkin Elmer Cat# NEL753001KT) for 1 hour. After incubation, embryos were washed (2 x 5min) in TNT and stored at 4 °C until ready for imaging.

2.6 *in situ* Hybridization on Mouse Cryosections

In situ hybridization procedure was adapted from Smith, Avaron, Guay, Padhi, & Akimenko, 2006 from and modified by Jing Zhang (March 2015). All breeding of mice and harvesting of embryonic tissue was performed by Jing Zhang according to the guidelines established by the Canadian Council on Animal Care (CCAC). Wildtype mice were bred in the Vanier Hall facility at the University of Ottawa and embryos were harvested at 13.5 days post coitus (dpc). Embryos were fixed in 4% PFA overnight and washed in PBS as previously described. The autopod region of the embryonic limb was dissected and stored in PBS solution containing 30% sucrose at 4 °C overnight. The next day, autopod tissue was oriented in plastic disposable base molds (Fisherbrand® 7 x 7 x 5 mm) and embedded in optimal cutting temperature (Fisher Healthcare™ Tissue-Plus™ O.C.T. Compound) medium according to standard freezing protocol. Autopod tissue was cut at 16 µm using Leica CM3050 S Research Cryostat, transferred to Superfront/Plus microscope slides (Fisherbrand®, catalog # 12 550-15), and allowed to dry at room temperature for 30 minutes. Tissue-affixed slides were stored in a light-sensitive box at -20 °C until further use. On day one, slides were defrosted at 60 °C for an hour, rinsed for 15 minutes with DEPC-PBS solution containing 0.3% Triton™ X-100, and washed (2 x 5 min) in DEPC-PBS solution. Next, slides were treated with Proteinase K (20 µl of 10 mg/ml of Proteinase K, 4 ml of 1M Tris HCl pH 8.0, 4 ml of 0.5M EDTA, and DEPC water to a total of 40 ml) for 15 minutes, followed by washes (2 x 5 min) in DEPC-PBS solution. After Proteinase K treatment, slides were fixed in 4% PFA in PBS for 20 minutes and washed (2 x 5 min) in DEPC-PBS. Following fixation, slides were immersed in acetylation solution (500 µl Triethanolamine, 108 µl of acetic anhydride, and 40 ml of DEPC water) for 5 minutes, washed (2 x 5 min) in DEPC water, and allowed to dry at room temperature. Thereupon, 200 ng of 1ng/µl RNA probe was diluted in hybridization buffer (1X salt

solution [0.2 M NaCl, 10 mM Tris HCl, 5 mM NaH_2PO_4, 5 mM Na_2HPO_4, 1 mM Tris-base, 5 mM EDTA], 50% deionised formamide, 10% dextran sulphate, 1 mg/ml yeast tRNA, 1X 50x Denhardts), mixed, denatured for 5-10 minutes at 70 °C, and chilled on ice. Slides were immersed with 500 µl of hybridization solution, covered with a coverslip, and stored overnight at 70 °C in a sealed chamber containing solution A (1X SSC, 50% formamide, 0.1% Tween®20). On day two, coverslips were removed and slides were washed (2 x 30 min) in solution A at 70 °C, followed by washes (2 x 30 min) in 1X TBST (140 mM NaCl, 2.7 mM KCl, 25 mM Tris HCl, 0.1% Tween®20) at room temperature. Subsequently, slides were blocked in 1X TBST solution containing 10% heat-inactivated calf serum for 1 hour at room temperature. Following blocking, slides were immersed in 450 µl of 1X TBST containing 10% inactivated calf serum and 1:2000 anti-DIG AP Fab fragment (Roche catalog # 1093274), covered with a coverslip, and incubated overnight at 4 °C in a humified chamber. On day three, slides were washed (5 x 20 min) in 1X TBST, washed in NTMT (100 mM NaCl, 100 mM Tris HCl pH 9.5, 50 mM $MgCl_2$, 0.1% Tween®20) for 10 minutes, and stained in NTMT solution containing with 225 µg/ml NBT and 175 µg/ml BCIP. Staining was allowed to proceed in the dark at 37 °C until the desired contrast is achieved. The staining reaction was stopped by washed (2 x 5 min) in autoclaved distilled water. Slides were then allowed to dry, covered with Aqua-Mount® mounting medium, and prepared for imaging.

2.7 Double Fluorescent *in situ* Hybridization on Mouse Cryosections

In situ hybridization procedure was adapted from Welten et al., 2006 and modified by Jing Zhang. All steps leading up to day two of *in situ* hybridization were carried out as previously described in section 2.5. Following washes with solution A and TBST, tissue-affixed slides were incubated in TNT solution containing 2% H_20_2 for 10 minutes and rinsed (4 x 5 min) in TNT. Next, slides were immersed with 300 µl of TBSTB blocking solution and incubated for 2-4 hours at room

temperature. Subsequently, slides were incubated with 100 µl of TBSTB solution containing 1:500 anti-DNP POD (TSA™ Plus DNP System, Perkin Elmer catalog # NEL747A001KT) and stored at 4 °C overnight. On day three, slides were washed (2 x 5 min, 2 x 10 min, 20 min, 30 min) with TNT and stained in the dark with 100 µl of Amplification Diluent containing 1: 100 Tyr-Cy3 (Perkin-Elmer Manufacturers protocols of TSA™ Plus Cyanine 3/Fluorescein System, Perkin Elmer catalog # NEL753001KT) for 10 minutes. All steps after staining were allowed to proceed in the dark. Once staining was complete, slides were rinsed (2 x 5 min) with TNT. Next, slides were treated with TNT solution containing 2% H_2O_2 for 30 minutes and washed (4 x 5 min) with TNT. To prepare for blocking, slides were immersed with 300 µl of TBSTB and incubated for 2-4 hours at room temperature. After blocking, slides were incubated with 100 µl of TBSTB containing 1:500 anti-DIG-POD (Roche catalog # 1207733) and stored overnight at 4 °C. On day four, slides were washed (2 x 5 min, 2 x 10 min, 20 min, 30 min) with TNT and subsequently stained with Amplification Diluent containing 1:100 Tyr-fluorescein (Perkin-Elmer Manufacturers protocols of TSA™ Plus Cyanine 3/Fluorescein System, Perkin Elmer catalog # NEL753001KT). After staining, slides were washed (3 x 5 min) with TNT and stored overnight at 4 °C in fresh TNT to remove background staining. On day five, slides were washed with autoclaved distilled water and mounted with Aqua-Mount® for imaging.

2.8 Probe Synthesis

Digoxygenin-labelled (DIG) antisense RNA probes were created by purifying template DNA plasmid from a QIAGEN HiSpeed® Midi Kit (catalog # 12643). Briefly, 10 µl of plasmid DNA was linearized using enzymatic digestion for 2 hours in a 37 °C water-bath using the appropriate restriction enzyme (see Table 2.1). The linearized DNA was purified using the GE Healthcare illustra™ GFX™ PCR DNA and Gel Band Purification Kit. The transcription reaction consisting

of 1 µl of purified linearized template DNA, 2 µl of DIG RNA labeling mix (Roche catalog # 11277073910), 2 µl of 10X transcription buffer, 0.5 µl RNaseOUT™ Recombinant Ribonuclease inhibitor (Invitrogen catalog # 10777-019), 2 µl of appropriate RNA polymerase (see Table 2.1), and autoclaved distilled water to a total of 20 µl were allowed to proceed in a 37 °C water-bath for 2 hours. For dinitrophenyl-labelled (DNP) antisense RNA probes, all steps were carried out similarly except 1 µl of each NTP and DNP-UTP were used to replace the 2 µl of DIG RNA labeling mix in the transcription reaction. Next, RNA probes were isolated and purified using the SigmaSpin™ Post-Reaction Clean-Up Columns (Sigma catalog # S5059-70EA) or standard Lithium Chloride precipitation protocol. Once purified, RNA probes were run on an RNAse-free gel to verify the size and subsequently stored at – 80 °C according to the procedure described by Poss et al., 2000.

Table 2.1 Antisense RNA probes for *in situ* hybridization experiments

Probe name	Label	Plasmid Vector	Restriction enzyme	RNA Polymerase
fli1a	DIG	pDrive[1]	*MluI*	Sp6
fli1b	DIG	pdonr221[1]	ApaI	T7
Fli1	DIG	pCR4-TOPO[2]	SpeI-HF	T7
Hoxa13	DIG	pCR-BluntII TOPO[3]	NotI-HF	Sp6
Hoxa13	DNP	pCR-BluntII TOPO[3]	NotI-HF	Sp6

[1] *375 pME-fli1a* (Addgene plasmid # 49001) and *pME-fli1b* (Addgene plasmid # 49019) were obtained from Nathan Lawson.

[2] *pCR4-TOPO Fli1* expressed sequence tag (EST) was obtained from Dharmacon™, product discontinued (catalog # EMM1002-213342120)

[3] *pCR-BluntII TOPO Hoxa13* complete coding sequence was obtained from Dharmacon™, product discontinued (catalog # MMM1013-211692838)

2.9 Plasmid Construction

All cloning and subcloning of *m-Inta11-βG:fli1a* were carried out according to the standard procedure described by Sambrook & Russell, 2001. The *375 pME-fli1a* plasmid, previously created by the Nathan Lawson Lab (Moore et al., 2013), was purchased from Addgene (Addgene plasmid # 49001; http://n2t.net/addgene:49001; RRID: Addgene_49001). The *fli1a* coding sequence was amplified using the FW *fli1a* AgeI primer (5'-ACCGGTATGGACGGAACTATTAAG GA-3') and Rev *fli1a* NotI primer (5'-GCGGCCGCTTAGTAGTAACTACC-3') and subsequently cloned into *pDrive* vector (QIAGEN). The *fli1a* coding sequence consisting of 1362 base-pairs (bp) was subcloned into the *m-Inta11-βG:eGFP* construct using AgeI and NotI restriction sites. The *m-Inta11: eGFP* plasmid was created by Rob L. Lalonde by modifying the original pEGFP-N1 vector (Kherdjemil et al., 2016). The cytomegalovirus (CMV) regulatory elements were taken out and replaced by *Tol2* transposon arms. The left arm was cloned between the AseI and NheI restriction sites, while the right arm was cloned at the AflII restriction site.

2.10 Microinjections

Microinjection solution was prepared immediately before use and consisted of 200 ng/µl of purified *m-Inta11-βG:fli1a* plasmid DNA, 4 µl of 2M KCl, 4 µl of 0.5% phenol red, and DEPC water to a total of 20 µl. Accordingly, 1 µl of microinjection solution containing 100 ng/µl of *m-Inta11:fli1a* plasmid was mixed with 1 µl of transposase RNA (50 ng/ml) and co-injected in transgenic (*m-Inta11:eGFP*) embryos at the one-cell stage. All microinjections were performed by Vishal Saxena using a Narishige IM300 microinjector and a Leica M27.5 microscope.

2.11 Whole Mount Proliferation Assay of Zebrafish Embryos

Proliferation assays were performed on whole-mount zebrafish embryos using Immunohistochemistry (IHC) with a polyclonal antibody that detects phosphorylation at the serine 10 site of Histone 3 and serves as a marker of mitosis. Briefly, embryos were fixed with a 9:1 ratio of formaldehyde (37%) to ethanol (95%) at 4 °C overnight, followed by washes (2 x 5 min) in PBS solution. On day one, embryos were incubated in pre-chilled 100% acetone for 20 minutes at -20 °C and washed (2 x 5 min) in PBS at room temperature. Next, embryos were immersed in a blocking solution (10% calf serum, 0.5% Triton™ X-100 in 1X PBS) for 1-3 hours. After blocking, embryos were incubated in a blocking solution containing 1:250 primary antibody (Anti-phospho-Histone H3 (Ser10) Rabbit Polyclonal Antibody Mitosis marker, Upstate, catalog # 06-570) for 3 hours at room temperature or overnight at 4 °C. On day two, embryos were washed (4 x 10 min) in PBST and immersed in PBST solution containing 1:500 secondary antibody (Alexa Fluor Goat anti-Rabbit IgG 594 Life technologies, catalog # A-11012) and kept in the dark for 3 hours at room temperature or overnight at 4 °C. Secondary antibody incubation was followed by PBST washes (4 x 10 min) in the dark and embryos were processed for imaging.

2.12 Whole Mount Cell Death Assay of Zebrafish Embryos

Embryos were fixed in PFA, washed in PBS, stored in methanol, and rehydrated as previously described in section 2.4. All procedures for cell death assay were carried out as described in the *In Situ* Cell Death Detection Kit, TMR red manual, version 11, April 2006 (catalog # 12 156 792 910). After rehydration, embryos were digested with 10 mg/ml Proteinase K in PBS solution for 5 minutes. Next, embryos were fixed in 4% PFA in PBS solution for 20 minutes and washed (5 x 5 min) in PBST. Embryos were then permeabilized by immersion in fresh 0.1% sodium citrate in PBST for 15 minutes at room temperature and washed (3 x 5 min) in PBST solution. A TUNEL

reaction mixture consisting of 45 µl of Label solution (vial 2) and 5 µl of Enzyme solution (vial 1) was prepared. A maximum of 10 embryos were incubated in TUNEL reaction mixture (50 µl) for 60 minutes at 37 °C in the dark, washed (3 x 5 min) in PBS solution, and prepared for imaging.

2.13 Quantitative Reverse Transcriptase Polymerase Chain Reaction

Ectopic *fli1a* and control larvae were anesthetized using tricaine (0.17mg/ml in E3 medium) and the pectoral fin was carefully dissected at 14 and 24 dpf using two needles (329424 - 1 mL BD™ U-100 insulin syringe with 28 G x 1/2). Pectoral fin dissections corresponding to 50-100 mg of tissue were transferred to TRIzol® reagent (Thermo Fisher) and RNA was isolated according to standard phenol-chloroform protocol. Next, 120 ng of template RNA was reverse transcribed into cDNA as described in the iScript™ cDNA Synthesis Kit manual (Bio-rad catalog # 1708890). Each qRT-PCR contained 5 µl of 2XPowerUp™ SYBR® Green Master Mix (Applies Biosystems catalog #A25741), 0.5 µl of forward and reverse primer (20 mM), 0.5 µl nuclease-free water, and 4 µl of cDNA. Primers were custom-designed from the Primer-BLAST tool provided by the National Center for Biotechnology Information (NCBI) website (see Table 2.2). Primer verification was carried according to MIQE guidelines (Bustin et al., 2009). qRT-PCR was allowed to proceed in the Eco™ Real-Time (Illumina Inc) machine for 2 minutes at 50 °C, 2 minutes at 95 °C, followed with 40 cycles of amplification; each consisting of 15 seconds at 95 °C and 1 minute at 60 °C. *β-actin* and *Efl1a* house-keeping genes were run in experimental duplicates and determined to be experimental stable between ectopic *fli1a* and control genotypes. Target genes were run in experimental triplicates and normalized to the expression of house-keeping genes. The Pfaffl method was used to generate fold expression values (Pfaffl, 2001). Data were illustrated using the GraphPad- Prism8 software.

Table 2.2 Custom-designed primers for reverse transcriptase polymerase chain reaction.

Primer Name	Primer Sequence (5' to 3')
β-actin Fw	GACACAGATCATGTTCGAGACC
β-actin Rev	CCATCACCAGAGTCCATCAC
Ef1a Fw	AAGCTCTTCCTGGGGACAAT
Ef1a Rev	ATGCTATGTGGGCTGTGTGA
hoxa13a Fw	CCCGACATGAGTCTTTACTGC
hoxa13a Rev	CTCCATGGGATACCTGACTCTGG
hoxa13b Fw	GGCAATCACTAACGGGTGGA
hoxa13b Rev	GACGTACTGAGGCTCCATCG
hoxd13 Fw	CCACCAACATTGGGACTGGT
hoxd13 Rev	AGGAACCCGCTTCTTTCTCC
eGFP Fw	ATGGTCAGCAAGGGCGAGGAG
eGFP Rev	TTACTTGTACAGCTCGTCCATGCCGA
fli1a Fw	GGCGAAACTGTCTCTGTCTC
fli1a Rev	CTGGCCGTAATCCTGAGTCC

2.14 Fin Fold Measurements

Median and pectoral fin dissections were generated and imaged using brightfield contrast as previously described in section 2.2. The sample size of median and pectoral fins (n=4) was generated from three separate breeding sessions (N=3) to account for differences between individual fish of the same transgenic line. The median fin fold was measured from the distal tip of the notochord (along the midline) to the outer-most fin tissue. The pectoral fin fold was

measured from the distal tip of the endoskeletal disc (ED), made visible by the marginal blood vessel (mbv), to the outer-most fin tissue. To account for human error, fin fold measurements were taken five times and averaged to correspond to a single value per fin tissue. All median and pectoral fin fold measurements were taken in pixels (px) using Photoshop CS6 software and subsequently converted to micrometers (μm).

2.15 Bone and Cartilage Staining

All bone and cartilage staining procedures were performed according to the protocol provided by Walker & Kimmel, 2007 with some modifications. Briefly, adult fish were anesthetized with 0.17 mg/ml tricaine and fixed with 4% PFA in PBS solution overnight at 4 °C. After fixation, fish were washed (2 x 5 min) in PBS and pectoral fin tissue was dissected. Next, pectoral fin tissue was dehydrated with a solution containing 50% ethanol for 10 minutes and stained in acid-free double stain solution overnight at room temperature with gentle shaking. The staining solution was prepared by mixing 1 part of Alizarin red (0.5% Alizarin Red S monosodium salt) with 1000 parts of Alcian Blue (0.02% Alcian Blue 8GX, 60 mM $MgCl_2$, 70% ethanol). After staining, pectoral fin tissue was washed (1 x 2 min) with water and incubated in bleaching solution (1.5% H_2O_2, 1% KOH) at room temperature for 20 minutes. Tissue clearing was then allowed to proceed overnight at room temperature in 20% glycerol and 0.25% KOH, followed by immersion in 50% glycerol and 0.25% KOH overnight at room temperature. Pectoral fin tissue was stored in a solution containing 50% glycerol and 0.1% KOH overnight at 4 °C and processed for imaging accordingly.

CHAPTER 3 RESULTS

3.1 The *m-Inta11* positive cells in the pectoral fin do not originate from the marginal blood vessel

The *m-Inta11* enhancer, previously described in section 1.4.2 and 1.4.3, is active in migrating cells of the median and pectoral fins during zebrafish development. The *m-Inta11* positive cells in the pectoral fin may emanate from the marginal blood vessel, the chondrocytes of the endoskeletal disc, or elsewhere in the fin. It was initially postulated that the *m-Inta11* positive cells in the pectoral fin may emerge from blood vessels given the proximity of the migrating cells to the marginal blood vessel (Figure 1.5B). To determine the source of migrating *m-Inta11* positive cells in the pectoral fin, the reporter activity of double transgenic *Tg*(*fli1a:eGFP*; *m-Inta11:mCherry*) live embryos was examined. If *m-Inta11* positive cells in the pectoral fin did indeed arise from the marginal blood, we would expect to observe an overlap between *fli1a* and *m-Inta11* reporter activity.

The development of the marginal blood vessel in the pectoral fin has been described in section 1.2 and 1.4.4. Briefly, two vessels invade the pectoral fin distally from the anterior and posterior direction, ultimately fusing in the posterior fin region to form the marginal blood vessel(T. Yano et al., 2012) (Figure 3.1 A). All blood vessels express *fli1a* during zebrafish development (Lawson & Weinstein, 2002). In addition, *fli1a* is expressed in a few cells of the endoskeletal disc. Starting at 50.5 hpf, *m-Inta11:mCherry* reporter activity is initially observed within the distal tip of the pectoral fin (Figure 3.1 B-D; yellow arrowheads). At the same time, *fli1a* reporter activity is concentrated in the anterior region of the presumptive endoskeletal disc (Figure 3.1B-C). Using confocal microscopy, 3D rendering of the pectoral fin tissue after a rotation at a 45° angle towards

the objective lens, reveals that the first *m-Inta11* positive cell is overlaying a population of *fli1a*-expressing cells in the anterior region of the developing fin (Figure 3.1B-C, white box). Moreover, single-cell resolution analysis of the front-and side-view planes demonstrates that while the first *m-Inta11* positive cell is overlaying *fli1a*-expressing cells (Figure 3.1 E-G), *m-Inta11* activity and *fli1a* expression are not overlapping or co-localized in the same cell (Figure 3.1 E'-G'). These images show that newly formed *m-Inta11* activity is complementary to *fli1a*-expressing cells in the distal anterior region of the fin, as evidenced by the lack of overlap between *m-Inta11* and *fli1a* reporter activity in the side-view (i.e. sagittal) plane (Figure 3.1 E'-G'). At the same time, the ends of anterior and posterior marginal blood vessels are restricted to the proximal portion of the pectoral anlage. The distal position where *m-Inta11* activity is first established relative to the proximally invading blood vessels indicates that the *m-Inta11* positive cells cannot originate from the marginal blood vessel (Figure 3.1 B-C).

Double Tg (*fli1a:eGFP; m-Inta11:mCherry*)

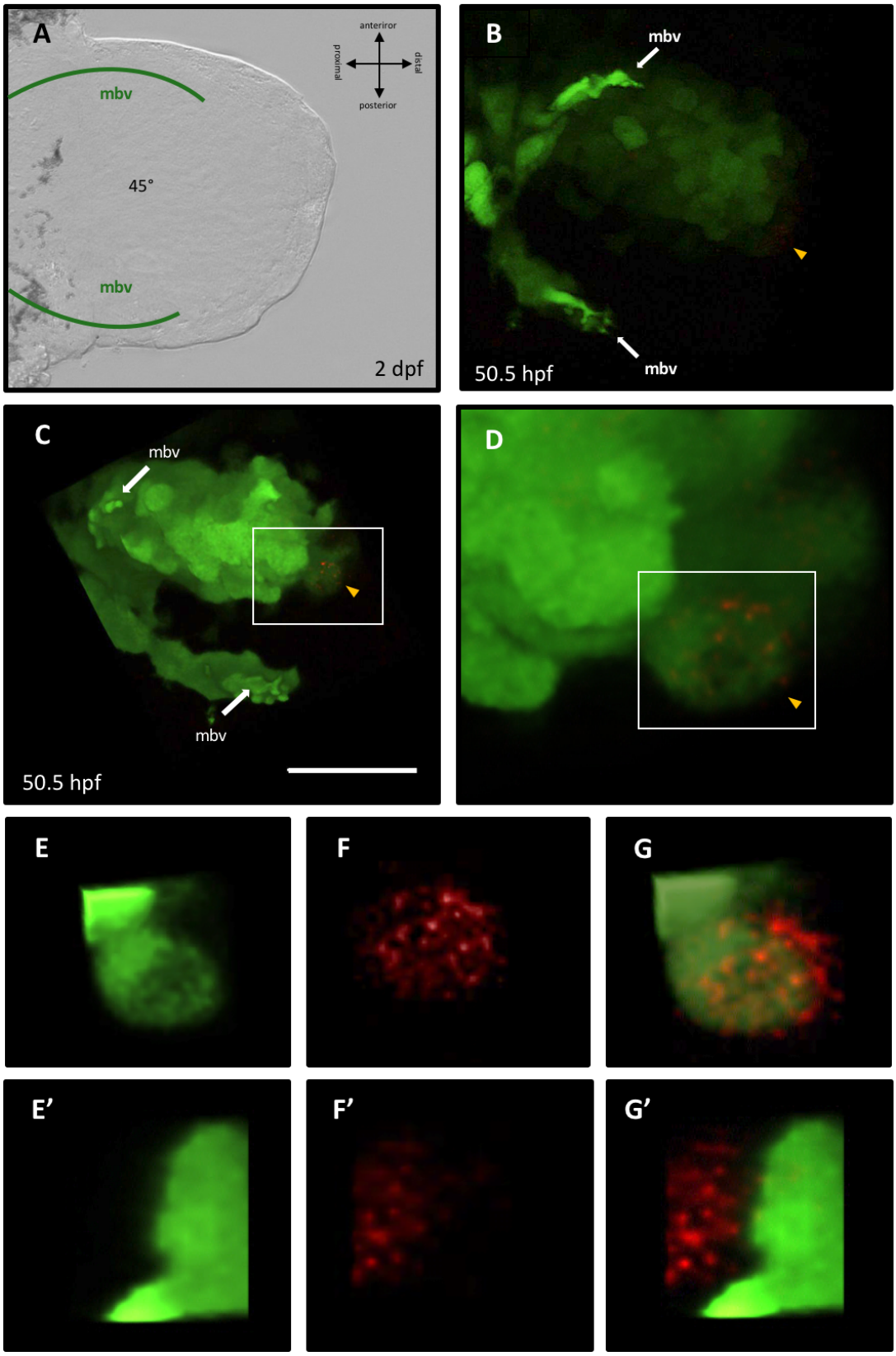

Figure 3.1: The *m-Inta11* positive cells in the pectoral fin do not originate from the marginal blood vessel and are complementary with the *fli1a* domain of expression. (A) Brightfield image of the pectoral fin at 2 dpf, showing the schematic position of the anterior and posterior invading blood vessels that later form the marginal blood vessel (B) Confocal imaging of the pectoral fin of double transgenic *Tg*(*fli1a:eGFP; m-Inta11:mCherry)* embryos at 50.5 hpf, showing the ends of the developing anterior and posterior marginal blood vessels (white arrows). Note, *m-Inta11:mCherry* reporter activity is first established at the anterior distal tip of the fin; yellow arrowheads (B-D). (C) 3D rendering of the pectoral fin in panel B after a rotation at an angle of 45° in the direction of the objective lens, showing the position of the marginal blood vessel relative to the beginning of *m-Inta11* reporter activity. (D) Higher magnification of panel C. (E-G) Higher magnification of panel D, showing single-cell resolution. (E'-G') Side-view (i.e. sagittal) plane of panels E, F, and G, showing a complementary pattern between *m-Inta11* and *fli1a* reporter activity. n = 6. n = sample size. mbv = marginal blood vessel. Scale bar of B, C = 100 μm.

3.2 The *m-Inta11* positive cells are complementary to the *fli1a* domain in the pectoral fin during embryonic development

Imaging of the double transgenic *Tg*(*fli1a:eGFP; m-Inta11:mCherry*) embryos at 50.5 hpf has demonstrated that *m-Inta11* positive cells in the pectoral fin could not originate from the marginal blood vessel. In addition, preliminary data have indicated the complementary pattern between *fli1a* and *m-Inta11* enhancer domains during pectoral fin development (Figure 1.8). A more rigorous time-course analysis of double transgenic *Tg*(*fli1a:eGFP; m-Inta11:mCherry*) embryos was undertaken using confocal microscopy and has shown that the complementary pattern (described in section 1.4.5) is maintained during embryonic pectoral fin development (Figure 3.2). Starting at 53 hpf, *m-Inta11:mCherry* reporter activity can be observed in the anterior and medial pectoral fin region (Figure 3.2A; white bracket). Between 54 and 58 hpf, the population of *m-Inta11* positive cells progressively increase in the posterior direction and follow the extension of the anterior marginal blood vessel (Figure 3.2BC; yellow arrowhead). By 58 hpf, the anterior marginal blood vessel continues to invade the pectoral fin around *fli1a*-expressing cells and grow towards the posterior marginal blood vessel (Figure 3.2F; yellow arrowhead). In contrast, the posterior portion of the marginal blood vessel does not interact with *m-Inta11* positive cells and grows at a slower rate than the anterior portion of the marginal blood vessel. We further observe that *fli1a* reporter activity is absent in the distal posterior part of the presumptive endoskeletal disc region during the progression of *m-Inta11* positive cells (Figure 3.2 A-F).

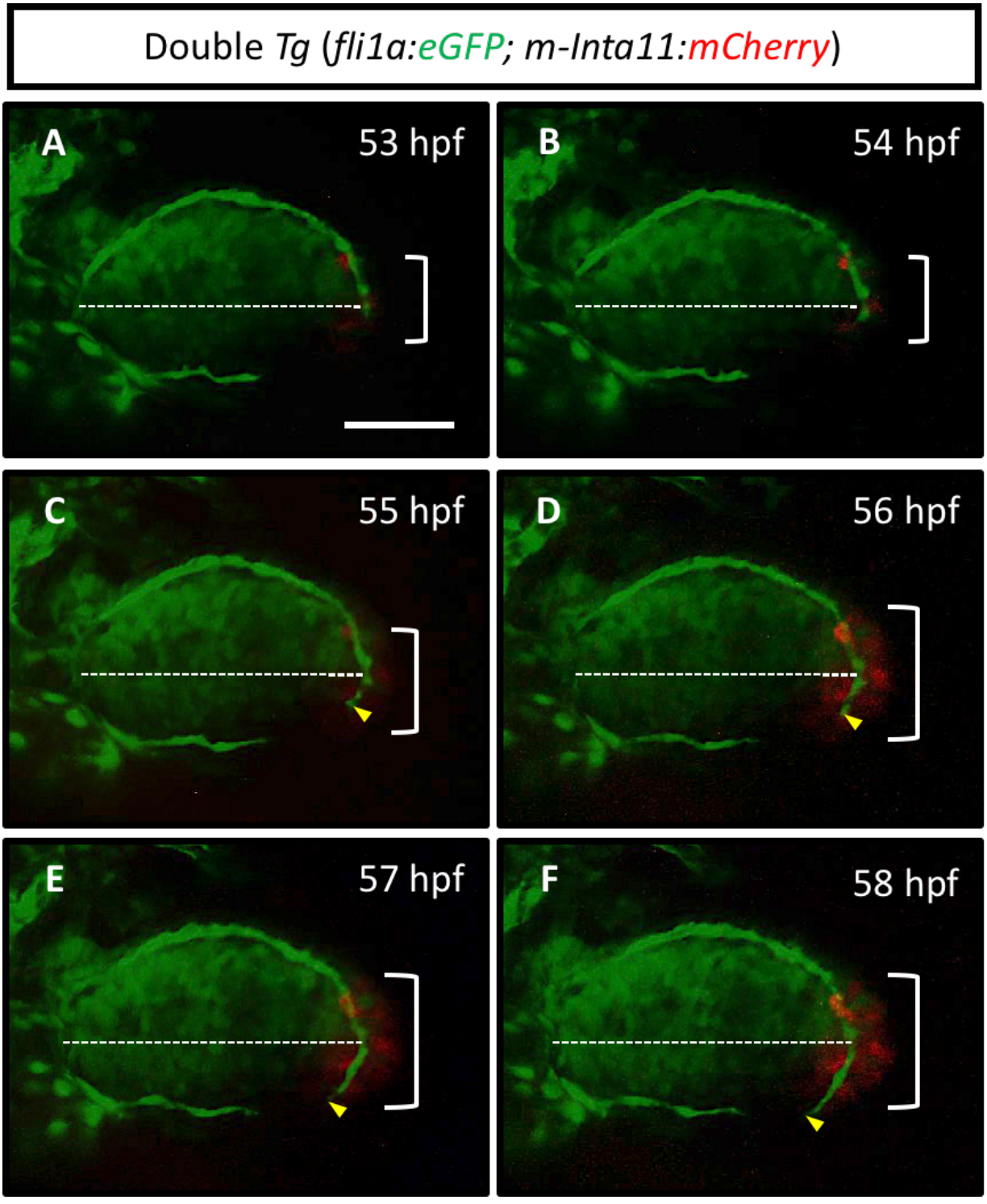
Double Tg (fli1a:eGFP; m-Inta11:mCherry)
A
53 hpf
B
54 hpf
C
55 hpf
D
56 hpf
E
57 hpf
F
58 hpf

Figure 3.2: The *m-Inta11* positive cells are complementary to the *fli1a* domain in the pectoral fin during embryonic development. (A-F) Time-course analysis of double transgenic *Tg*(*fli1a:eGFP*; *m-Inta11:mCherry*) pectoral fin tissue captured by confocal microscopy between 53 hpf and 58 hpf, showing the progression of *m-Inta11* positive cells in the posterior direction of the fin region (white bracket). Note, the anterior marginal blood vessel can be seen extending around *fli1a*-expressing cells and towards the posterior marginal blood vessel (yellow arrowheads). n = 4. The dashed line represents the midline of the pectoral fin. Scale bar of A-F = 50 μm.

3.3 The pectoral fin *m-Inta11* positive cells originate from chondrocytes of the endoskeletal disc

Next, double transgenic *Tg*(*KR19; m-Inta11:eGFP*) embryos were examined to determine if chondrocytes of the endoskeletal disc could give rise to *m-Inta11* positive cells. In the *KR19* transgenic enhancer trap line, chondrocytes of the pectoral fin ED among other regions (ie. choroid plexus, jaw, hindbrain) can be labeled with the fluorescent reporter *KillerRed* membrane-tethered expression (Teh et al., 2010). The *KR19* transgene is integrated at a site 32, 151 bp downstream of *foxp3b* and at a second integration site that is unknown (Teh et al., 2010). Time-course analysis of double transgenic *Tg*(*KR19; m-Inta11:eGFP)* embryos using Z-stacking images of confocal microscopy and 3D rendering shows that *m-Inta11* positive cells in the pectoral fin arise from chondrocytes of the endoskeletal disc (Figure 3.3). The acquisition of a single image from a Z-stack at 49.5 hpf demonstrates that *m-Inta11* activity and *KR19* expression are found within the same cell (Figure 3.3 A-D). More specifically, *m-Inta11* reporter activity is localized to the cytoplasm while *KR19* expression is bound to the plasma membrane (Figure 3.3 B, C). At that time, *m-Inta11* positive cells have the characteristic shape of chondrocytes (Figure 3.3 C). To ensure that eGFP and KR19 proteins are located within a single cell layer, the optical depth of a single image from a Z-stack was narrowed to 0.95 μm, which is less than the width of a cell in Figure 3.3. By 52 hpf, the *m-Inta11* positive cells lose their regular shape that is common to chondrocytes, change their cell morphology, and begin to migrate towards the fin fold as evidenced by the presence of filopodia-like protrusions (Figure 3.3 E-H). At the same time, the killer red expression of *KR19* is weakened at the leading edge of the endoskeletal disc while *m-Inta11* reporter activity becomes stronger (Figure 3.3 H). Thus, we can confirm that *m-Inta11* positive

cells of the pectoral emerge from chondrocytes of the endoskeletal disc during embryonic development.

Double *Tg* (*KR19; m-Inta11:eGFP*)

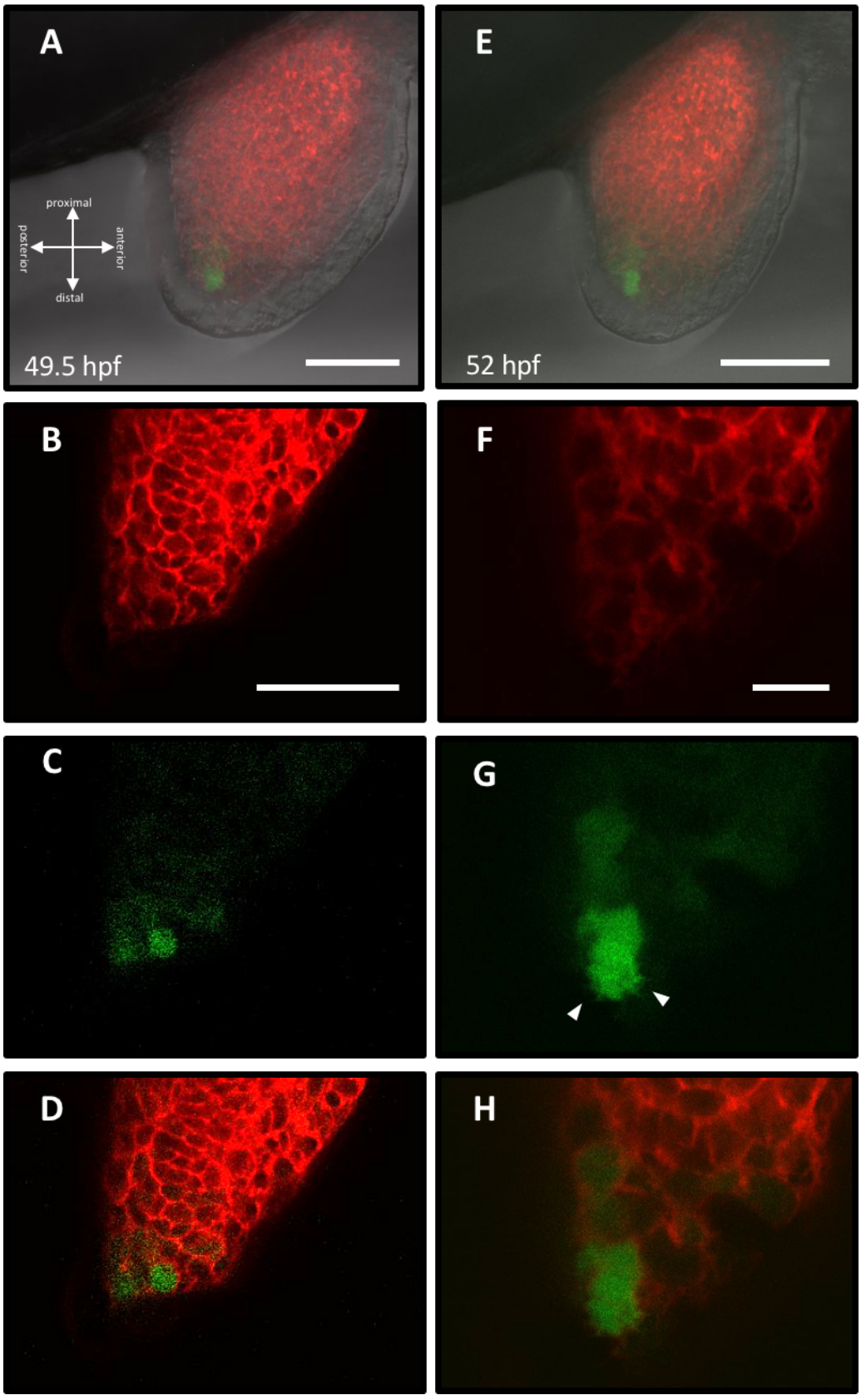

Figure 3.3: The *m-Inta11* positive cells in the pectoral fin arise from chondrocytes of the endoskeletal disc during embryonic development. (A-H) Time-course analysis of double transgenic (*KR19; m-Inta11:eGFP*) pectoral fin development between 49.5 hpf and 52 hpf. (A) The pectoral fin of double transgenic (*KR19* x *m-Inta11:eGFP*) embryos at 49.5 hpf (B-D) single Z-stack from the acquired image in panel A, showing *m-Inta11* eGFP reporter activity and *KR19* expression around found within the same cell. Note, eGFP and KR19 are localized to the cytoplasm and plasma membrane, respectively. (E) The pectoral fin of double transgenic (*KR19 x m-Inta11:eGFP*) embryos at 52 hpf. (F-H) single Z-stack from the acquired image in panel E, showing *m-Inta11* positive cells lose their regular shape, change their cell morphology, and begin to migrate towards the fin fold. Note, filopodia-like protrusions are visible in panel G (arrowheads). n = 8. Scale bar of A, E = 100 μm, B-D = 25 μm, F-H = 10 μm.

3.4 *fli1b* is expressed in the endoskeletal disc of the pectoral fin

Previous data indicate the *fli1a* and *fli1b* have comparable domains of expression in the vasculature during somitogenesis and embryonic development (see section 1.2 and 1.4.4) (Craig et al., 2015). However, little is known about the similarity between the expression domains of *fli1a* and *fli1b* elsewhere in the embryo. The expression of *fli1a* in chondrocytes of the endoskeletal disc prompted to examine whether its paralog *fli1b* has a similar expression pattern during pectoral fin development. Gene expression analysis using whole-mount *in situ* hybridization demonstrates that *fli1b* is active in chondrocytes of the endoskeletal disc at 2 and 3 dpf (Figure 3.4 A-B). In addition, *fli1b* can be observed in the blood vessels of the head and trunk. However, it is unclear if *fli1b* is expressed in the distal posterior region of the endoskeletal disc or the marginal blood vessel due to microscope limitations at the time of imaging.

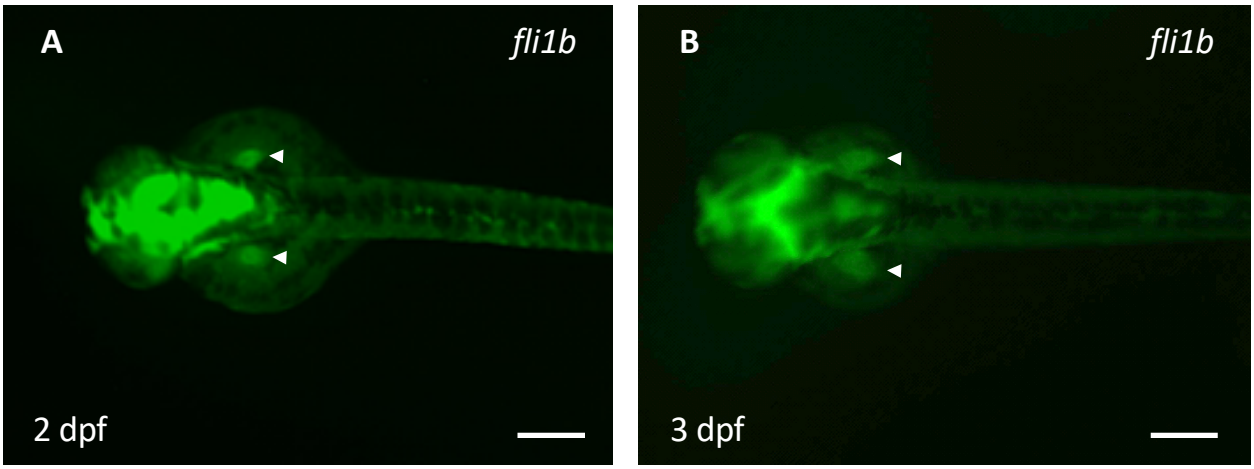

Figure 3.4: *fli1b* is expressed in the pectoral endoskeletal disc. Whole-mount *in situ* hybridization of 2 dpf embryo (A) and 3 dpf larvae (B), showing *fli1b* expression in the chondrocytes of the endoskeletal disc (white arrowheads). Note, *fli1b* expression is present in blood vessels of the head and trunk. n = 12. Scale bar of A, B = 200 µm.

3.5 Contributions of *m-Inta11* positive and *fli1a*-expressing cells during pectoral fin development.

Previous imaging analysis of double transgenic *Tg*(*fli1a:eGFP; m-Inta11:mCherry*) embryos at 3 dpf suggested that the initiation of *m-Inta11* enhancer activity in migrating pectoral fin cells correlates with the absence of *fli1a* reporter expression in the distal posterior chondrocytes of the endoskeletal disc (Figure 1.8). In addition, the *m-Inta11* and *fli1a* enhancer activities appear to be complementary, as evidenced by the lack of overlap between *mCherry* and *eGFP* reporter expression in the front-view plane. Accordingly, we wondered if *m-Inta11* and *fli1a* enhancer activity domains may be complementary during later stages of pectoral fin development. At the same time, we wished to determine the contributions of *m-Inta11* positive and fli1a-expressing cells to adult structures in the pectoral fin.

3.5.1 The *m-Inta11* and *fli1a* enhancer domains are confirmed to be complementary during early larval development

First, we had to investigate whether *m-Inta11* and *fli1a* enhancer domains of activity are complementary across all geometric planes at 3 dpf. Accordingly, we proceeded to examine double transgenic *Tg*(*fli1a:eGFP; m-Inta11:mCherry*) pectoral fin tissue using confocal imaging (Figure 3.5 A). Z-stacking and 3D rendering analysis confirms that *m-Inta11* and *fli1a* enhancer domains are in fact complementary, as evinced by the lack of overlap between *mCherry* and *eGFP* expression in the side-view (i.e. sagittal) plane (Figure 3.5 B). Furthermore, time-course analysis of double transgenic *Tg*(*fli1a:eGFP; m-Inta11:mCherry*) larvae demonstrates the *m-Inta11*

positive cells continue to migrate towards the pectoral fin fold from the distal posterior region of the endoskeletal disc where there is no *fli1a* reporter activity (data not shown).

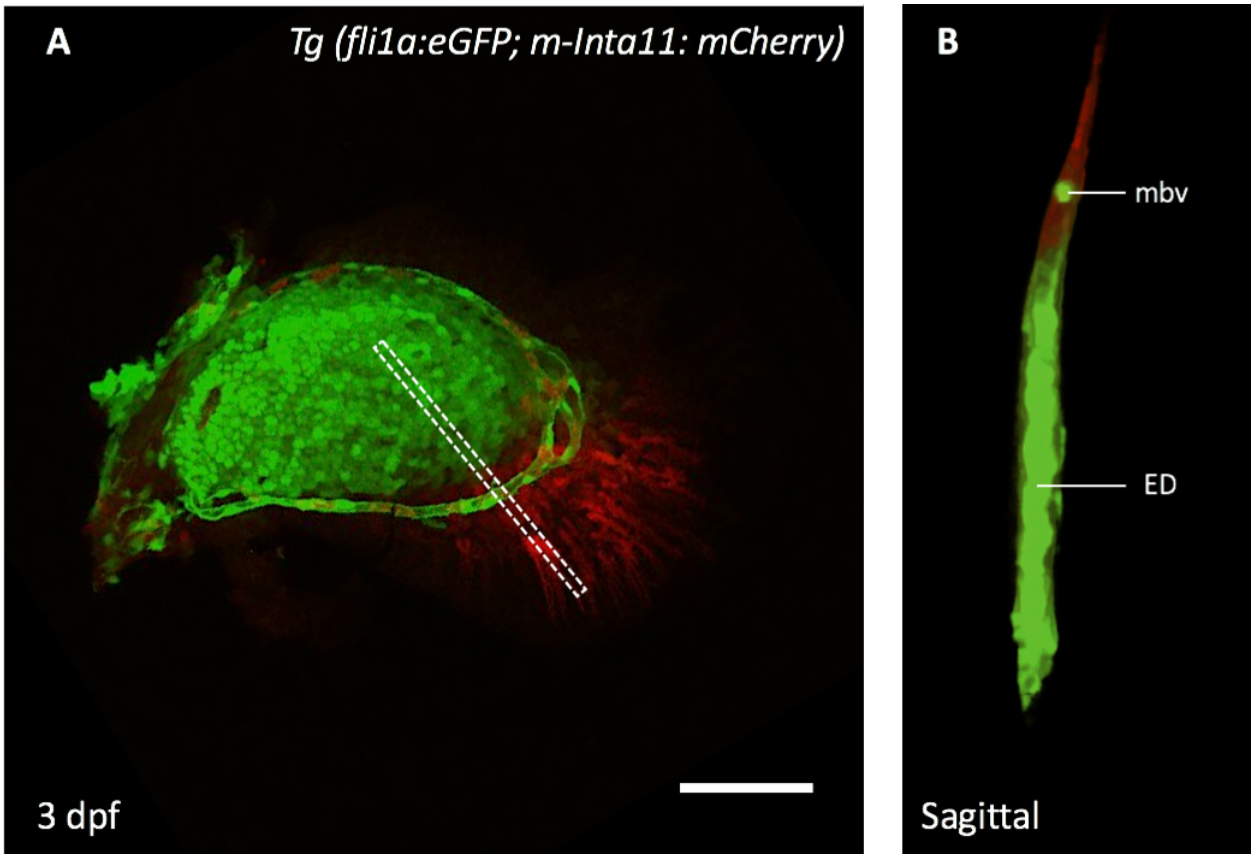

Figure 3.5: The *m-Inta11* and *fli1a* enhancer domains are complementary during early larval development. Confocal imaging of a double transgenic (*fli1a:eGFP; m-Inta11:mCherry*) pectoral fin at 3 dpf, showing a lack of overlap between *eGFP* and *mCherry* reporter expression. (A) Dorsal view (B) Sagittal view of the dashed line in panel A. n = 6. mbv = marginal blood vessel, ED = endoskeletal disc. Scale bar of A=100 μm.

3.5.2 Brighter *fli1a*-expressing cells in the anterior endoskeletal disc give rise to distal radials and are complementary to *m-Inta11* activity during larval development.

While *m-Inta11* positive cells are migrating towards the pectoral fin fold, some *fli1a*-expressing cells in the endoskeletal disc are being reorganized. In fact, time-course analysis of double transgenic *Tg*(*fli1a:eGFP; KR19)* larvae identified a brighter population of *fli1a*-expressing cells in the anterior region of the endoskeletal disc that gives rise to distal radials during pectoral fin development (Figures 3.4-3.6). The brighter *fli1a*-expressing cells can be visualized as early as 12 dpf (data not shown). This group of *fli1a*-expressing cells extends in the distal direction and displays brighter eGFP reporter activity compared to the rest of the endoskeletal disc, postcoracoid process, or scapulocoracoid (Figure 3.6). The postcoracoid process and scapulocoracoid are visible at 14 dpf underneath and proximal to the endoskeletal disc, respectively (Figure 3.6 B; pop and sco). At this stage, we also report an elaborated network of blood vessels, particularly around the distal edge of the endoskeletal disc (Figure 3.6 B; white arrowhead, 3.7 B). Importantly, the brighter *fli1a* reporter activity in the endoskeletal disc does not seem to be associated with blood vessel reorganization in Figure 3.6. By 15 dpf, *m-Inta11* positive cells have extended to the anterior region of the fin such that *m-Inta11* enhancer activity is uniform across the pectoral fin fold (Figure 3.7). A small population of *m-Inta11* positive cells can be seen overlaying chondrocytes at the distal edge of the endoskeletal disc (Figure 3.7 D; white arrowhead). Meanwhile, the brighter *fli1a*-expressing cell population continues to be visible in the anterior endoskeletal disc region (Figure 3.7B). By 19 dpf, the brighter *fli1a*-expressing cells transform to define the rudiments of the first and second most anterior distal radials in the anterior pectoral fin region (Figure 3.8 B; white arrows). At the same time, brighter *fli1a* reporter activity can be seen extending in the proximal

direction (Figure 3.8 B). Despite the transformation of brighter *fli1a*-expressing cells in the anterior endoskeletal fin region, *fli1a* reporter *eGFP* expression remains absent in the distal posterior region of the endoskeletal disc (Figure 3.8 B). In addition, the postcoracoid process has elongated in the distal direction (Figure 3.8B; pink arrow). Meanwhile, actinotrichia fibrils adjacent to the newly formed distal radials appear to have reorganized and condensed to lay the groundwork for the formation of lepidotrichia (Figure 3.8 A; yellow arrowhead). In addition to the formation of actinotrichia, extensive invasion and growth of the marginal blood vessel network can be observed outside of the endoskeletal disc, particularly in the posterior fin region (Figure 3.8 B; white arrowhead). By 20 dpf, we discover that the *m-Inta11* enhancer shows different domains and activity of reporter expression in the anterior and posterior fin regions (Figure 3.9 A-L). In the anterior fin region, the activity of *m-Inta11* is reduced and adjacent to strong *fli1a* reporter expression (Figure 3.9 E-H). In addition, the *m-Inta11* activity appears to be organized along the plane of newly formed distal radials, as determined by the absence of *m-Inta11:mCherry* reporter expression in the interray tissue (Figure 3.9 E-H). In the posterior fin region, *m-Inta11: mCherry* reporter expression is uniform and localized to the fin fold (Figure 3.9 I-L).

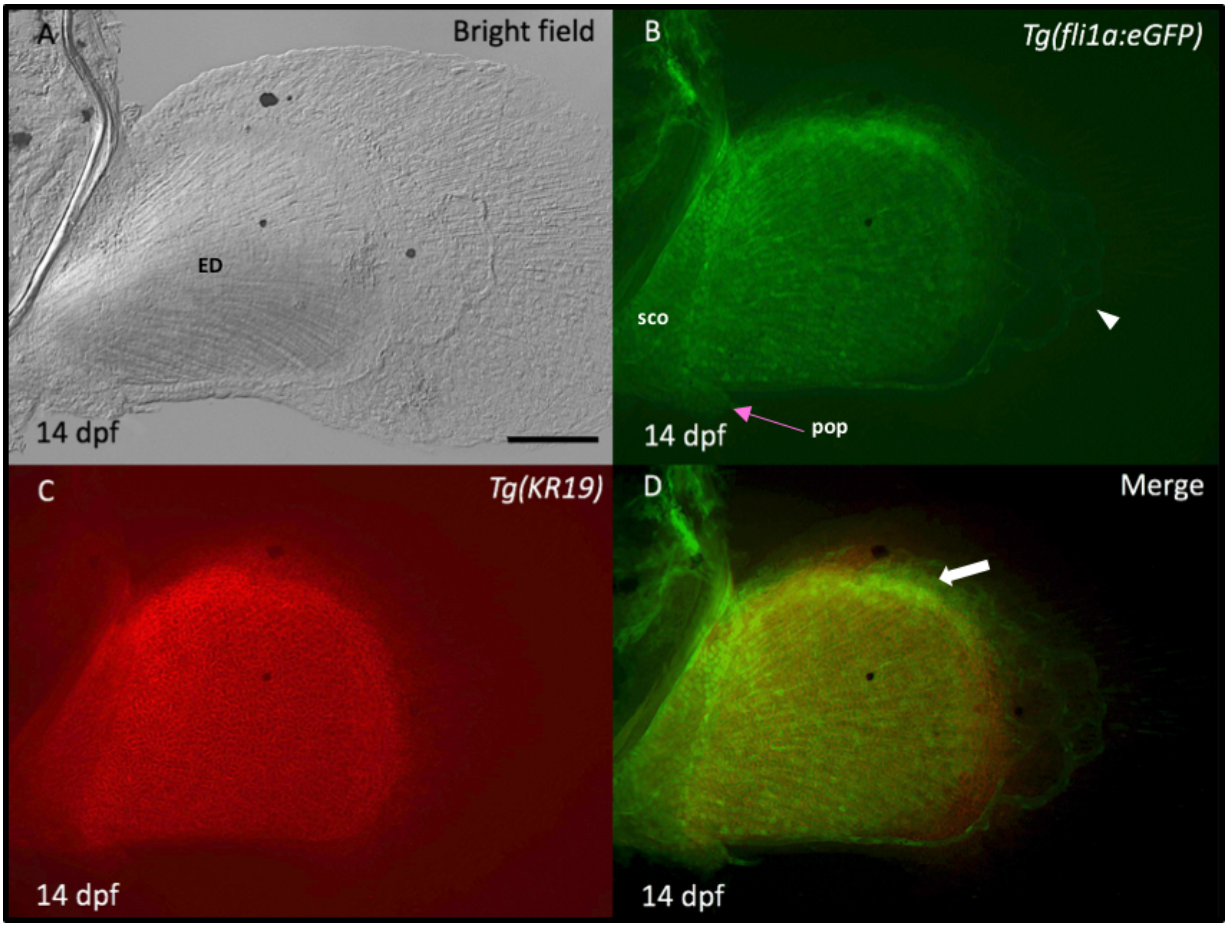

Figure 3.6: The distal radials arise from a population of brighter *fli1a*-expressing cells in the anterior endoskeletal disc during pectoral fin development. (A-D) The pectoral fin of double transgenic (*fli1a:eGFP; KR19*) larva at 14 dpf. (A) Brightfield (B) *fli1a* enhancer drives reporter *eGFP* expression in blood vessels and the endoskeletal disc of the pectoral fin, including the postcoracoid process (pink arrow) and scapulocoracoid. The marginal blood vessel has transformed into an elaborate network of blood vessels (white arrowhead). Note, there is no *eGFP* expression in the distal posterior portion of the endoskeletal disc. (C) KR19 label chondrocytes of the endoskeletal disc with a membrane-bound red fluorescent molecule. (D) Merged image of panel B and C, showing brighter *fli1a*-expressing cells in the anterior endoskeletal disc of the pectoral fin (white arrow). n = 10. ED = endoskeletal disc. pop = postcoracoid process. sco = scapulocoracoid. Standard length = 5.42 mm. Scale bar of A-D = 100 μm.

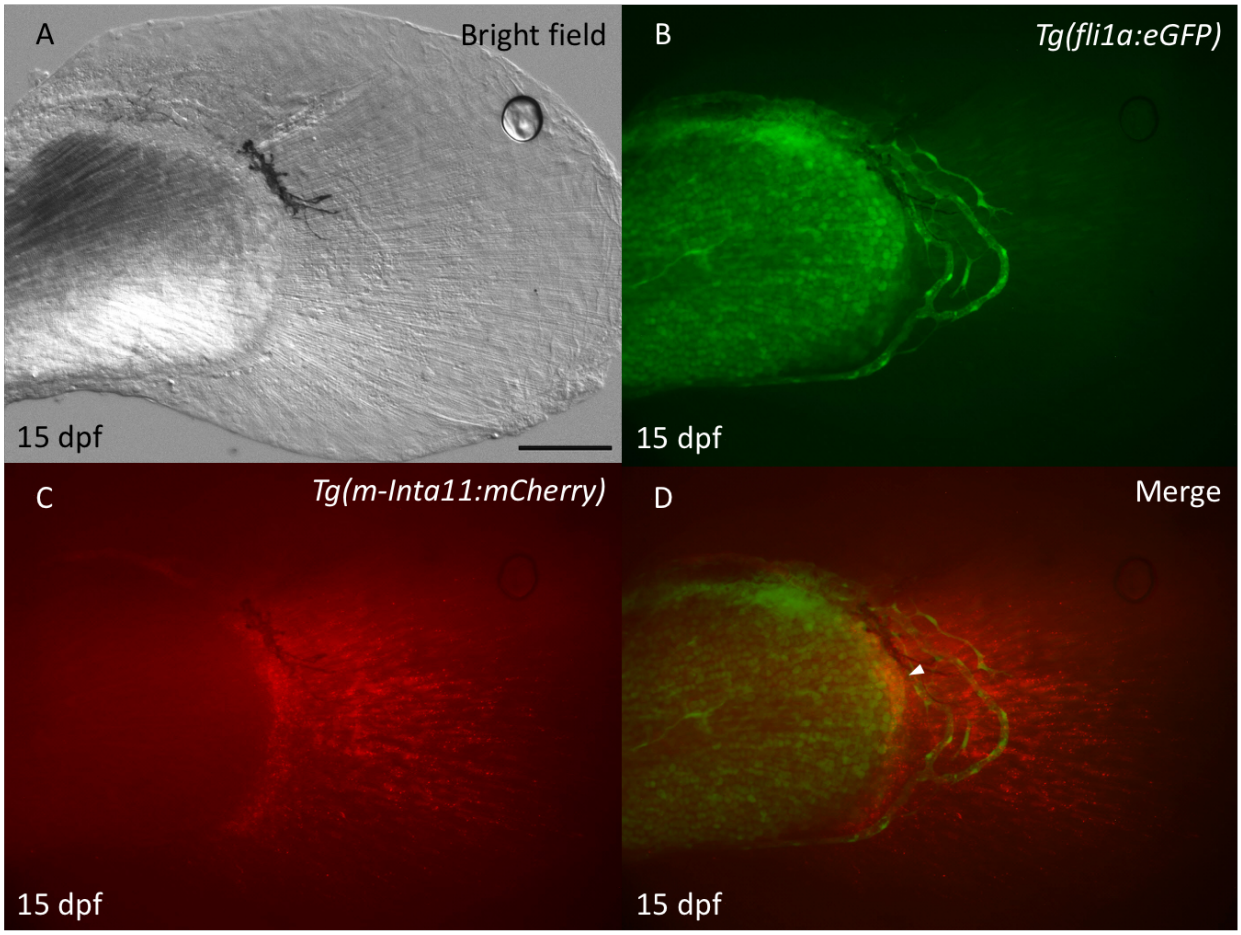

Figure 3.7: The activity of the *m-Inta11* enhancer is uniform in the pectoral fin fold during larval development. The pectoral fin of a double transgenic (*fli1a:eGFP; m-Inta11: mCherry*) larva at 15 dpf. (A) Brightfield image, showing endoskeletal disc and pectoral fin fold. (B) *fli1a* reporter eGFP activity is increased in the anterior endoskeletal disc regions. The brighter *fli1a*-expressing cell population can be observed in the anterior endoskeletal disc (C) *m-Inta11* reporter mCherry activity is uniform in the fin fold (D) Merge image of panel B and C, showing a complementary pattern between *m-Inta11* and *fli1a* enhancer domains. Note, a population of *m-Inta11* positive cells is overlaying *fli1a*-expressing cells at the edge of the endoskeletal disc (white arrowhead). n = 10. Standard length = 5.5 mm. Scale 100 µm.

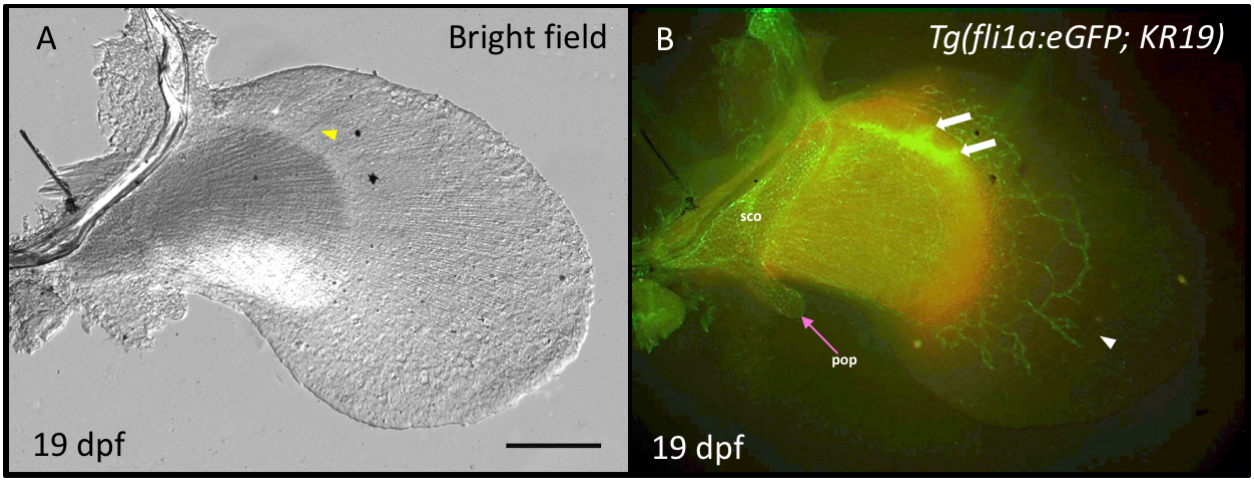

Figure 3.8: The brighter *fli1a*-expressing cell population transforms to define the rudiments of the two most anterior distal radials during pectoral fin development. The pectoral fin of double transgenic (*fli1a:eGFP; KR19*) larva at 19 dpf. (A) Brightfield image, showing the condensation of actinotrichia in the anterior pectoral fin region (yellow arrowhead). (B) Merged image of *fli1a:eGFP* and *KR19* activity, showing the formation of the two most anterior distal radials (white arrows). Note, the postcoracoid process has elongated in the distal direction (pink arrow). There is no *eGFP* expression in the distal posterior region of the endoskeletal disc. White arrowhead in panel B shows extensive growth of the marginal blood vessel network in the posterior pectoral fin region. n = 10. pop = postcoracoid process. sco = scapulocoracoid. Standard length = 6.7 mm. Scale bar of A-B = 100 μm.

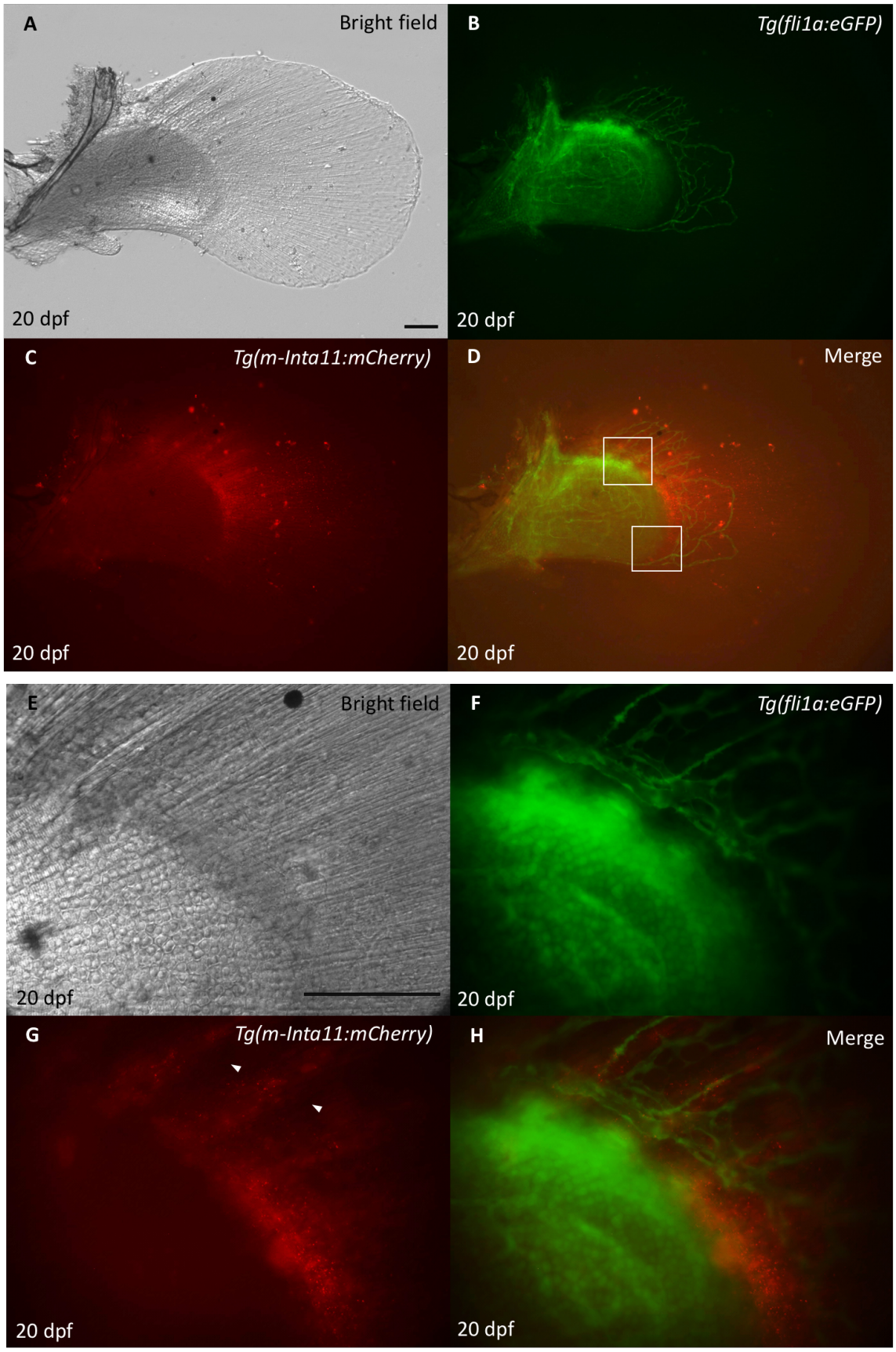
A
Bright field
20 dpf
B
Tg(fli1a:eGFP)
20 dpf
C
Tg(m-Inta11:mCherry)
20 dpf
D
Merge
20 dpf
E
Bright field
20 dpf
F
Tg(fli1a:eGFP)
20 dpf
G
Tg(m-Inta11:mCherry)
20 dpf
H
Merge
20 dpf

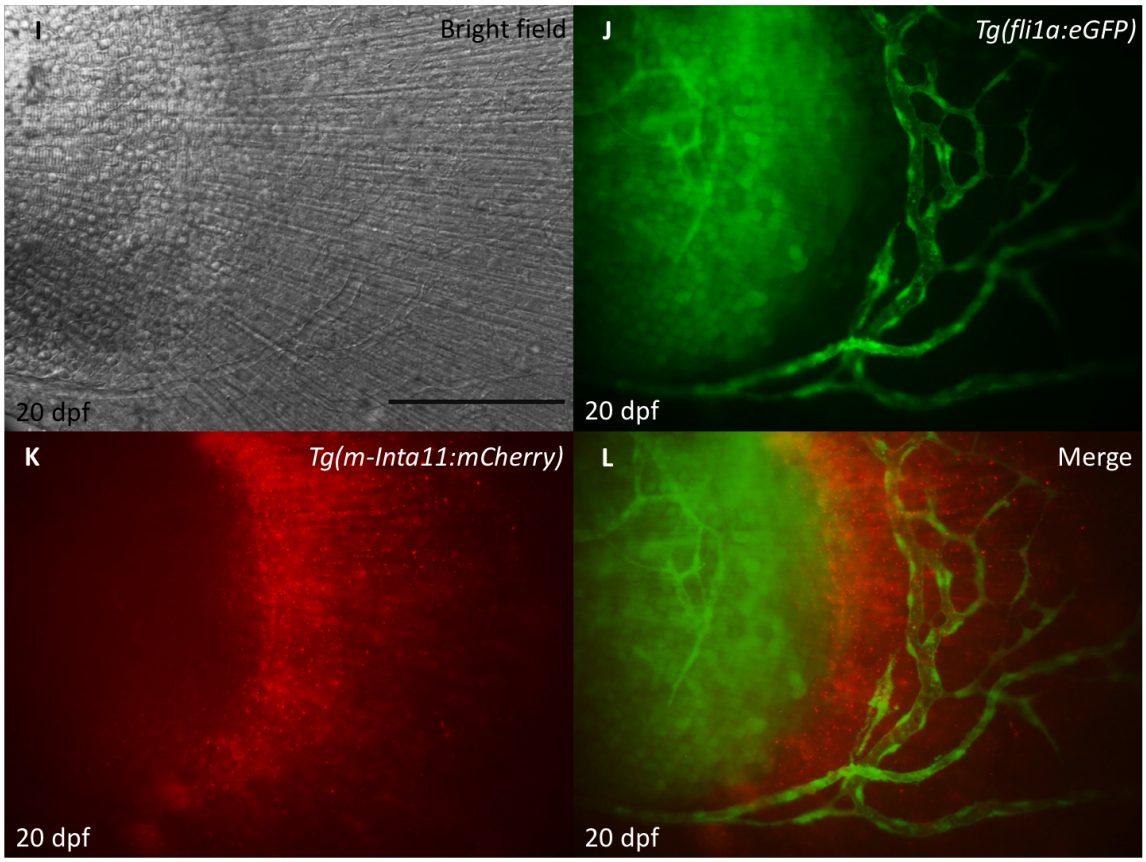
I
Bright field
20 dpf
J
Tg(fli1a:eGFP)
20 dpf
K
Tg(m-Inta11:mCherry)
20 dpf
L
Merge
20 dpf

Figure 3.9: The *m-Inta11* enhancer shows different domains and activity of reporter expression in the anterior and posterior fin region during larval development. The pectoral fin of a double transgenic *(fli1a:eGFP; m-Inta11: mCherry*) larva at 20 dpf. (A) Brightfield image. (B) *fli1a* reporter activity is increased in newly formed distal radials compared to the rest of the endoskeletal disc. (C) *m-Inta11* reporter activity is differentially organized in the anterior and posterior fin regions. (D) Merge image of panel B and C, showing anterior and posterior fin regions (white boxes). (E-H) Higher magnification of the anterior fin region in panel D, showing decreased *m-Inta11* activity that is confined along the plane of newly formed distal radials and associated with strong *fli1a* reporter *eGFP* expression. Note, *m-Inta11* reporter expression is absent in the anterior interray tissue (arrowheads). *m-Inta11* activity proceeds in an anterior-posterior direction. (I-L) Higher magnification of posterior fin region in panel D, showing increased *m-Inta11* activity that is uniform and localized to the fin fold. Notice, the domains of *m-Inta11* and *fli1a* enhancer activity are complementary during larval development. There is little to no overlap of the *m-Inta11* and *fli1a* enhancer domains of activity as shown by their respective *mCherry* and *eGFP* reporter expression. n = 10. Standard length = 7.7 mm. Scale bar of A-L = 100 µm.

3.5.3 Blood vessel remodeling correlates with distal radial and fin ray formation during pectoral fin development

In addition to showing that a subpopulation of *fli1a*-expressing cells contributes to the formation of distal radials, time-course analysis of double transgenic (*fli1a:eGFP; KR19*) larvae has provided insights into the remodeling of pectoral fin blood vessels. Recall, the marginal blood vessel can be observed undergoing arborization and extensive growth by 19 dpf. At 24 dpf, we show that blood vessel remodeling in the pectoral fin correlates with the formation of the distal radials and fin rays (Figure 3.10 A-B). In the posterior fin region where neither distal radials nor fin rays have formed, the blood vessel network is disorganized (Figure 3.10 B; white bracket). In the anterior fin region, blood vessels are remodeled where distal radials and fin rays have formed. The earliest indication of vascular remodeling can be observed along the axis of the most anterior distal radial, which displays strong *fli1a* reporter activity. Once the first distal radial has formed, *fli1a* reporter *eGFP* expression diminishes (Figure 3.10 B; most anterior white arrowhead). Accordingly, blood vessels that support fin rays are remodeled in an anterior to posterior direction, concomitant with the formation of distal radials and fin rays. In addition, blood vessel invasion of the endoskeletal disc can be observed along with the regression of the postcoracoid process (Figure 3.10 B; pink arrow). It is also worth noting that the *fli1a* reporter activity continues to be absent in the distal posterior region of the endoskeletal disc during larval development.

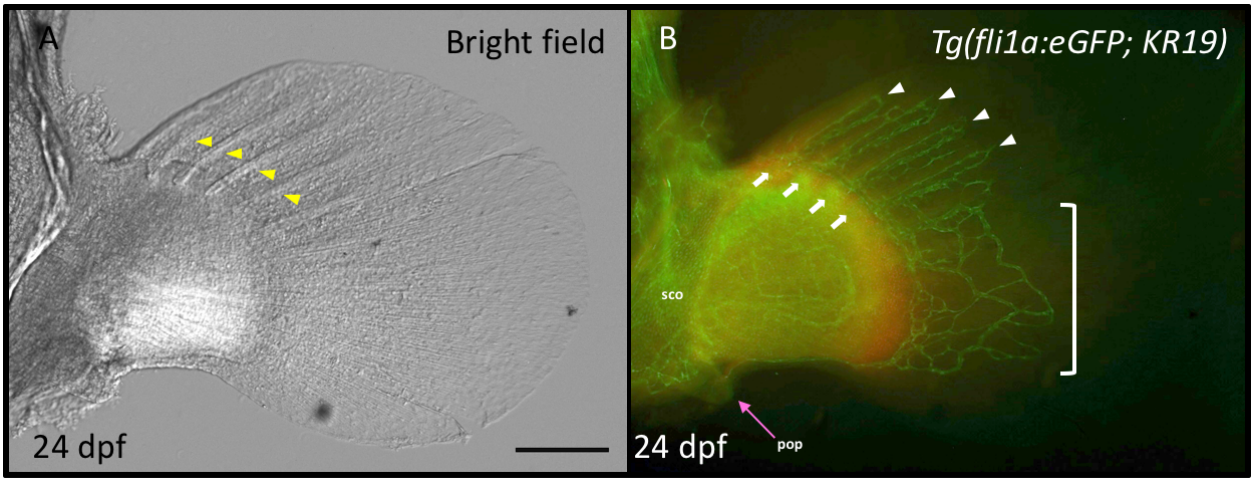

Figure 3.10: Blood vessel remodeling in the pectoral fin correlates with distal radial and fin ray formation during larval development. The pectoral fin of double transgenic *(fli1a:eGFP; KR19)* larva at 24 dpf. (A) Brightfield image, showing the formation of fin rays in an anterior to posterior direction (yellow arrowheads). (B) Merged image of *fli1a:eGFP and KR19* activity, showing the blood vessel remodeling coincide with distal radial and fin ray formation. In the posterior fin region where distal radials and fin rays have not yet formed, the blood vessel network is disorganized (white bracket). In the anterior fin region, blood vessels are remodeled (white arrowheads) where distal radials (white arrows) and fin rays (yellow arrowheads) have formed. Blood vessel invasion of the endoskeletal disc can be seen along with the regression of the postcoracoid process. Note, there is no *fli1a* reporter *eGFP* expression in the distal posterior region of the endoskeletal disc. n = 10. pop = postcoracoid process. sco = scapulocoracoid. Standard length = 7 mm. Scale bar of A-B = 100 μm.

3.5.4 *m-Inta11* activity localizes within presumptive fin rays and is complementary to the *fli1a* enhancer domain during late larval development

Despite drastic changes in the modeling of pectoral fin blood vessels, the *m-Inta11* enhancer continues to display different domains of reporter expression in the anterior and posterior fin region (Figure 3.11 B). Using confocal imaging, we show the activity of *m-Inta11* in the posterior fin region remains uniform and localized to the cells of the fin fold at 26 dpf (Figure 3.11 B). In the anterior fin region, however, the activity of *m-Inta11* is localized within presumptive fin rays as evinced by the lack of reporter *mCherry* expression in the interray tissue (Figure 3.11 B, B'). Furthermore, it becomes evident that the localization of *m-Inta11* activity proceeds in an anterior to posterior direction, in synchrony with the formation of distal radials, patterning of fin rays, and remodeling of fin ray blood vessels (Figure 3.11 B). Meanwhile, brighter *fli1a* reporter activity continues to be restricted in the anterior endoskeletal disc region, both in the proximal and distal direction (Figure 3.11 A, C). Moreover, our analysis of 3D rendering confirms that, despite changes in the *m-Inta11* and *fli1a* enhancer domains of activity, *mCherry* and *eGFP* reporter expression is not overlapping in any geometric view, including the sagittal plane, as determined by the absence of yellow fluorescence (Figure 3.11 C, C', C''). In fact, the *m-Inta11* and *fli1a* enhancer domains are complementary at all time points examined during larval development. Nonetheless, it is worth noting that there is little to no overlap at the margins of *m-Inta11* and *fli1a* enhancer domains, as shown by their respective reporter expression.

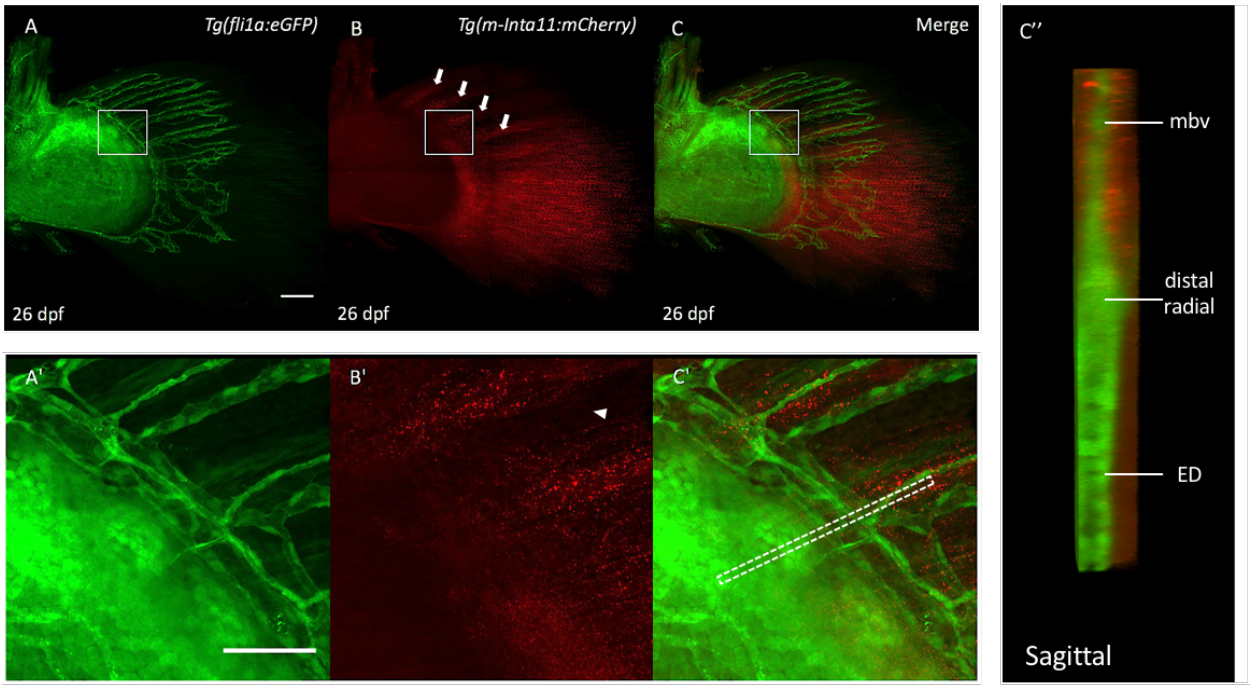

Figure 3.11: The *m-Inta11* activity localizes within presumptive fin rays and is complementary to the *fli1a* enhancer domain during late larval development. The pectoral fin of a double transgenic (*fli1a:eGFP; m-Inta11: mCherry*) larva at 26 dpf. (A) *fli1a* reporter activity is increased within newly formed distal radials. (B) *m-Inta11* reporter activity is localized within presumptive fin rays in the anterior fin region. (C) Merge image of panel A and B (A') Higher magnification of panel A (B') Zoom-in of panel B, showing lack of *m-Inta11* reporter mCherry expression in interray tissue (arrowheads). (C') Higher magnification of panel C. (C'') Sagittal view of the dashed line in panel C, showing a complementary pattern between *m-Inta11* and *fli1a* enhancer domains, as demonstrated by lack of overlap between *mCherry* and *eGFP* reporter expression. Standard length = 6.7 mm. n = 4. Scale bar of A-C = 100 µm. Scale bar of A'-C' = 50 µm. Confocal images were captured by Jing Zhang.

3.6 The *m-Inta11* and *fli1a* enhancer domains of activity are complementary during caudal fin regeneration.

The presence of a complementary pattern between *m-Inta11* and *fli1a* enhancer domains of activity during embryonic and larval pectoral fin development made us wonder if such domains are complementary during other processes. More specifically, we sought to examine if *m-Inta11* and *fli1a* enhancer activity is complementary in the context of fin regeneration. The caudal fin is well characterized and frequently used in regeneration studies. Confocal imaging analysis of adult double transgenic (*fli1a:eGFP; m-Inta11:mCherry*) caudal fin regenerates was performed 4 days post-amputation (dpa). Accordingly, we revealed a complementary pattern between *m-Inta11* activity in newly formed joints within the most proximal region of the regenerate tissue and surrounding *fli1a*-expressing blood vessels (Figure 3.12B). In addition, the sagittal plane of newly formed joints demonstrated that *m-Inta11* and *fli1a* domains of activity are mutually exclusive, as determined by the lack of overlap between reporter *mCherry* and *eGFP* expression (Figure 3.12C).

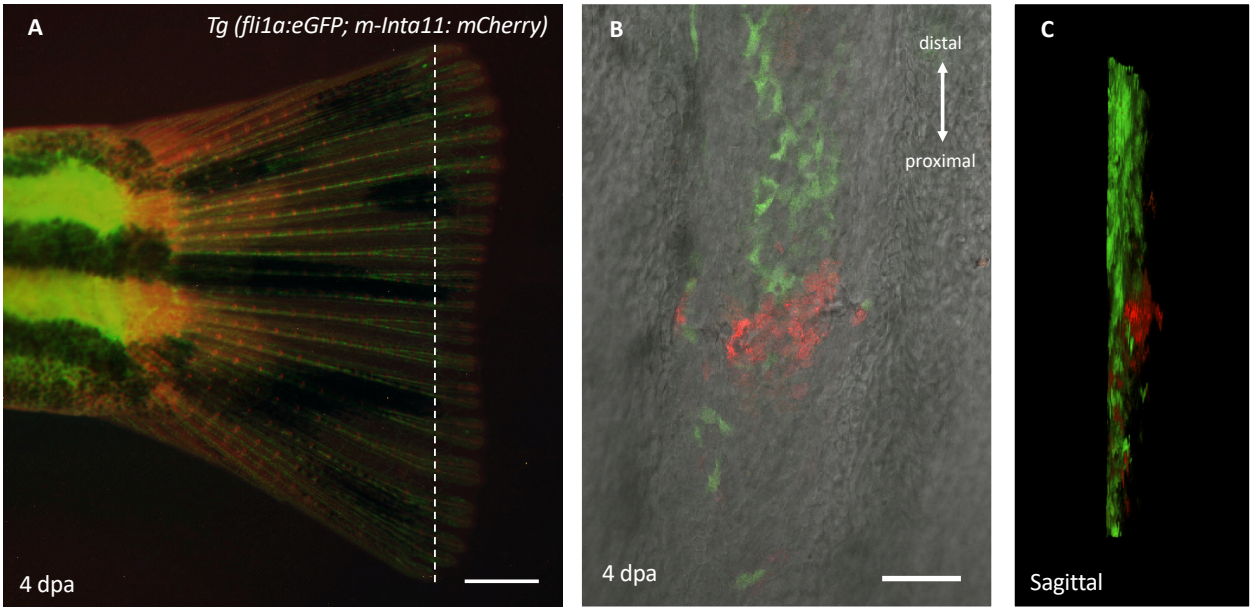

Figure 3.12: The *m-Inta11* and *fli1a* enhancer domains are complementary in newly formed joints during caudal fin regeneration. (A) The caudal fin regenerate of an adult double transgenic (*fli1a:eGFP; m-Inta11:mCherry*) fish 4 days post-amputation. (B) Confocal imaging of newly formed joint in the most proximal region of the caudal fin regenerate, showing a complementary pattern between *m-Inta11* activity and *fli1a*-expressing blood vessels. (C) Sagittal view of panel B showing a lack of overlap between *m-Inta11* and *fli1a* enhancer domains. The dashed line in panel A shows the plane of amputation. n = 4. Scale bar of A = 500 μm. Scale bar of B = 50 μm.

3.7 The overall expression domains of *Fli1* and *Hoxa13* are complementary in the mouse autopod at 13.5 dpc.

The existence of a complementary pattern between *m-Inta11* and *fli1a* enhancer domains of activity during pectoral fin development led us to investigate whether *Hoxa13* and *Fli1* expression domains may be complementary during limb development. First, we wished to characterize *Fli1* expression and examine *Hoxa13* expression in the mouse autopod. *In situ* hybridization with antisense *RNA* probes on mouse forelimb autopod cryosections at 13.5 days post coitum (dpc) reveals that *Fli1* is expressed in chondrogenic condensations but absent in joints (Figure 3.13A). In contrast, *Hoxa13* is expressed in the mesenchyme surrounding the chondrogenic condensation and at the level of the joints (Figure 3.13B). Moreover, double fluorescent *in situ* hybridization with antisense *RNA* probes on mouse hindlimb autopod cryosections was imaged using confocal microscopy, showing that the overall expression domains of *Fli1* and *Hoxa13* are complementary at 13.5 dpc, as evidenced by the lack of a yellow fluorescent signal that would be expected if *Fli1* and *Hoxa13* expression overlapped (Figure 3.14). A small population of *Hoxa13*-expressing cells can be seen overlaying the distal tip of the developing phalanges (Figure 3.14C).

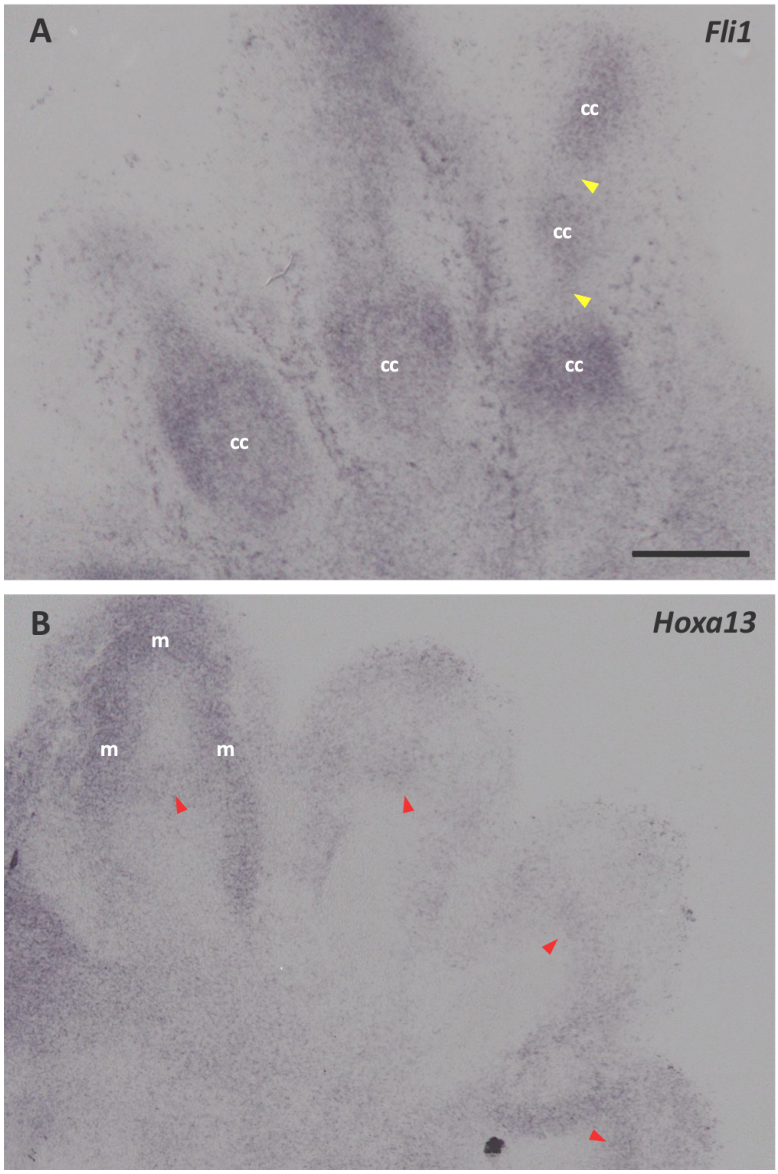

Figure 3.13: *Fli1* is expressed in chondrogenic condensations and surrounded by *Hoxa13*-expressing mesenchyme. Single *in situ* hybridization on mouse forelimb autopod cryosections at 13.5 dpc. (A) *Fli1* is expressed in chondrogenic condensations of the autopod but absent within joint tissue (yellow arrowheads). (B) *Hoxa13* is active in the mesenchyme surrounding chondrogenic condensations and at the level of the joints (red arrowheads). n = 34. cc = chondrogenic condensation. m = mesenchyme. Scale bar of A and B = 200 µm.

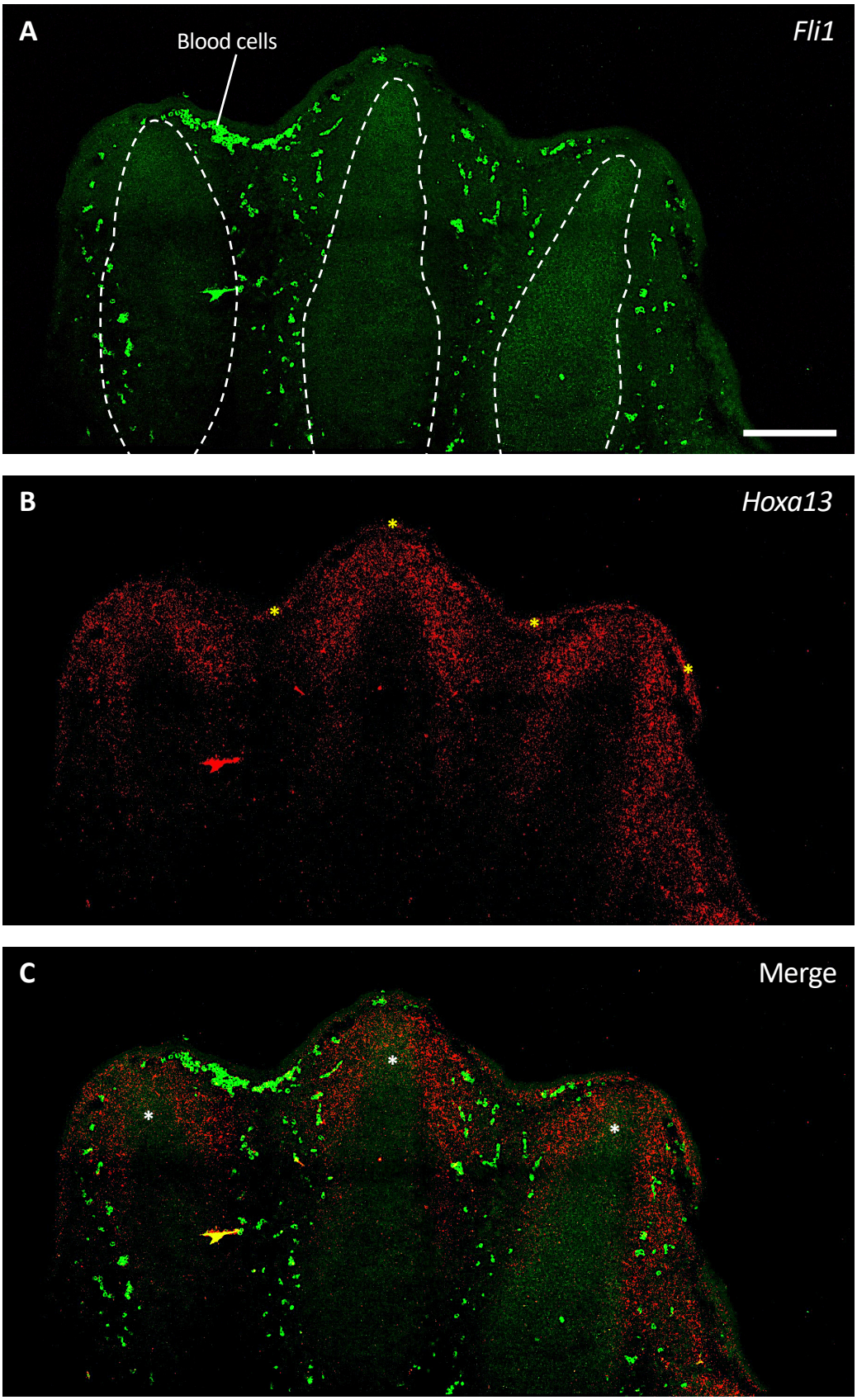
A
Blood cells
Fli1
B
Hoxa13
C
Merge

Figure 3.14: The overall expression domains of *Fli1* and *Hoxa13* are complementary in the mouse autopod. Double fluorescent *in situ* hybridization of mouse hindlimb autopod cryosections was imaged at 13.5 dpc using confocal microscopy. (A) *Fli1* is active in chondrogenic condensations. (B) *Hoxa13* is active in the mesenchyme surrounding chondrogenic condensations. Note, background staining can be observed in the ectodermal layer (yellow asterisks). (C) Merge image of panels A and B, showing a general complementary pattern between *Fli1* and *Hoxa13* expression domains. Note, a small population of *Hoxa13*-expressing cells can be observed overlapping the distal tip region of the developing phalanges (white asterisks). Blood cells are visible around chondrogenic condensations. The dashed line in panel A delineates chondrogenic condensations. n = 28. Scale bar of A, B, and C = 200 μm.

3.8 Ectopic *fli1a* expression in the *m-Inta11* domain induces cell clustering, defects in cell migration, and strong reporter activity in the median and pectoral fins during development.

The persistence of a complementary pattern between *m-Inta11* and *fli1a* enhancer domains during pectoral fin development suggested that there may be a regulation between *hox13* and *fli1a* genes. To elucidate the regulation underlying the complementary pattern, we wished to ectopically express *fli1a* in the *m-Inta11* domain. The *m-Inta11-βG:fli1a* construct was created and injected into transgenic *Tg(m-Inta11:eGFP)* embryos. An analysis of *eGFP* expression was performed on primary injected larvae (P^0) at 3 dpf and the majority of medians fins displayed clusters of eGFP with round cell morphology (data not shown). Once P^0 larvae reached adulthood, they were crossed with wild-type fish to identify a founder fish transmitting the transgene to the next generation. The F1 larvae, obtained from a cross between positive founder and wildtype fish, were screened at 3 dpf exhibiting either low or high eGFP fluorescence levels. PCR and *in situ* hybridization analysis showed the presence of the *fli1a* transgene in larvae with high eGFP expression (data not shown). Larvae with low *eGFP* expression lacked the *fli1a* transgene, had eGFP levels comparable to the transgenic *Tg(m-Inta11:eGFP)* line, and served as a control group in subsequent analyses. For screening consistency purposes, larvae with the highest eGFP reporter levels in each of the ectopic *fli1a* and control groups were selected to be raised. Confocal imaging analysis of F2 embryos showed that ectopic *fli1a* expression in the median and pectoral fin *m-Inta11* positive cells display cell clustering, defects in cell migration, and enhanced *m-Inta11* reporter eGFP levels compared to control larvae during early larval development (Figure 3.15 A-D). In addition, median fins with ectopic *fli1a* expression show arborization of melanocytes

(Figure 3.15 B). It is worth noting that ectopic *fli1a*-expressing larvae have increased *m-Inta11* reporter activity in the urogenital pore (data not shown).

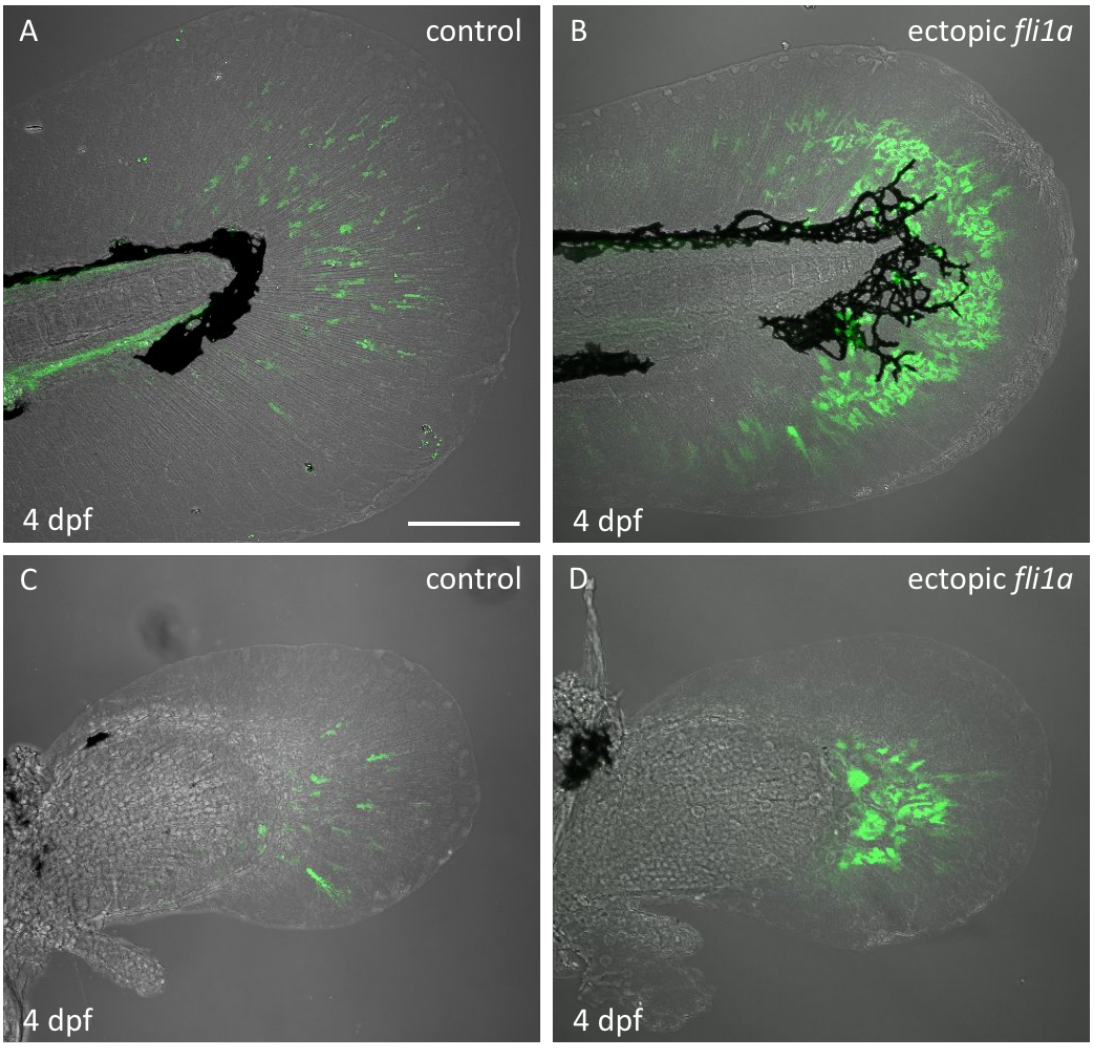

Figure 3.15: Ectopic *fli1a* expression induces cell clustering, defects in cell migration, and enhanced *m-Inta11* reporter eGFP levels in the median and pectoral fins during early larval development. Confocal imaging analysis of control larvae at 4 dpf, showing *m-Inta11* reporter *eGFP* expression in migrating *m-Inta11* positive cells of the (A) median and (C) pectoral fins. Ectopic *fli1a*-expressing larvae at 4 dpf, showing cell clustering, defects in cell migration, and stronger eGFP levels in the (B) median and (D) pectoral fins. Note, arborization of median fin melanocytes is visible around the notochord. n ≈ 300. Scale bar of A-D = 100 μm.

3.9 Ectopic *fli1a* expression result in shorter median and pectoral fin folds.

Morphological analysis of ectopic *fli1a*-expressing larvae suggests that the median and pectoral fin may be shorter in length compared to control larvae. Accordingly, measurements of the median and pectoral fin folds were undertaken at 4 dpf. Using a one-tailed t-test at a significance level of 0.05, the median fin fold of ectopic *fli1a*-expressing larvae (177.32 ± 1.92 μm) was determined to be significantly shorter than that of control (234.52 ± 2.72 μm) larvae (Figure 3.16). Furthermore, ectopic *fli1a*-expressing pectoral fin folds (167.46 ± 2.05 μm) were shorter than their control counterparts (172.40 ± 3.14 μm) but the difference was not statistically significant (Figure 3.16).

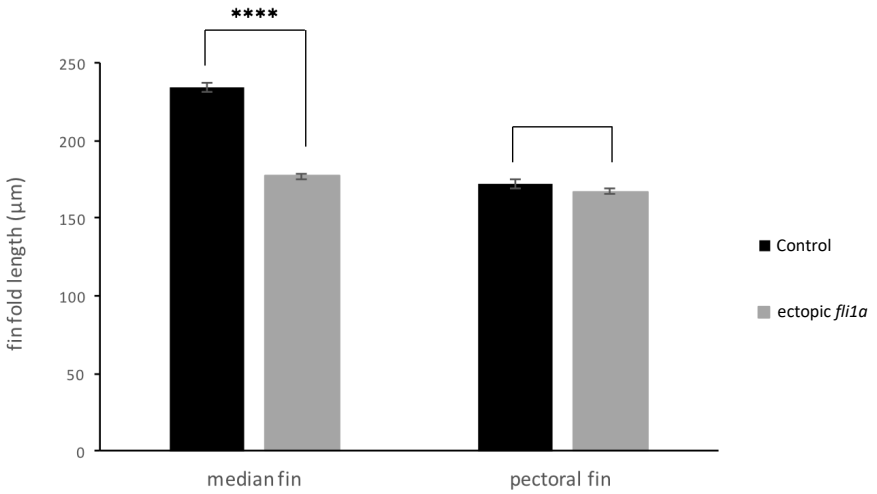

Figure 3.16: The median and pectoral fin folds of ectopic *fli1a*-expressing larvae are shorter compared to control larvae. Ectopic *fli1a*-expressing larvae have significantly shorter median fin folds compared to control larvae (ectopic *fli1a* expression = 177.32 ± 1.92 μm, control = 234.52 ± 2.72 μm, **** P = <0.0001, n =12). Ectopic *fli1a*-expressing larvae have shorter pectoral fin folds compared to control larvae, but difference is not significant (ectopic *fli1a* expression = 167.46 ± 2.05 μm, control = 234.52 ± 2.72 μm, P = 0.201702, n =12).

3.10 Ectopic *fli1a* expression does not influence cell death activity in the median and pectoral fins at 3dpf.

The presence of defects in the migration of *m-Inta11* positive cells within the median and pectoral fins of ectopic *fli1a*-expressing larvae made us wonder if ectopic *fli1a* expression could induce cell death. Interestingly, analysis of whole-mount TUNEL assay staining revealed no difference in cell death activity between the median and pectoral fins of ectopic *fli1a*-expressing and control larvae at 3 dpf (Figure 3.17; white arrowheads). It is worth noting that some apoptotic activity can be observed in the head as well as the trunk region of both ectopic *fli1a*-expressing and control larvae, thus serving as an internal control.

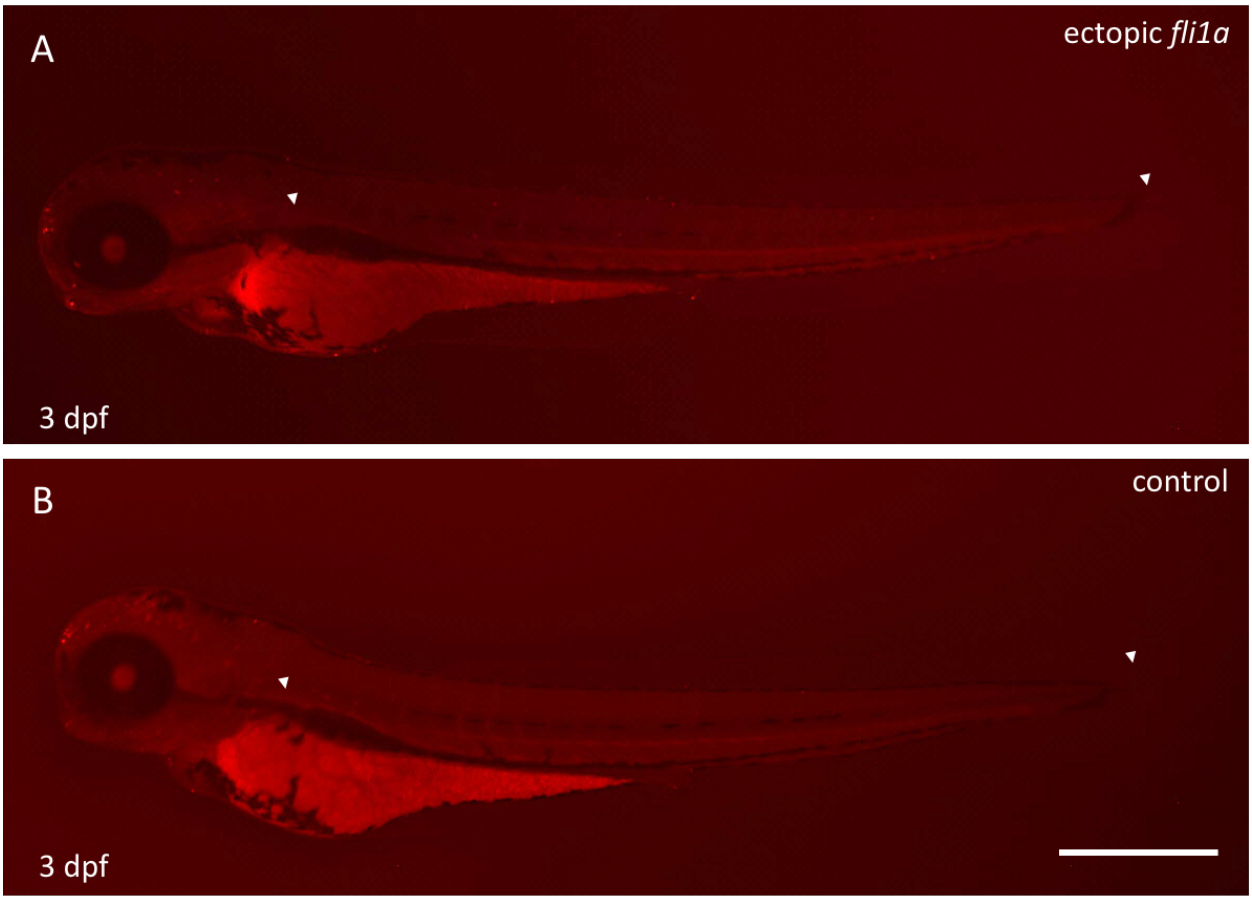

Figure 3. 17: Ectopic *fli1a* expression does not influence the rate of apoptotic activity in the median and pectoral fins during development. Whole-mount TUNEL assay staining of control ectopic *fli1a*-expressing (A) and control (B) larvae at 3 dpf, showing no difference in the rate of cell death activity in the median and pectoral fins (white arrowheads). Note, some TUNEL staining can be observed in the head and trunk region of both control and ectopic *fli1a*-expressing larvae. n =10 per group. Scale bar of A-B = 500 μm.

3.11 Ectopic *fli1a* expression does not perturb cell proliferation activity in the median and pectoral fins at 3dpf

The clustering of *m-Inta11* positive cells and enhanced reporter activity in the median and pectoral fins of ectopic *fli1a*-expressing larvae prompted us to investigate whether ectopic *fli1a* expression could influence the rate of proliferation during development. Analysis of whole-mount immunohistochemical staining at various magnifications using the α-phospho Histone 3 (Ser10) proliferative marker showed no discernable difference in mitotic activity between the median and pectoral fins of control and ectopic *fli1a*-expressing larvae at 3 dpf (Figure 3.18 A-D).

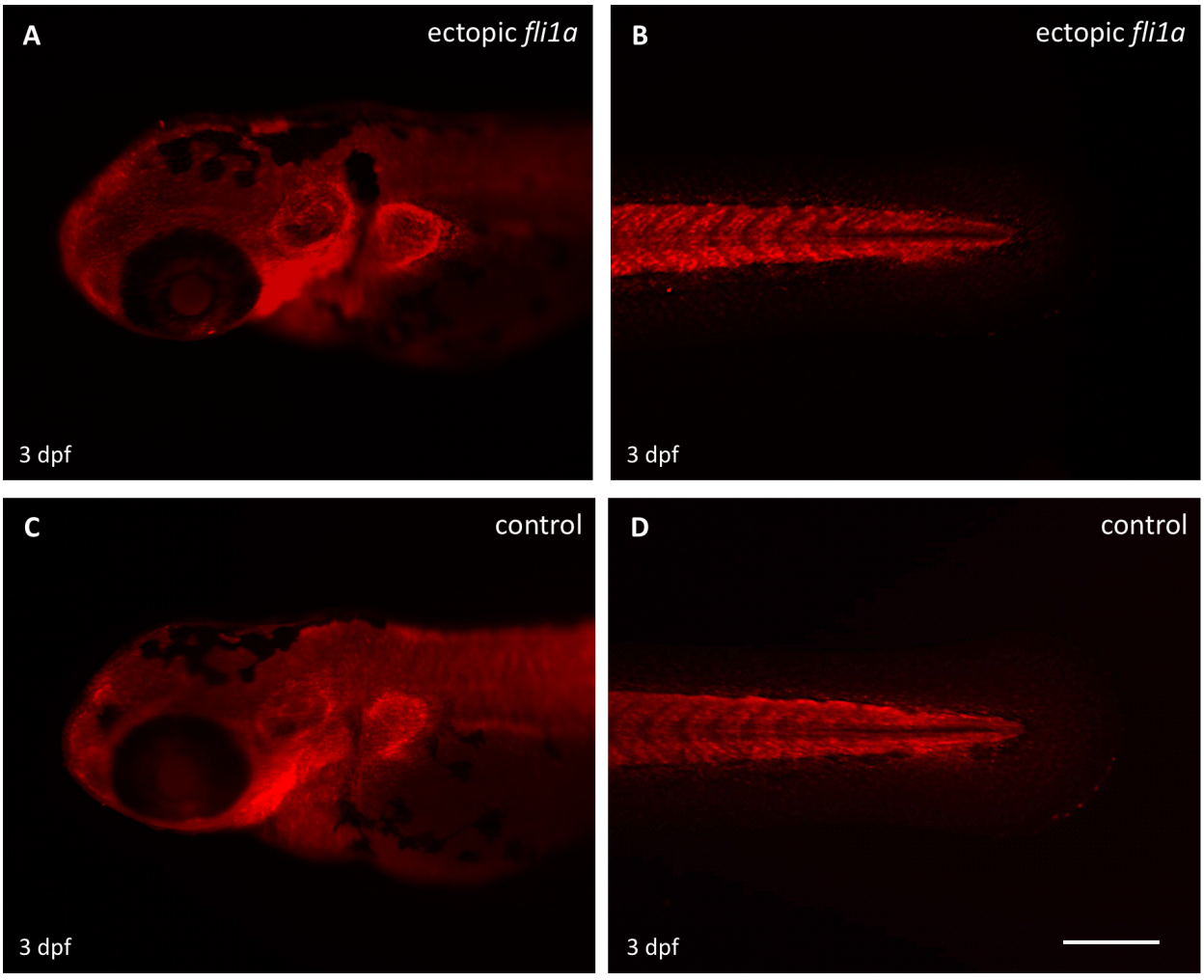

Figure 3.18: Ectopic *fli1a* expression does not perturb the proliferation rate in the median and pectoral fins during development. Whole-mount immunohistochemical staining of the α-phospho Histone 3 (Ser10) mitotic marker. The pectoral (A) and median (B) fins of ectopic *fli1a*-expressing larvae at 3 dpf, showing no difference in staining compared to the pectoral (C) and median (D) fins of control larvae. n =40 per group. Scale bar of A-D = 200 μm.

3.12 Ectopic *fli1a* expression demonstrate continued cell clustering, enhanced *m-Inta11* activity, and fin deformities during late larval development

The presence of cell clustering, defects in cell migration, and strong *m-Inta11* reporter activity in the median and pectoral fins of ectopic *fli1a*-expressing larvae at 4 dpf led us to investigate whether such changes would persist during later stages of development. Time-course analysis of ectopic *fli1a*-expressing larvae shows that clustering of *m-Inta11* positive cells and enhanced *m-Inta11* reporter activity are sustained during late larval pectoral fin development (Figure 3.19). It is important to note that *eGFP* reporter expression is not visible in control larvae after 5 dpf, which is comparable to the *Tg(m-Inta11:eGFP)* line (data not shown). Recall, control larvae are siblings of ectopic *fli1a*-expressing fish that carry the *m-Inta11:eGFP* transgene but lack the *m-Inta11:fli1a* transgene.

Morphological analysis of ectopic *fli1a*-expressing larvae demonstrates clustering of *m-Inta11* positive cells in the fin fold outside the endoskeletal disc and predominantly in the posterior fin fold region at 14 dpf (Figure 3.19 A; yellow arrowheads). Interestingly, *m-Inta11* cell clustering continues to be concentrated in the posterior fin region during later stages of larval development (Figure 3.19 B-C; yellow arrowheads). By 27 dpf, we observe a pronounced difference between the size of the anterior and posterior fin regions (Figure 3.19 D). In fact, the posterior part of the fin fold, where there are no fin rays yet, is reduced and forming a protrusion compared to the rest of the fin, where fin rays have already formed (Figure 3.19 D; dotted line). This aberration is not present in the pectoral fin during normal development (Figure 3.19 E, Figure 3.8 A, Figure 3.9 A). At the same time, some *m-Inta11* activity fails to localize within presumptive fin rays, as evidenced

by the presence of reporter *eGFP* expression in the interray tissue (Figure 3.19 C, white arrowhead). Additionally, we report that continued clustering of *m-Inta11* positive cells in the posterior fin region is associated with a curvature of the presumptive fin rays (Figure 3.19 C; pink arrowheads). Our analysis also reveals defects in the anterior fin region as early as 21 dpf. At that time, some *m-Inta11* positive cells can be seen organizing within presumptive fin rays in the anterior fin region (Figure 3.19 B). Nonetheless, the larval pectoral fin begins to display deformities in the anterior fin fold, particularly in the distal portion corresponding to the formation of exoskeletal fin rays (Figure 3.19 B). More specifically, the distal edge of the anterior fin rays is not round but rather serrated (Figure 3.19 B; white asterisk). This deformity is not consistent with normal development (Figure 3.19 E, Figure 3.8 A, Figure 3.9 A) and is maintained at 24 dpf (Figure 3.19 C; white asterisk), as well as 27 dpf albeit being less severe.

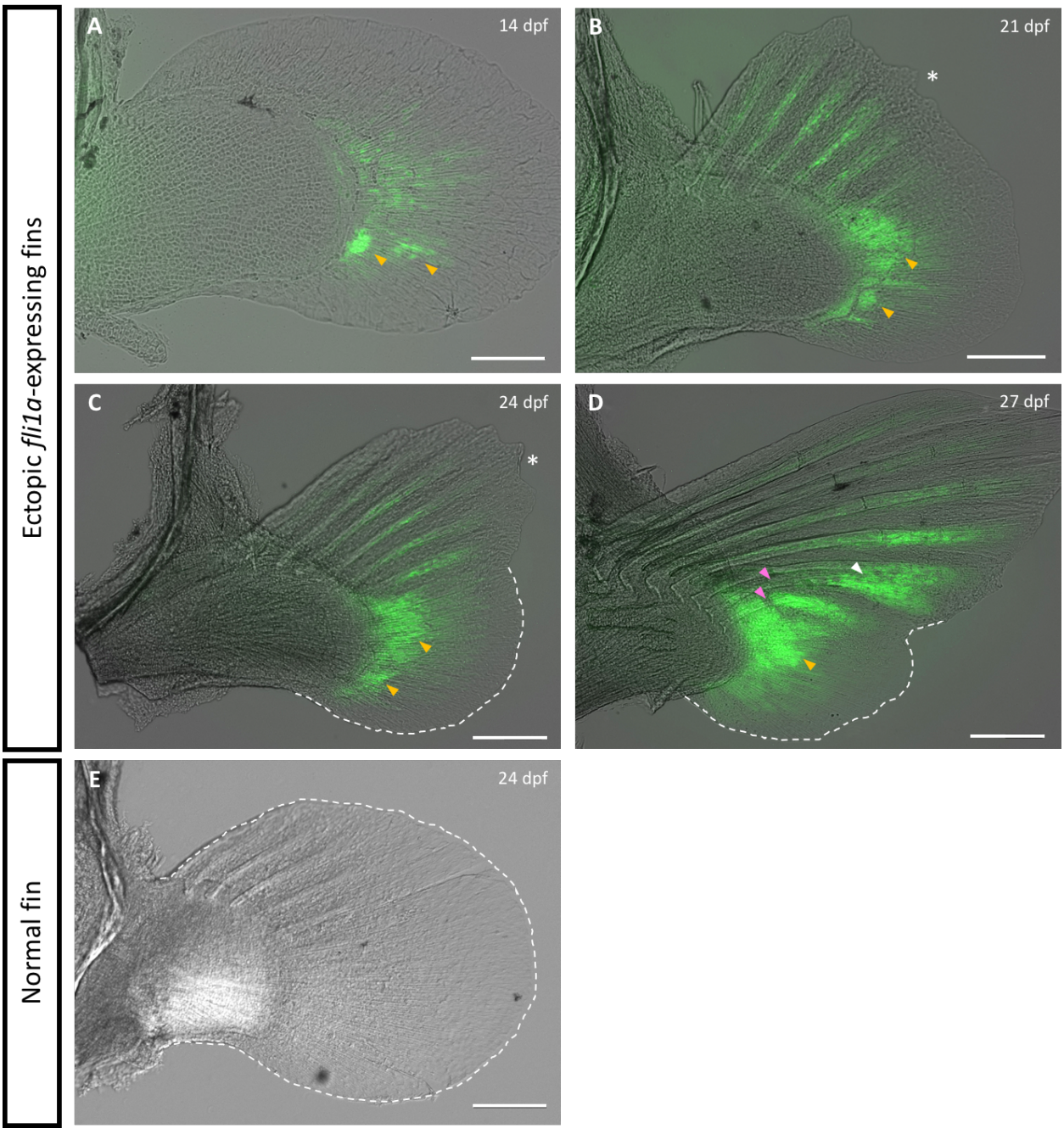
Ectopic *fli1a*-expressing fins
A
14 dpf
B
21 dpf
*
C
24 dpf
*
D
27 dpf
Normal fin
E
24 dpf

Figure 3.19: Ectopic *fli1a* expression results in sustained clustering of *m-Inta11* positive cells, enhanced *m-Inta11* reporter activity, and fin deformities in the pectoral fin during late larval development. The pectoral fin of ectopic *fli1a*-expressing larvae at 14, 21, 24, and 27 dpf. (A) Clustering of *m-Inta11* positive cells can be seen predominantly in the posterior fin region (orange arrowheads). (B-C) some *m-Inta11* positive cells organize within presumptive fin rays, while others continue to be concentrated in the posterior fin region (orange arrowheads). Note, the pectoral fin display deformities in the anterior fin region. The distal edge of the anterior fin rays is serrated (white asterisk in panel B and C). (D) Some *m-Inta11* activity fails to localize within presumptive fin rays, as demonstrated by the presence of reporter *eGFP* expression in the interray tissue (white arrowhead). Note, the curvature of posterior presumptive fin rays is visible (pink arrowheads). (E) A normal pectoral fin at 24 dpf; image obtained from Figure 3.10. The dotted line in panel C-E delineates the edge of the pectoral fin fold. n = 10 per time point. Standard length of larva in A = 5.1 mm, B = 8.1 mm, C = 8.2 mm, D = 10.65 mm. Scale bar of A, E = 100 μm, B-D = 200 μm.

3.13 Ectopic *fli1a* expression increases *hox13* expression and *m-Inta11* reporter *eGFP* expression in the developing pectoral fin

Following analysis of ectopic *fli1a*-mediated defects in late larval pectoral fins, we wished to investigate whether ectopic *fli1a* expression could influence the regulation of *hox13* genes during fin development. The pectoral fin tissue of ectopic *fli1a*-expressing and control larvae was dissected and accordingly used to extract RNA for quantitative reverse transcriptase polymerase chain reaction (qRT-PCR) in order to quantify *hox13* transcripts at 14 and 24 dpf. Analysis of qRT-PCR showed that ectopic *fli1a* expression increases *hox13* expression and *m-Inta11* reporter *eGFP* levels during pectoral fin development (Figure 3.20). At 14 dpf, ectopic *fli1a*-expressing larvae displayed an approximately 4-fold increase in *hoxa13a* and an approximately 3-fold increase in *hoxa13b*. Most prominently, we observed an approximately 6-fold increase in *hoxd13a* expression. Furthermore, *fli1a* and *eGFP* showed a nearly 2-fold and 3-fold increase in relative expression, respectively. By 24 dpf, the pectoral fin of ectopic-*fli1a* expressing larvae demonstrated less elevation of *hoxa13a, hoxd13a, fli1a,* and *eGFP* relative expression. Indeed, *hoxa13a* only showed a 1.5-fold increase in relative expression. Similarly, *hoxd13a* and *eGFP* merely displayed a 2-fold increase in relative expression. Meanwhile, *fli1a* relative expression was slightly increased, while *hoxa13b* showed a slight reduction in expression compared to control larvae.

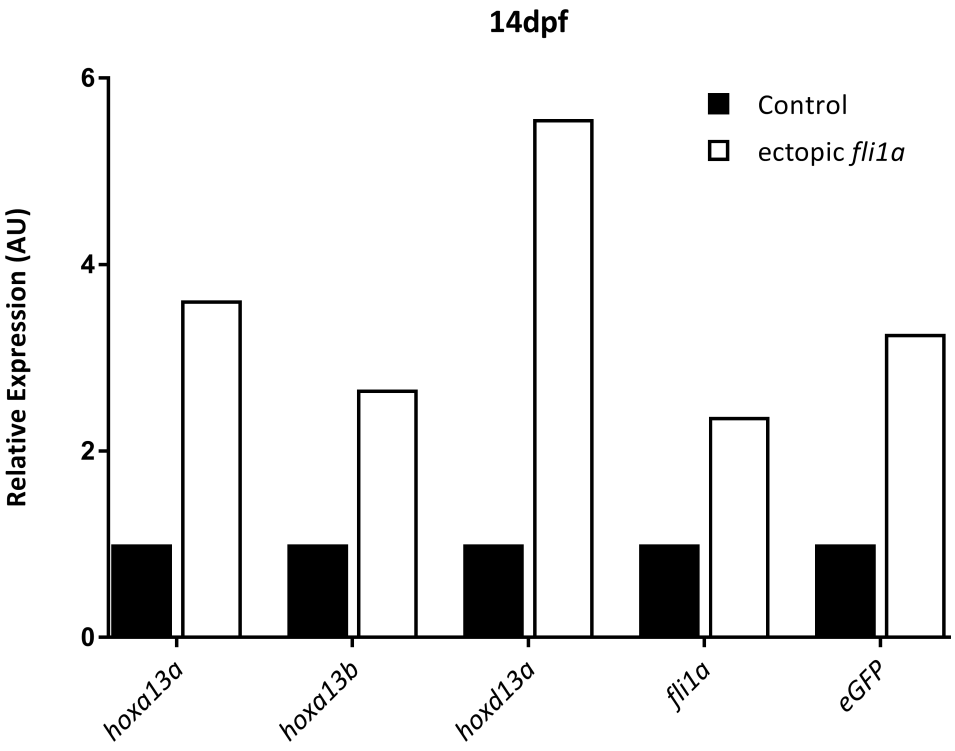
14dpf
Control
ectopic fli1a
Relative Expression (AU)
6
4
2
0
hoxa13a
hoxa13b
hoxd13a
fli1a
eGFP

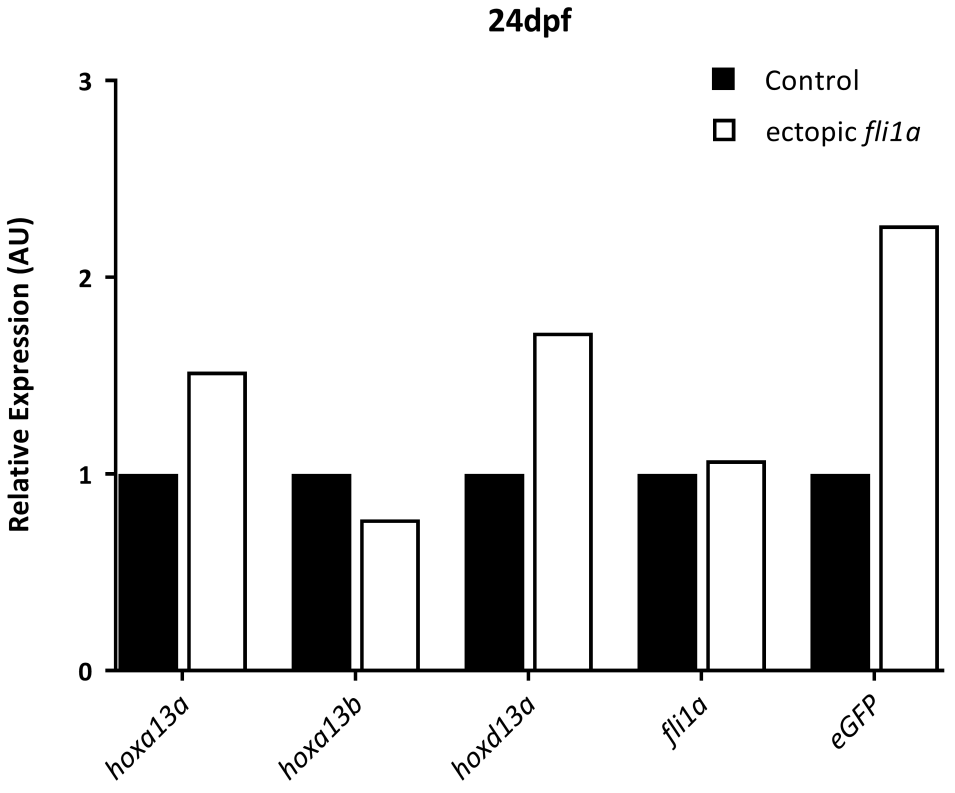
24dpf
Control
ectopic fli1a
Relative Expression (AU)
3
2
1
0
hoxa13a
hoxa13b
hoxd13a
fli1a
eGFP

Figure 3.20: Ectopic *fli1a* expression increases *hox13* and *m-Inta11* reporter *eGFP* expression during pectoral fin development. qRT-PCR analysis of ectopic *fli1a*-expressing pectoral fin tissue at 14 and 24 dpf, showing an increase in the relative expression of *hox13* and *eGFP* compared to control. Reported expression values are normalized to the geometric average of *β-actin* and *ef1a* housekeeping genes. A total of 40 and 20 pectoral fin dissections were used to create the cDNA library at 14 and 24 dpf, respectively. n = 1. qRT-PCR was run by Simon Monis and graphs were prepared using Prism8 software.

3.14 Ectopic *fli1a* expression results in additional bone nodules in the posterior region and produces defects in the formation of fin rays within the adult pectoral fin

The persistence of clustering and increased reporter eGFP activity in the *m-Inta11* positive cells of the pectoral fin during late larval development prompted us to investigate the effects of ectopic *fli1a* expression on the adult pectoral fin. To further examine the pectoral fin, analysis of bone and cartilage was performed on control and ectopic *fli1a*-expressing adult fish using Alcian blue and Alizarin red staining. Surprisingly, our analysis of the pectoral endoskeleton revealed that ectopic *fli1a*-expressing fish have additional bone nodules in the posterior region of the fin compared to control fish. The endoskeleton of control fish contained seven distal radials (Figure 3.21 A). In contrast, ectopic *fli1a*-expressing fish possessed, on average, seven distal radials, between two to five additional bone nodules, and disordered fin rays (Figure 3.21 B). Moreover, all ectopic *fli1a*-expressing pectoral fins displayed various defects in the formation of dermal bone fin rays (Figure 3.21 B-D). In fact, the proximal regions of posterior fin rays are particularly disordered and fail to properly articulate to the endoskeleton when compared to control fish (Figure 3.21 A-B, Figure 3.22 A-B). Other defects in the posterior fin region are present in some but not all examined ectopic *fli1a*-expressing fish. This includes deformed fin rays that bifurcate at a proximal position and fuse back at a distal position (Figure 3.22 C, pink arrowhead), visible in two out of the four examined pectoral fins. In addition, a trifurcation of a posterior fin ray can be observed in one of the four ectopic *fli1a*-expressing pectoral fins (Figure 3.22 C, orange arrowhead). It is important to note that not all fin ray defects are restricted to the poster fin region. In fact, three out of the four ectopic *fli1a*-expressing pectoral fins demonstrated a bifurcation in the upper sister ray of the second most anterior fin ray, which is not consistent with normal development (Figure 3.22 D).

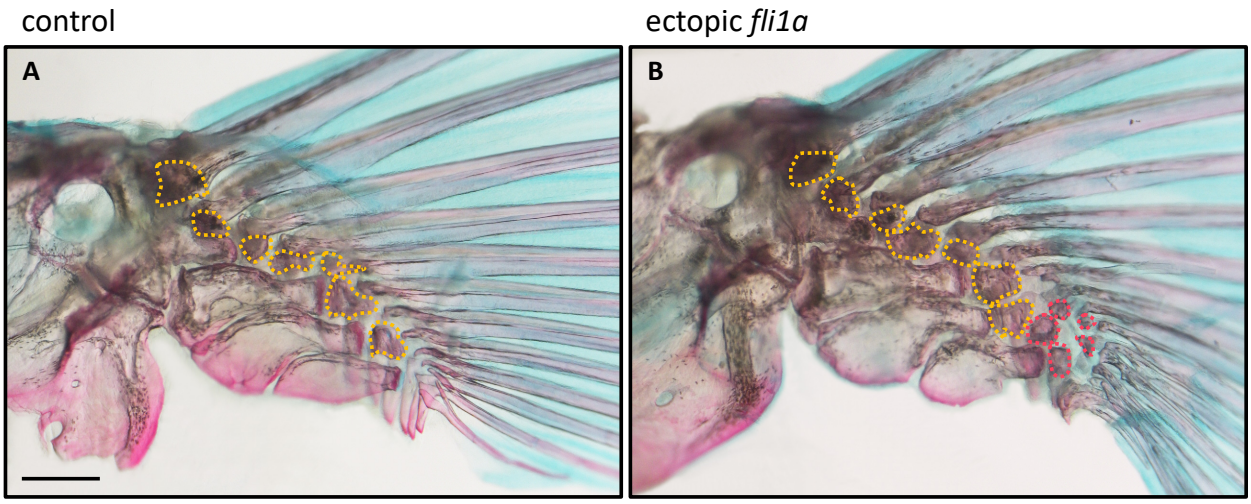

Figure 3.21: Ectopic *fli1a* expression results in the formation of additional bone nodules in the posterior fin region of the adult pectoral fin. Alcian blue and Alizarin red staining of control and ectopic fli1a-expressing fish, showing the endoskeleton of the adult pectoral fin. (A) The endoskeleton of control fish showing seven distal radials and organized articulating fin rays. (B) The endoskeleton of ectopic *fli1a*-expressing fish, showing seven distal radials, five additional bone nodules, and disordered fin rays in the posterior region. The orange dotted line delineates distal radials. The red dotted line represents the additional bone nodules. n= 4 (two fish per group). The number of distal radials in control fish = 7. The number of distal radials and additional bone nodules in ectopic *fli1a*-expressing fish = 12, 9, 10, 12. Scale bar of A and B = 200 µm.

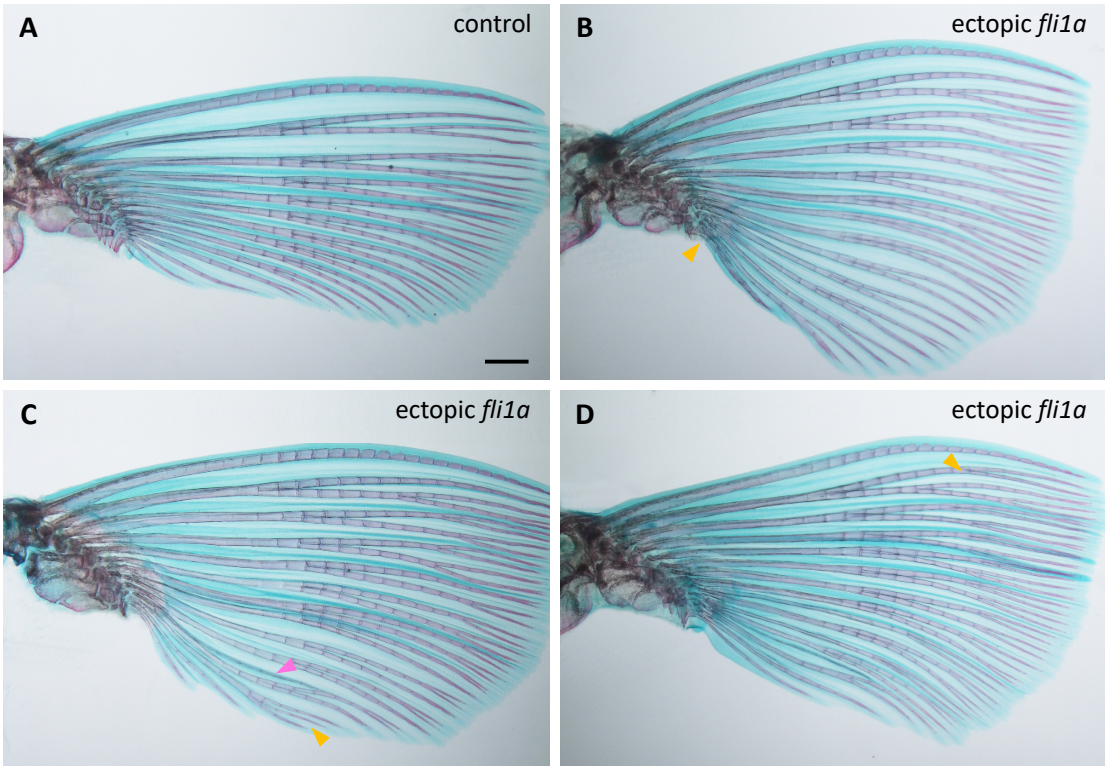

Figure 3.22: Ectopic *fli1a* expression leads to defects in the formation of fin rays in the adult pectoral fin. Alcian blue and Alizarin red staining of control and ectopic *fli1a*-expressing fish, showing the dermal and endochondral skeleton of the adult pectoral fin. (A) The pectoral fin of control fish, showing organized dermal bone fin rays. (B) The pectoral fin of ectopic *fli1a*-expressing fish, showing disordered fin rays in the posterior fin region (orange arrowhead, proportion of fish with phenotype: 4/4). (C) The pectoral fin of ectopic *fli1a*-expressing display aberrant bifurcation at a proximal position, followed by fusion at a distal position (pink arrowhead, proportion of fish with phenotype: 2/4). Note, a trifurcation of a posterior fin ray can be observed in panel C (orange arrowhead, proportion of fish with phenotype: 1/4). (D) The pectoral fin of ectopic *fli1a*-expressing fish showing bifurcation in the upper sister-ray of the second most anterior fin ray (orange arrowhead, proportion of fish with phenotype: 3/4). n=4 (two fish per group). The number of fin rays in control fish = 12, 12, 14, 14. The number of fin rays in ectopic *fli1a*-expressing fish = 15, 15, 13, 15. Scale bar of A-D = 500 µm.

CHAPTER 4 DISCUSSION

The next sections will discuss the results gathered in this dissertation and their implications for the development of the pectoral fin. Our discussion will be focused on insights gained from identifying the source of migrating *m-Inta11* positive cells, determining the contributions of *m-Inta11* positive and *fli1a*-expressing cells to adult structures, and elucidating the regulation between *fli1a* and *hox13* during development. In doing so, we will put forward a mechanism for the regulation of *fli1a* and *hox13* and address the relevance of our study for the pathology of Ewing sarcoma.

4.1 Characterization of the source of migrating *m-Inta11* positive cells in the pectoral fin

In this study, we have sought to determine the source of migrating *m-Inta11* positive cells in the pectoral fin. Previous data had suggested that the marginal blood vessel may give rise to *m-Inta11* positive cells in the pectoral fin during development. Time-course analysis of double transgenic (*fli1a:eGFP; m-Inta11:mCherry*) embryonic pectoral fins has ruled out the marginal blood vessel as a source for the emergence of *m-Inta11* positive cells (Figure 3.1). Nonetheless, analysis during later stages of fin development suggests that the marginal blood vessel may control the activation of *m-Inta11* leading to the progressive extension of *m-Inta11* positive cells towards the posterior pectoral fin region. More specifically, the anterior portion of the marginal blood vessel appears to come into contact with *m-Inta11* positive cells and may contribute to the progressive activation of the *m-Inta11* domain into the posterior direction (Figure 3.2). Alternatively, the anterior marginal blood vessel may serve as a scaffold for the migration of *m-Inta11* positive cells in the posterior region. Despite that, the anterior portion of the marginal blood vessel continues to grow around the presumptive endoskeletal disc region and towards the posterior marginal blood vessel. The

described development of the marginal blood vessel in the pectoral fin is consistent with previous studies that demonstrate two vessels invading from the anterior and posterior edge that later join in the posterior fin region (T. Yano et al., 2012). So far, there is no evidence in the pectoral fin to support blood vessel-mediated cell migration. If confirmed, the purported role of the anterior marginal blood vessel in the migration of *m-Inta11* positive cells would be reminiscent of actinotrichia fibrils that guide migrating mesenchyme into the fin fold during embryonic pectoral fin development. In fact, studies in the mammalian brain provide evidence of vessel-mediated cell migration wherein blood vessels act as a substrate for the movement of neural precursors towards their destination (Bovetti et al., 2007; Ulrich, Ma, Baker, & Torres-Vázquez, 2011; Xi et al., 2015). This modality of cell migration, known as vasophilic migration, is dependent on interactions between the extracellular matrix of migrating cells and supporting cells that wrap around blood vessels (Segarra, Kirchmaier, & Acker-Palmer, 2015). To test the role of blood vessels on the migration of *m-Inta11* positive cells or progressive activation of the *m-Inta11* domain, bevacizumab, an anti-VEGF antibody can be used to inhibit the growth of the marginal blood vessel (Zhang, Gao, Zhang, Qian, & Xiang, 2018). If the rate of *m-Inta11* cell migration or extension of *m-Inta11* domain is hindered with bevacizumab treatment, this could suggest that the marginal blood vessel is crucial for the motility or activity of *m-Inta11* positive cells during embryonic pectoral fin development. To determine whether *m-Inta11* positive cells are migrating along the anterior marginal blood vessel or undergoing progressive activation of the *m-Inta11* domain in the posterior direction, we could create a transgenic line expressing the photoconvertible kaede fluorescent reporter under the control of *m-Inta11*. Using UV light, kaede can be irreversibly photoconverted from green to red fluorescence at a single-cell resolution, allowing us to follow the fate of a photoconverted *m-Inta11* positive cell during embryonic pectoral fin development.

Next, we wondered whether *m-Inta11* positive cells in the pectoral fin could emerge from chondrocytes of the endoskeletal disc. To investigate a chondrogenic source for *m-Inta11* cell migration, we utilized the *KR19* transgenic line which labels chondrocytes of the endoskeletal disc with red fluorescence. Time-course analysis of double transgenic (*KR19; m-Inta11:eGFP*) embryos has revealed that the source of *m-Inta11* positive cells in the pectoral fin originates from chondrocytes of the endoskeletal disc (Figure 3.3). Starting at 49.5 hpf, *m-Inta11* reporter *eGFP* expression can be observed in the cytoplasm of cells at the leading edge of the endoskeletal disc, along with strong *KR19* reporter expression. By 52 hpf, *m-Inta11* reporter *eGFP* expression is increased while *KR19* expression is diminished in the same cells expressing *eGFP*. Thereupon, *m-Inta11* positive cells lose their regular shape (i.e. round cell morphology) and acquire filopodia-like protrusions that are necessary for cell migration. The decrease in *KR19* activity, increase in *eGFP* reporter expression, and change in cell morphology suggest that *m-Inta11* positive cells lose their chondrocyte attributes and transition into migratory cells. The identification of the source of migrating *m-Inta11* positive cells in the pectoral fin is in agreement with previous lineage tracing experiments suggesting that late phase *hox*-expressing cells emerge from the endochondral disc (Nakamura et al., 2016).

To the best of our knowledge, this is the first study to closely examine the changes in cell morphology that occur in chondrocytes and give rise to migratory cells within the leading edge of the endoskeletal disc. Moreover, the behavior of *m-Inta11* positive cells in the pectoral fin is reminiscent of the epithelial-to-mesenchymal transition. Studies in the past have described an epithelial-to-mesenchymal like transition of chondrocytes within the growth plate region of the mouse femur and distal tibia (Zhou, Shen, Wang, & Li, 2015). More specifically, chondrocytes in the proliferative zone showed increased expression of mesenchymal-like factors (i.e. *Smad3*

Ctnnb1, *Acta2*) and little to no epithelial-like markers (i.e. *Cdh1*, *Lamc1*, *Cldn6*, *Krt19*, *Col4a1*) In contrast, chondrocytes within the resting and hypertrophic zones demonstrated enhanced epithelial-like factors and a lack of mesenchymal-like factors. We suspect a similar process may be involved in the emergence of *m-Inta11* positive cells from chondrocytes of the endoskeletal disc. During the nascent stages of fin development, mesenchymal cells are known to form a chondrogenic condensation that will later give rise to chondrocytes of the endoskeletal disc (Grandel & Schulte-Merker, 1998). It is possible that some chondrocytes at the leading edge of the disc revert to a more mesenchymal state, retain, or acquire mesenchymal-like factors, and as such, serve as a source for the emergence of *m-Inta11*-positive cells. In fact, previous studies of chick micro-mass culture have indicated that HOXA13 and HOXD13 transcription factors inhibit chondrocyte differentiation in primary mesenchymal limb progenitor cells (Jerković et al., 2017). Accordingly, we predict that the onset of *hox13* expression may contribute to the loss of chondrocyte identity in *m-Inta11* positive cells and facilitate their migration during embryonic pectoral fin development. The identification and quantitative analysis of epithelial- and mesenchymal-like factors in chondrocytes and *m-Inta11* positive cells, along with detailed *hox13* expression, could further characterize the chondrocyte-to-migratory cell transition during early embryonic pectoral fin development.

It is important to note that *m-Inta11* positive cells represent a subpopulation of migrating cells in the pectoral fin fold. To illustrate this, the transgenic *Tg(m-Inta11:mCherry)* can be crossed with the enhancer trap (*ET5*) line. This transgenic *Tg(ET5)* line recapitulates the activity of Sall4, a transcription factor that is associated with the maintenance of embryonic stem cells, and labels all migrating cells of the pectoral fin fold during development (Jackson et al., 2013). Future studies

could utilize the transgenic *Tg(ET5)* line in a similar time-course analysis to infer the source of other *fli1a*-negative migrating cells within the pectoral fin fold.

4.2 The *fli1a* and *m-Inta11* reporter lines give evidence to regulation between *fli1a* and *hox13* during pectoral fin development

In this study, we have sought to follow the progression of *m-Inta11*-positive and *fli1a*-expressing cells during pectoral fin development, as well as determine their contributions to adult structures. Previous data have indicated that the activity of the *m-Inta11* correlates with the absence of *fli1a* expression in the distal posterior region of the endoskeletal disc at 3 dpf (Figure 1.8). Using time-course analysis, we show that *m-Inta11* and *fli1a* enhancer domains are indeed complementary during embryonic and larval pectoral fin development (Figure 4.1). Starting at 50.5 hpf, we observe that the beginning of *m-Inta11* activity, reporting *hox13* expression, is mutually exclusive with the *fli1a* expression domain. The inception of *m-Inta11* reporter *mCherry* expression in the pectoral fin is comparable to previous data showing *m-Inta11* reporter *eGFP* expression as early as 49.5 hpf (Figure 3.1 and 3.3). The discrepancy in *m-Inta11* onset may be due to individual variation in embryonic development. Alternatively, it may be attributed to intrinsic translational properties of the reporter mCherry and eGFP proteins, which exhibit patchy and uniform activity levels, respectively. Shortly after the start of *m-Inta11* activity in the pectoral fin, *m-Inta11* positive cells begin to display changes in cell morphology that are consistent with cell migration regardless of reporter expression. By 58 hpf, *m-Inta11* positive cells spread in the posterior direction. At 72 hpf, *m-Inta11* positive cells occupy the distal posterior region of the endoskeletal disc where *fli1a* reporter expression is absent and concurrently undergo extensive migration towards the fin fold.

As the pectoral fin grows, *m-Inta11* cell migration shows uniform reporter mCherry expression across the fin fold at 15 dpf. Meanwhile, the *fli1a* domain demonstrates brighter *eGFP* reporter expression in the anterior region of the endoskeletal disc. This brighter *fli1a*-expressing cell population transforms into precursor condensations that give rise to distal radials in an anteroposterior direction during larval development. Once a distal radial is formed, Fli1a activity is diminished, as can be seen with the most anterior distal radial (Figure 3.10 B). We also observe brighter *fli1a* activity in the anterior proximal region of the endoskeletal disc. This activity likely corresponds to tissue reorganization leading to articulation between the most anterior distal radial and the scapula, suggesting that increased Fli1a activity may be a marker of tissue organization in the endoskeletal disc. During that time, the domains and levels of *m-Inta11* and *fli1a* activity change yet continue to be characterized by the lack of overlap between reporter *mCherry* and *eGFP* expression (Figure 4.1). In fact, the activity of *m-Inta11* and *fli1a* appears to be coordinated since both enhancer domains are well-defined in the anterior region yet diffuse in the posterior region. In the anterior region, *m-Inta11* activity is organized along the plane of newly formed distal radials and progressively localized within presumptive fin rays, concomitant with remodeled blood vessels in the fin fold. In the posterior region, the dispersion of *m-Inta11* positive cells is emulated by an unorganized network of fin fold blood vessels. Furthermore, we suspect that the remodeling of blood vessels may facilitate *m-Inta11* cell localization within presumptive fin rays. Consistent with the purported role of the marginal blood vessel in *m-Inta11* cell migration during embryonic development, blood vessel remodeling may serve as a prerequisite for the formation of fin rays during larval development. In fact, Huang and colleagues have demonstrated that a mutation in collagen IX (col9α1) disrupts the modeling of blood vessels, leading to perturbed patterning of fin rays in the caudal fin (Huang et al., 2009). To test whether blood vessel remodeling drives fin ray

formation, we could use VEGF inhibitors to conditionally stunt the growth of blood vessels in the pectoral fin fold during late larval development (Zhang et al., 2018). Subsequently, we could analyze the effects of VEGF treatment on the organization of *m-Inta11* positive cells and the patterning of fin rays.

Another study has recently examined the morphological variation within and between various zebrafish strains and determined that pectoral fin rays are patterned along the anterior-to-posterior axis according to their articulation to distal radials (Hamada et al., 2019). The synergistic formation of distal radials and fin rays is mediated by the expression of *lhx* genes, which show anterior-posterior patterning activity during limb and pectoral fin development (Hamada et al., 2019) *lhx2b*, in particular, is expressed in distal radials and fin rays during development and is thought to be regulated by Shh signaling (Hamada et al., 2019). It is possible that strong *fli1a* expression in the distal rim of the endoskeletal disc not only provides positional information for the formation of distal radials but also interacts with *lhx2b* to coordinate the patterning of fin rays. To the best of our knowledge, this is the first study to examine the formation of distal radials prior to the appearance of precursor condensations and associate their emergence to increased Fli1a activity, concomitant with the patterning of fin rays and blood vessel remodeling. Most importantly, we argue that the persistence of a complementary pattern between *m-Inta11* and *fli1a* enhancer domains provide evidence for a regulatory relationship between *hox13* and *fli1a* during embryonic and larval development. This complementary pattern is not only limited to pectoral fin development but can also be observed during caudal fin regeneration as well as limb development (see section 4.3). This provides further support for the proposed regulation and suggests that the mechanism regulating *hox13* and *fli1a* expression during pectoral fin development is recapitulated during fin regeneration.

Future studies may focus on characterizing *fli1b* expression in the endoskeletal disc during embryonic and larval development. Preliminary expression analysis illustrates that *fli1b* is active in the endoskeletal disc at 2 and 3 dpf. It is yet to be determined if *fli1b* is absent in the distal posterior region of the endoskeletal disc and whether its expression domain is complementary to that of *hox13*. A comparable expression profile between *fli1a* and *fli1b* could suggest that both genes have similar roles during pectoral fin development.

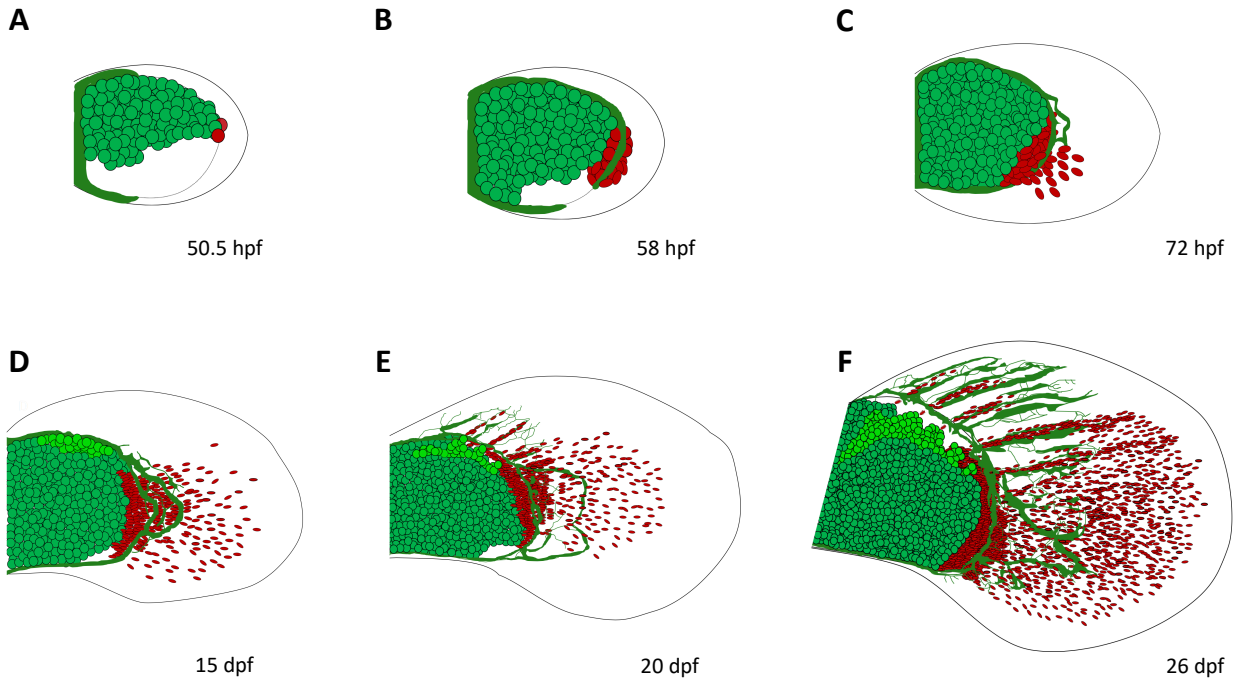

Figure 4.1: The *m-Inta11* and *fli1a* enhancer domains of activity are complementary in the pectoral fin during embryonic and larval development. A little amount of overlap between reporter expression is to be expected at the margins of the enhancer domains. Note, schematics are not to scale and do not show the network of blood vessels within the endoskeletal disc. The dotted line in panel A and B delineates the boundaries of the presumptive region of the endoskeletal disc.

4.3 *Fli1* and *Hoxa13* expression may be complementary during limb development

In addition to characterizing the domains of *m-Inta11* and *fli1a* during zebrafish pectoral fin development, we have sought to examine *Fli1* and *Hoxa13* expression during mouse forelimb and hindlimb development. Accordingly, we report that *Fli1* is expressed in chondrogenic condensations within the autopod at 13.5 dpc. At the same time, HOXA13 is active at the level of the joints and in mesenchymal tissue that surrounds chondrogenic condensations. Most importantly, we reveal that the overall domains of *Fli1* and *Hoxa13* expression are complementary at 13.5 dpc, as determined by the lack of overlap between fluorescent probes (Figure 3.14). The expression of *Hoxa13* at the distal tip of the autopod appears to correspond to regions that experience the most amount of morphological change or outgrowth during limb development (Perez et al., 2010). In contrast, *Fli1* expression is associated with condensation of endochondral tissue that contributes to the formation of digits. The activity of *Fli1* in chondrogenic condensations of the autopod is in agreement with *fli1a* expression analysis in the endoskeletal disc and distal radials, suggesting that *Fli1* and its ortholog *fli1a*, are involved in endochondral bone formation. Furthermore, the expression profile of *Hoxa13* shares resemblance with the domain of *hoxa13a*, with both genes showing activity in mesenchymal cells and at the levels of joints (McMillan et al., 2018; Perez et al., 2010). Taken together, this data provides additional support for the proposed regulation between *fli1a* and *hox13* during fin development and suggests that such regulation may be potentially conserved during limb development. In this study, we have only examined the expression of *Fli1* and *Hoxa13* in the autopod at 13.5 dpc. In the future, we wish to employ the RNAscope® method to undertake a detailed time-course analysis of *Fli1*, *Hoxa13*, and *Hoxd13* expression during limb development. The RNAscope® technique reduces

background noise, is much more sensitive, and has higher specificity compared to the standard *in situ* hybridization approach (H. Wang et al., 2015). If the activity of *Fli1* is determined to be complementary to that of *Hoxa13* or *Hoxd13* throughout limb development, this would provide further inclination for a conserved regulatory relationship between the *Fli1* member of the ETS family and homeobox-13 transcription factors.

4.4 Functional analysis of ectopic *fli1a* expression in the pectoral fin

In order to elucidate the regulation between *fli1a* and *hox13*, we have undertaken a functional analysis of the effects of ectopic *fli1a* expression in *m-Inta11* positive cells during pectoral fin development. Here, we report that ectopic *fli1a* expression leads to clustering of *m-Inta11* positive cells and enhanced reporter *eGFP* activity in the median and pectoral fins at 4 dpf (Figure 3.15). More specifically, the median fin of ectopic *fli1a*-expressing larvae exhibit fin fold collapse and pronounced arborization of melanocytes. These melanocytes come into contact with some ectopic-*fli1a* expressing cells. Melanocytes have intrinsic properties that increase their propensity to undergo cell transformation (Gupta et al., 2005; Uong & Zon, 2010). One potential hypothesis is that extensions of melanocytes could invade the intracellular space generated by the lack of *m-Inta11* cell migration and compensate for reduced median fin fold outgrowth. The arborization of melanocytes is limited to the median fin fold since melanocytes appear in the pectoral fin fold at a later stage during larval development. Furthermore, fin fold measurements reveal that ectopic *fli1a*-expressing larvae have significantly shorter median fin folds compared to control larvae. However, the pectoral fin fold of ectopic *fli1a*-expressing larvae is not significantly shorter than control larvae. Nonetheless, the difference in pectoral fin fold length may be biologically significant. Accordingly, we speculate that the length of the median and pectoral fin fold is

correlated to the number of *m-Inta11* positive cells that ectopically express *fli1a* in the median and pectoral fins. Given that the median fin contains more *m-Inta11* positive cells compared to the pectoral fin, we expect to observe more defects in cell migration and further truncations of the fin fold.

Next, we investigated whether clustering of *m-Inta11* positive cells may be associated with changes in proliferative and apoptotic activity. Previous studies using human and murine models of erythroleukemia have demonstrated that ectopic *Fli-1* expression in erythroleukemic cells inhibits differentiation, promotes non-restrained proliferation, and suppresses cell death activity (Cui, Vecchiarelli-Federico, Li, Wang, & Ben-David, 2009; Li et al., 2015; Vecchiarelli-Federico et al., 2017). In our study, we show that ectopic *fli1a* expression did not lead to a discernable change in the rate of proliferation or apoptotic activity in *m-Inta11* positive cells of the median and pectoral fins at 3 dpf (Figure 3.17, 3.18). It is important to note that changes in proliferation may not be detectable at this level of analysis. Therefore, closer analysis and quantification of proliferating cells may be necessary to confirm the effect of ectopic *fli1a* expression on *m-Inta11* cell proliferation. Nonetheless, our data could suggest that the introduction of *fli1a* alone is not sufficient to induce proliferation or suppress apoptosis in an otherwise healthy *m-Inta11* cell population. In a pathological context where various growth regulatory networks are comprised, constitutive activation of *fli1a* could contribute to proliferation and cell survival. Moreover, the effects of ectopic *fli1a* expression on cellular growth could vary depending on the cell lineage, not only influencing proliferation or cell death but also cell migration. For instance, studies in human epithelial breast cancer cell lines show that low *Fli-1* activity levels are correlated with enhanced tumor progression and that *Fli-1* re-expression reduces the ability of cells to undergo migration

and invasion during metastasis (Scheiber et al., 2014). This finding supports a role for *fli1a* in the disruption of *m-Inta11* cell morphology and migration during fin development.

Interestingly, we report that ectopic *fli1a*-mediated defects in *m-Inta11* cell migration are sustained during late larval pectoral fin development (Figure 3.19). Our data show that the clustering of *m-Inta11* positive cells is mild in the anterior fin region and predominantly concentrated in the posterior fin region as early as 14 dpf. The disproportionate aggregation of ectopic *fli1a*-expressing cells correlates with the intensity of *m-Inta11* activity and generates distinct morphological defects in the anterior and posterior fin regions. In the anterior region where *m-Inta11* activity is starting to organize within presumptive fin rays, defects are concentrated at the tip of the fin rays. By 21 dpf, we discover that the distal edge of the anterior fin rays is serrated and not round as would be expected during normal development. This aberration indicates that *m-Inta11* positive cells in the anterior fin region are capable of localizing within presumptive fin rays but may not be migrating adequately in the distal direction during fin ray formation. As the patterning of fin rays proceeds in an anterior to posterior direction, we detect more defects in fin morphology and a marked reduction in the size of the posterior fin region. We speculate that the difference between the size of the anterior and posterior fin region is attributed to the pronounced clustering of *m-Inta11* positive cells in the posterior fin region. This anomaly hinders the motility of *m-Inta11* positive cells and their prospective localization within presumptive fin rays, leading to stunted fin outgrowth and defects in the patterning of fin rays by 27 dpf.

In addition to morphological analysis of *m-Inta11* cell migration, we show that reporter *eGFP* activity is augmented at all of the examined time points during late larval development. Although qRT-PCR was performed once and would need to be repeated for statistical analysis, our data

corroborate that the introduction of *fli1a* more than doubles relative *eGFP* expression in the pectoral fin at 14 dpf. At the same time, we show that ectopic *fli1a* activity elevates relative *hox13* expression, with *hoxd13a* presenting the most notable increase compared to *hoxa13a* and *hoxa13b*, respectively (Figure 3.20). Interestingly, the relative expression of *hox13* and *eGFP* in the pectoral fin appear to be less elevated at 24 dpf. This suggests that ectopic *fli1a* expression modulates the activity of *hox13* more strongly during earlier stages of larval development and these effects could be mitigated during later stages of pectoral fin development. Nonetheless, the augmentation of reporter *eGFP* levels indicates that *fli1a* positively regulates the *m-Inta11* enhancer and leads to an increase in *hox13* expression during fin development. This is in addition to previous evidence in Ewing sarcoma showing that ectopic FLI1 activation positively regulates *HOXA13* and *HOXD13* expression (Svoboda et al., 2014).

As ectopic *fli1a*-expressing larvae mature into adulthood, we demonstrate that the severity of defects in the adult pectoral fin corresponds to the extent of *m-Inta11* cell clustering during larval development (Figure 3.21). Not surprisingly, the anterior fin region displays minor morphological disparities of the exoskeleton, particularly during bifurcation events. Meanwhile, the posterior fin region shows various abnormalities in the morphology and organization of both the endoskeleton and exoskeleton. Indeed, we describe the formation of additional bone nodules in the posterior fin region, where ectopic *fli1a*-expressing cells were once clustered (Figure 3.22). These nodules associate with disordered fin rays that exhibit fusion and bifurcation events. We postulate that ectopic *fli1a*-mediated increase of *hox13* expression during larval development contributes to the formation of bone nodules in the adult pectoral fin. Previous studies in zebrafish have shown that overexpression of *hoxd13a* promotes proliferation of chondrogenic tissue leading to a distal expansion of the endoskeletal disc as well as a fin fold reduction at 120 hpf (Freitas, Gómez-Marín,

Wilson, Casares, & Gómez-Skarmeta, 2012b). However, we did not observe a discernable increase in the proliferation of chondrocytes or a distal expansion of endoskeletal tissue at comparable time points. This outcome may be due to a difference in the timing and domain of *hox13* over-expression. Using alternative methods (i.e. corticosteroid hormone inducible system, *hsp70* and *col2a1a* tissue-specific promoters), Freitas and colleagues induced *hoxd13a* overexpression at specific time points (i.e. 30 and 32 hpf) prior to the anterior expansion of endogenous *hoxd13a* in the pectoral fin (Ahn & Ho, 2008). The over-expression of *hoxd13a* could potentiate a larger anterior expansion of the *hoxd13a* domain and encode further elaboration of distal endochondral structures in the pectoral fin. In our ectopic *fli1a* study, *hox13* expression is increased in *m-Inta11* positive cells only and not in other cells of the pectoral fin. In addition, the misexpression of *fli1a* likely perturbs the expression of other factors, which promote clustering and impede the ability of *hox13*-expressing cells to migrate to the fin blade. This could explain the lack of discernable proliferation and distal expansion that would otherwise be anticipated with *hoxd13a* over-expression. Thus far, we have chosen to focus our analysis of ectopic *fli1a* expression on the development of the pectoral fin. Current experiments are underway to examine the effects of ectopic *fli1a* expression in the caudal fin throughout larval development and adulthood. In addition, we wish to investigate the effects of ectopic *fli1a* expression on the development and remodeling of blood vessels in the caudal and pectoral fins.

4.5 Implications of ectopic *fli1a* expression for Ewing Sarcoma

Our functional analysis of ectopic *fli1a* expression not only sheds light on the regulatory relationship between *fli1a* and *hox13* in the pectoral fin but also carries implications for the pathology of Ewing sarcoma. Notably, the *m-Inta11* positive cells that mis-express *fli1a* are of

mesenchymal origin. Similarly, the source of Ewing sarcoma, while subject to much debate, is presumably derived from mesenchymal cells (Amaral et al., 2014). In view of this, the misexpression of *fli1a* appears to partially recapitulate some of the defects that have been previously described in EWS-FLI1 positive cells. Indeed, we observe aberrations in the morphology and migrating potential of ectopic *fli1a*-expressing cells that are comparable to the changes in the adhesion, morphology, and migration of *EWS-FLI1* transformed cells (Chaturvedi, Hoffman, Welm, Lessnick, & Beckerle, 2012; Svoboda et al., 2014). Furthermore, both ectopic activation of *fli1a* and transduction of *EWS-FLI1* are associated with a dysregulation in the expression of *hox13* and *HOX13*, respectively (Svoboda et al., 2017, 2014; von Heyking et al., 2016). More importantly, our data reveal a drastic elevation of *hoxd13a* that is similar to the marked over-expression of *HOXD13* in Ewing sarcoma cell lines (Svoboda et al., 2017; von Heyking et al., 2016). In Ewing sarcoma, increased expression of *HOXD13* is affiliated with the maintenance of malignant bone and soft tissue (Svoboda et al., 2017; von Heyking et al., 2016). In the case of ectopic *fli1a* expression, we speculate that the elevation of *hoxd13a* is involved in the transformation of osteochondrogenic progenitors leading to the formation of additional bone nodules in the adult pectoral fin. It thus becomes evident that *fli1a,* like *EWS-FLI1*, has the capacity to stimulate the progression of bone-forming tissue. Nonetheless, the mechanism by which *fli1a* modulates the expression of *hox13* remains elusive. Recent evidence in Ewing sarcoma cell lines has identified a critical role for chromatin remodeling complexes that confer transcriptional accessibility to the posterior *HOXD* locus (Svoboda et al., 2017). We suspect that a similar process is initiated by ectopic *fli1a* and responsible for the dysregulation of *hox13* during pectoral fin development.

Taken together, our findings suggest that changes in the cytoskeleton, dysregulation of *hox13*, and aberrant morphogenesis of bone-forming tissue are not limited to ectopic *fli1a*-expressing cells but also prevalent in EWS-FLI1 positive cells. Consistent with this, both the native form of Fli1a and the chimeric EWS-FLI1 fusion protein retain the C-terminus with the ETS DNA binding domain (Coles, Lawlor, & Bronner-Fraser, 2008). This domain elicits the activation of Fli1a and FLI1 downstream targets, respectively. In this regard, we anticipate that similar targeting by EWS-FLI1 and Fli1a leads to phenotypic similarities between our study and models of Ewing sarcoma. Nonetheless, the genomic targeting by the EWS-FLI1 does not completely resemble that of native FLI1 (Coles et al., 2008). In fact, the EWS-FLI1 fusion protein, comprising the N-terminal transactivation domain of EWS and the C-terminal ETS binding domain of FLI1, is a potent transcriptional activator (Bernstein et al., 2006; Coles et al., 2008). It is uncommon for secondary genetic events to occur in Ewing sarcoma thereby suggesting that EWS-FLI1 alone is sufficient to drive malignant transformation (Pfaltzgraff et al., 2019). The EWS-FLI1 fusion protein acquires the ability to remodel chromatin complexes and potentiates differential activation of downstream targets (Kikuchi et al., 2007; May et al., 1993; Patel et al., 2012; Truong & Ben-David, 2000). The ensuant global transcriptional dysregulation could account for phenotypes that are present in EWS-FLI1 positive cells but absent in ectopic *fli1a*-expressing cells, including non-restrained proliferation and malignant transformation. Furthermore, the cell lineage of transfected cells could contribute to the heterogeneity between EWS-FLI1 positive cells and ectopic *fli1a*-expressing cells. Recent studies have demonstrated that osteochondrogenic mesenchymal progenitor cells have a differential propensity to undergo *EWS-FLI1* transformation depending on their anatomical location during limb development (Pfaltzgraff et al., 2019). More specifically, osteochondrogenic progenitors located in the embryonic superficial zone at the surface of bones, recently conceived

as likely cells of origin for Ewing sarcoma, resemble *m-Inta11* positive cells at the distal edge of the endoskeletal disc in the pectoral fin (Tanaka et al., 2014). Current studies are underway to determine if *m-Inta11* positive cells are susceptible to *EWS-FLI1* transformation. To this end, we have created constructs that drive chimeric *EWS-FLI1* and *EWS-fli1a* in *m-Inta11* positive cells (see appendix A). Screening of primary injected *EWS-FLI1* and *EWS-fli1a* fish is in progress to identify a transgenic line. Thereupon, a comparative analysis will be carried out between ectopic *fli1a*, *EWS-FLI1*, and *EWS-fli1a* fish. This would not only allow us to further dissect the functional role of *fli1a* as well as its contributions to the Ewing sarcoma phenotype but also shed light on Ewing sarcoma cells of origin.

Our data could also help explain why Ewing sarcoma is not prevalent in the autopod bone-forming regions. In fact, Ewing sarcoma of the hand bones (i.e. proximal phalanges, metacarpals) is very rare, accounting for 1% of all Ewing sarcoma cases (Rajappa, Menon, & Sundaram, 2016; Shekhar, Korlhalli, & Murgod, 2015). In Ewing sarcoma, EWS-FLI1 disrupts the regulation of 5'*HOX* genes, leading to an upregulation of *HOXA13* and *HOXD13*, as well as a downregulation of *HOXA11* (Svoboda et al., 2014). Interestingly, *HOXA11* expression is downregulated in 45% of all Ewing sarcoma cases (Park, Jung, Kim, & Park, 2014). During normal limb development, HOXA11 expression is restricted to the zeugopod (Tohru Yano & Tamura, 2013). Meanwhile, HOXA13 and HOXD13 transcription factors are elevated in the autopod and activate the *m-Inta11* enhancer which ultimately leads to a downregulation of *HOXA11* expression in distal cells (Kherdjemil et al., 2016; Yano & Tamura, 2013). Recent studies show that *HOX* expression is maintained in post-embryonic and adult bone marrow mesenchymal stem cells, recapitulating the regionally restricted pattern of HOX expression during embryonic development (Rux et al., 2016; Rux & Wellik, 2017). We, therefore, suspect that EWS-FLI1 induced increases in

HOXA13/HOXD13 expression and decreases in *HOXA11* expression may not have major effects in autopod bone-forming regions but could have detrimental effects elsewhere in the body.

4.6 Proposed Model for the regulation of *fli1a* and *hox13*

Multiple studies have, thus far, focused on the actions of *fli1a* during embryonic vascular development. Meanwhile, little is known about the contribution of *fli1a* to chondrocyte maturation and development. Importantly, the activity of *fli1a* in chondrocytes is complementary to *hox13* expression in migrating cells of the pectoral fin. In this dissertation, we put forward that *fli1a* is involved in the condensation of cells while *hox13* are associated with the migration of cells in a dosage-dependent manner. According to previous data from our lab, *hoxa13b* and *hoxd13a* expression intrude towards the proximal region of the endoskeletal disc (Lalonde & Akimenko, 2018b). Therefore, some *fli1a*-expressing cells contain low levels of *hoxa13b* and *hoxd13a* during embryonic fin development. Contrarily, *m-Inta11* positive cells are void of *fli1a* but express high levels of *hox13a*, *hoxa13b*, and *hoxd13a*. The increased expression of *hox13* indicates that hox13 loci are accessible to transcription factors.

Herein, we propose that mis-expression of *fli1a* in *m-Inta11* positive cells of the pectoral fin increases *hox13* expression because ectopic FLI1 activity has been shown to activate HOXA13 and HOXD13 in models of Ewing sarcoma (Svoboda et al., 2014) (Figure 4.2). Subsequently, more Hox13 is available to activate the m-*Inta11* enhancer. Once active, the *m-Inta11* drives the expression of *fli1a* which further elevates *hox13* expression, resulting in a positive feedback loop between Fli1a and Hox13. At the same time, the activation of *m-Inta11* directs the expression of reporter *eGFP* and leads to enhanced fluorescence. Under normal conditions, *fli1a* expression is

inhibited in *m-Inta11* positive cells and unable to stimulate the activation of *hox13* expression. In *fli1a*-expressing cells, however, Fli1a may strive to activate *hox13* expression at a time when chromatin landscapes surrounding *hox13* loci are closed or partially closed. This could explain the presence of some *hoxa13b* and *hoxd13a* expression in *fli1a*-expressing cells during embryonic development. We further suspect that high levels of Hox13 could act on *cis*-acting regulatory elements to inhibit *fli1a* expression in *m-Inta11* positive cells under normal conditions and in the context of ectopic *fli1a* expression. In support of this, qRT-PCR analysis in ectopic *fli1a*-expressing pectoral fins has demonstrated a decrease in relative *fli1a* expression during later stages of larval development, concomitant with sustained *hox13* elevation (see Figure 3.20).

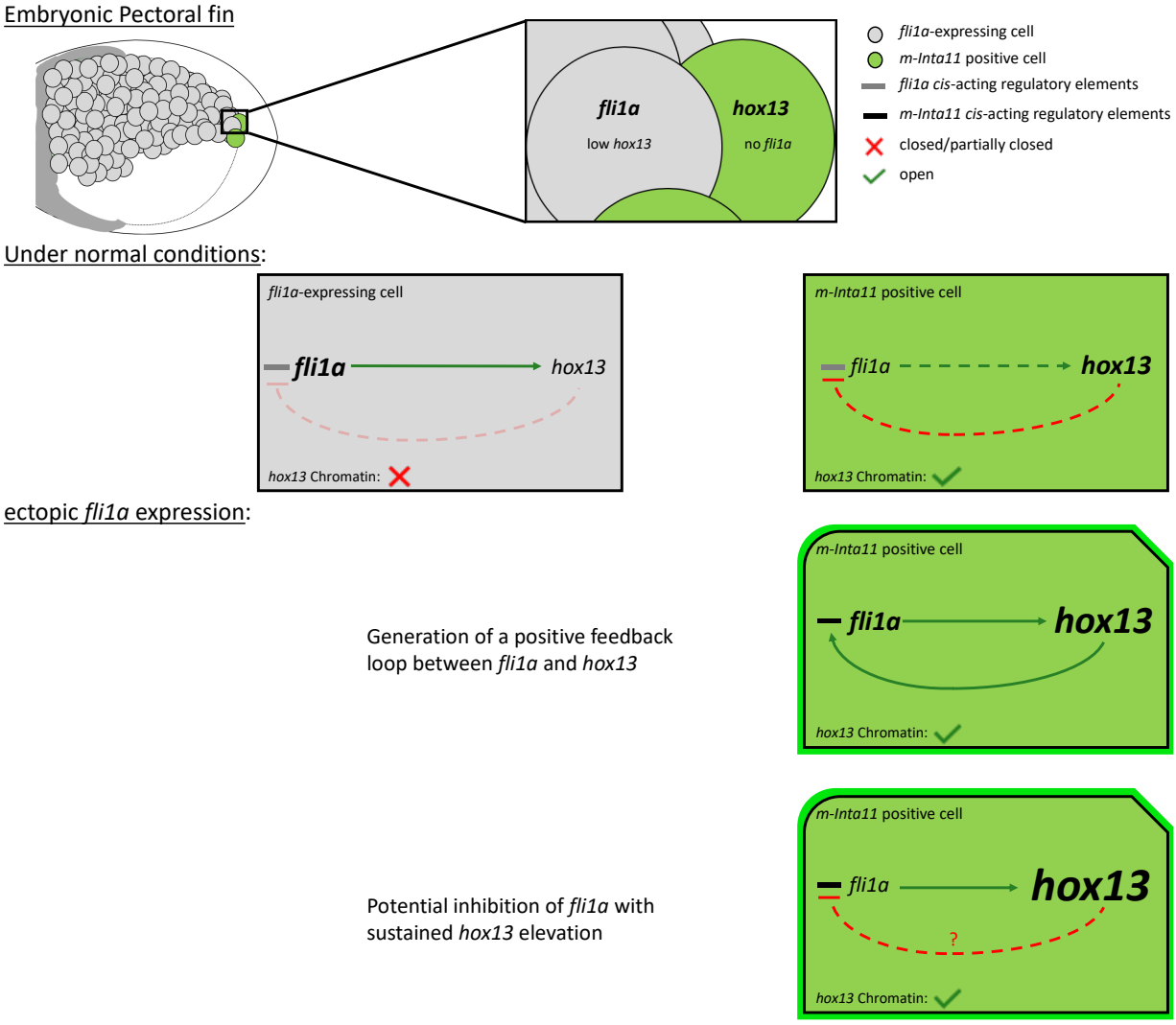

Figure 4.2: Proposed model for the regulation of *fli1a* and *hox13* during embryonic pectoral fin development.

Furthermore, our ectopic *fli1a* expression study shows that the amalgamation of Fli1a not only upregulates *hox13* expression but also promotes clustering of incumbent *m-Inta11* positive cells. This has long-lasting effects on the morphology of the pectoral fin during larval development and adulthood. Given the migration trajectory of *m-Inta11* cells of the pectoral fin, we contend that ectopic *fli1a* expression exerts dosage-dependent effects and leads to differential phenotypes in the anterior and posterior fin regions (Figure 4.3). In this manner, cells with the highest exposure to *fli1a* aggregate and fail to migrate outside the posterior fin region. This aggregation resembles the behavior of strong *fli1a*-expressing cells that give rise to distal radials. Although ectopic *fli1a* expression is accompanied with *hox13* elevation, Fli1a is thought to disrupt the expression of other genes and override increases in *hox13* that would promote *m-Inta11* cell migration. Hence, while continued exposure to *fli1a* sustains cell aggregation, increased *hox13* expression could contribute to the formation of additional bone nodules. In contrast, cells with lower *fli1a* exposure manage to migrate in the distal direction, despite exhibiting some defects in cell morphology. The limited exposure to *fli1a* is offset by high levels of *hox13*, making it possible for *m-Inta11* positive cells to localize within presumptive fin rays. Nonetheless, limited *fli1a* exposure is affiliated with some changes in *m-Inta11* cell morphology and adhesion, thereby impacting the patterning of fin rays, particularly during bifurcation events.

In Ewing sarcoma, the ETS binding domain of FLI1 is under the influence of novel *cis*-acting regulatory elements, owing to the chromosome translocation and contributions from *EWSR1*(Grohar et al., 2016). Ectopic activation of FLI1 targets, through the actions of the EWS-FLI1 fusion protein, is evinced to positively regulate HOXA13 and HOXD13 gene expression (Svoboda et al., 2014). Consistent with this, recent studies have identified an enhancer within the

conserved posterior HOXD locus that binds EWS-FLI1 and activates *HOXD13* expression (Apfelbaum, Svoboda, Magnuson, Ljungman, & Lawlor, 2019). Despite mounting evidence of FLI1 positively regulating *HOX13* expression, little is known about the effects of HOX13 elevation on *FLI1* expression. In our study, we speculate that rising levels of Hox13 negatively regulate *fli1a* expression. To test this negative feedback, we wish to undertake ectopic *hox13* expression in the *fli1a* endoskeletal disc domain using the mouse *m-Prxx1* enhancer and accordingly examine changes in *fli1a:eGFP* reporter activity in the pectoral fin (Hernández-Vega & Minguillón, 2011).

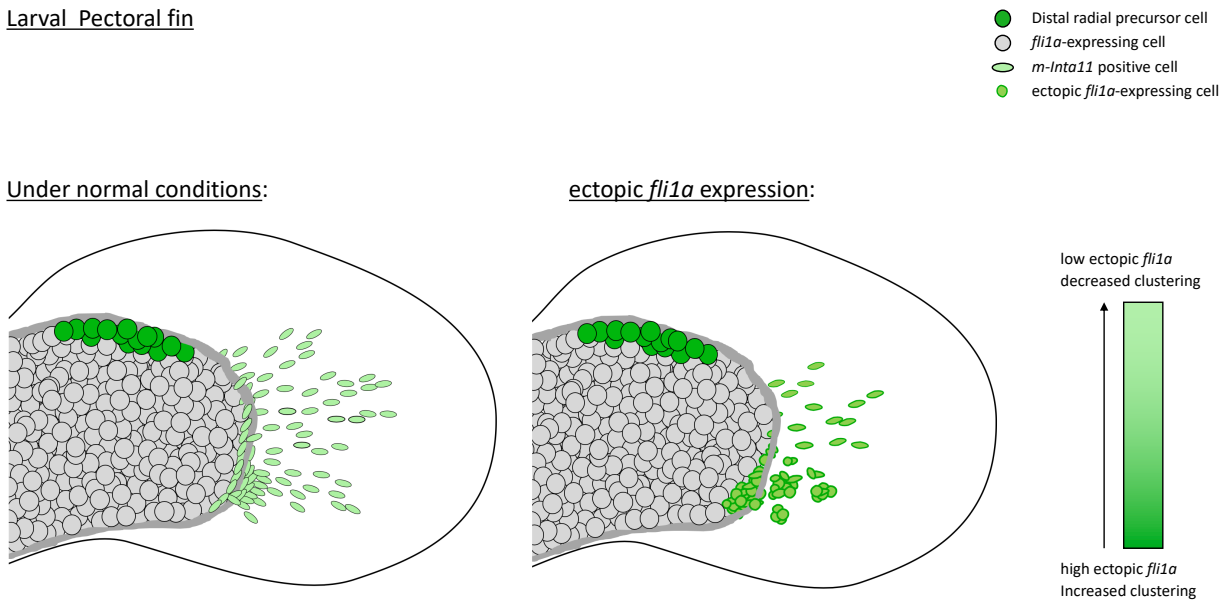

Figure 4.3: The ectopic expression of *fli1a* in *m-Inta11* positive cells of the pectoral fin is thought to generate dosage-dependent effects, leading to differential defects in the anterior and posterior fin regions.

CHAPTER 5 GENERAL CONCLUSION

The studies described in this dissertation further our understanding of cellular and molecular mechanisms underlying the development of the zebrafish pectoral fin. Using a transgenic approach, we have focused on elucidating the contributions of *fli1a* and *hox13* during embryonic and larval fin development.

In the current study, we have identified the source of migrating *m-Inta11* positive cells in the pectoral fin. Contrary to previous speculations, we report that *m-Inta11* positive cells in the pectoral fin do not emerge from the marginal blood vessel but rather arise from chondrocytes of the endoskeletal disc. In doing so, we have described the morphology changes that underlie the chondrocyte-to-*m-Inta11* cell transition, starting with a gradual loss of chondrocyte cell characteristics and followed with a progressive acquisition of migratory cell morphology.

In addition to identifying the source of migrating *m-Inta11* positive cells during embryonic development, we have determined the contributions of *m-Inta11* positive and *fli1*-expressing cells to adult structures in the pectoral fin. Using time-course analysis, we show that a population of brighter *fli1a*-expressing cells give rise to distal radials, while *m-Inta11* positive cells localize within presumptive fin rays. Our analysis also revealed that the formation of distal radials and patterning of fin rays correlate with the remodeling of fin fold blood vessels in an anterior to posterior direction. Surprisingly, the *m-Inta11* and *fli1a* enhancer domains of activity remained complementary throughout larval development. This pattern was also observed in the context of fin regeneration and appears to be recapitulated in the mouse autopod. Our data provide further support for a regulatory relationship between *fli1a* and *hox13* genes during pectoral fin development and suggests a conserved mechanism during limb development.

In order to examine the regulation between *fli1a* and *hox13*, we have induced ectopic *fli1a* expression in *m-Inta11* positive cells. The mis-expression of *fli1a* led to an increase in reporter *eGFP* expression and accumulation of defects in *m-Inta11* cell morphology and migration, resulting in shorter median and pectoral fin folds. Despite a reduction in fin fold length, ectopic *fli1a* expression did not seem to influence the proliferation or apoptotic activity of *m-Inta11* positive cells. Nonetheless, the introduction of *fli1a* was associated with an elevation of *hox13* expression during larval development and sustained *m-Inta11* cell defects, leading to aberrations in the endoskeleton and exoskeleton of the adult pectoral fin.

In Ewing sarcoma, the introduction of the EWS-FLI1 fusion protein is affiliated with ectopic stimulation of FLI1 targets, changes in cell adhesion, and overexpression of *HOXA13*, as well as *HOXD13* genes (Svoboda et al., 2014). Our findings suggest that ectopic *fli1a* expression recapitulates some of the phenotypes previously described in Ewing sarcoma, likely through the actions of the ETS binding domain of the C-terminus, which is common to both the EWS-FLI1 fusion and native Fli1a proteins. The functional analysis of ectopic *fli1a* expression in *m-Inta11* positive cells has helped us devise a proposed model for the regulation of *fli1a* and *hox13* genes during pectoral fin development. Taken together, the aforementioned results support our hypothesis and **confirm that *fli1a* and *hox13* participate in pectoral fin tissue organization and remodeling during embryonic and larval development**. To the best of our knowledge, this is the first study to examine the regulatory relationship between *fli1a* and *hox13* genes during pectoral fin development. We have put forward exciting future directions that could help elucidate the regulatory roles of *fli1a* and *hox13* during normal development and shed light on molecular hallmarks of Ewing sarcoma.

REFERENCES

Ahn, D., & Ho, R. K. (2008). Tri-phasic expression of posterior Hox genes during development of pectoral fins in zebrafish: Implications for the evolution of vertebrate paired appendages. *Developmental Biology*, *322*(1), 220–233. https://doi.org/10.1016/j.ydbio.2008.06.032

Amaral, A. T., Manara, M. C., Berghuis, D., Ordóñez, J. L., Biscuola, M., Lopez-García, M. A., … de Álava, E. (2014). Characterization of Human Mesenchymal Stem Cells from Ewing Sarcoma Patients. Pathogenetic Implications. *PLoS ONE*, *9*(2), e85814. https://doi.org/10.1371/journal.pone.0085814

Amores, A., Force, A., Yan, Y. L., Joly, L., Amemiya, C., Fritz, A., … Postlethwait, J. H. (1998). Zebrafish hox clusters and vertebrate genome evolution. *Science*, *282*(5394), 1711–1714. https://doi.org/10.1126/science.282.5394.1711

Apfelbaum, A. A., Svoboda, L., Magnuson, B., Ljungman, M., & Lawlor, E. (2019). EWS-FLI1 activates HOXD13 expression through enhancer reprogramming. *Cancer Research*, *79*(13 Supplement), 5205–5205. https://doi.org/10.1158/1538-7445.am2019-5205

Balamuth, N. J., & Womer, R. B. (2010). Ewing's sarcoma. *The Lancet Oncology*, *11*(2), 184–192. https://doi.org/10.1016/S1470-2045(09)70286-4

Bernstein, M., Kovar, H., Paulussen, M., Randall, R. L., Schuck, A., Teot, L. A., & Juergens, H. (2006). Ewing's Sarcoma Family of Tumors: Current Management. *The Oncologist*, *11*(5), 503–519. https://doi.org/10.1634/theoncologist.11-5-503

Bovetti, S., Hsieh, Y. C., Bovolin, P., Perroteau, I., Kazunori, T., & Puche, A. C. (2007). Blood vessels form a scaffold for neuroblast migration in the adult olfactory bulb. *Journal of Neuroscience*, *27*(22), 5976–5980. https://doi.org/10.1523/JNEUROSCI.0678-07.2007

Burchill, S. A. (2003). Ewing's sarcoma: diagnostic, prognostic, and therapeutic implications of molecular abnormalities. *Journal of Clinical Pathology*, *56*(2), 96–102. https://doi.org/10.1136/jcp.56.2.96

Bustin, S. A., Benes, V., Garson, J. A., Hellemans, J., Huggett, J., Kubista, M., … Wittwer, C. T. (2009). The MIQE Guidelines: Minimum Information for Publication of Quantitative Real-Time PCR Experiments. *Clinical Chemistry*, *55*(4), 611–622. https://doi.org/10.1373/clinchem.2008.112797

Chaturvedi, A., Hoffman, L. M., Jensen, C. C., Lin, Y.-C., Grossmann, A. H., Randall, R. L., … Beckerle, M. C. (2014). Molecular dissection of the mechanism by which EWS/FLI expression compromises actin cytoskeletal integrity and cell adhesion in Ewing sarcoma. *Molecular Biology of the Cell*, *25*(18), 2695–2709. https://doi.org/10.1091/mbc.E14-01-0007

Chaturvedi, A., Hoffman, L. M., Welm, A. L., Lessnick, S. L., & Beckerle, M. C. (2012). The EWS/FLI Oncogene Drives Changes in Cellular Morphology, Adhesion, and Migration in Ewing Sarcoma. *Genes and Cancer*, *3*(2), 102–116. https://doi.org/10.1177/1947601912457024

Coles, E. G., Lawlor, E. R., & Bronner-Fraser, M. (2008). EWS-FLI1 Causes Neuroepithelial Defects and Abrogates Emigration of Neural Crest Stem Cells. *Stem Cells*, *26*(9), 2237–2244. https://doi.org/10.1634/stemcells.2008-0133

Craig, M. P., Grajevskaja, V., Liao, H.-K., Balciuniene, J., Ekker, S. C., Park, J.-S., … Sumanas, S. (2015). Etv2 and fli1b function together as key regulators of vasculogenesis and angiogenesis. *Arteriosclerosis, Thrombosis, and Vascular Biology*, *35*(4), 865–876. https://doi.org/10.1161/ATVBAHA.114.304768

Cui, J. W., Vecchiarelli-Federico, L. M., Li, Y. J., Wang, G. J., & Ben-David, Y. (2009). Continuous Fli-1 expression plays an essential role in the proliferation and survival of F-MuLV-induced erythroleukemia and human erythroleukemia. *Leukemia*, *23*(7), 1311–1319. https://doi.org/10.1038/leu.2009.20

Dewit, J., Witten, P. E., & Huysseune, A. (2011). The mechanism of cartilage subdivision in the reorganization of the zebrafish pectoral fin endoskeleton. *Journal of Experimental Zoology Part B: Molecular and Developmental Evolution*, *316B*(8), 584–597. https://doi.org/10.1002/jez.b.21433

Duboule, D. (2007). The rise and fall of Hox gene clusters. *Development (Cambridge, England)*, *134*(14), 2549–2560. https://doi.org/10.1242/dev.001065

Durán, I., Marí-Beffa, M., Santamaría, J. A., Becerra, J., & Santos-Ruiz, L. (2011). Actinotrichia collagens and their role in fin formation. *Developmental Biology*, *354*(1), 160–172. https://doi.org/10.1016/j.ydbio.2011.03.014

Ellertsdóttir, E., Lenard, A., Blum, Y., Krudewig, A., Herwig, L., Affolter, M., & Belting, H.-G. (2010). Vascular morphogenesis in the zebrafish embryo. *Developmental Biology*, *341*(1), 56–65. https://doi.org/10.1016/j.ydbio.2009.10.035

Freitas, R., Gómez-Marín, C., Wilson, J. M., Casares, F., & Gómez-Skarmeta, J. L. (2012a). Hoxd13 Contribution to the Evolution of Vertebrate Appendages. *Developmental Cell*, *23*(6), 1219–1229. https://doi.org/10.1016/J.DEVCEL.2012.10.015

Freitas, R., Gómez-Marín, C., Wilson, J. M., Casares, F., & Gómez-Skarmeta, J. L. (2012b). Hoxd13 Contribution to the Evolution of Vertebrate Appendages. *Developmental Cell*, *23*(6), 1219–1229. https://doi.org/10.1016/j.devcel.2012.10.015

Fromental-Ramain, C., Warot, X., Messadecq, N., LeMeur, M., Dollé, P., & Chambon, P. (1996). Hoxa-13 and Hoxd-13 play a crucial role in the patterning of the limb autopod. *Development (Cambridge, England)*, *122*(10), 2997–3011. Retrieved from http://www.ncbi.nlm.nih.gov/pubmed/8898214

Gore, A. V, Monzo, K., Cha, Y. R., Pan, W., & Weinstein, B. M. (2012). Vascular development in the zebrafish. *Cold Spring Harbor Perspectives in Medicine*, *2*(5), a006684. https://doi.org/10.1101/cshperspect.a006684

Grandel, H., & Schulte-Merker, S. (1998). The development of the paired fins in the Zebrafish (Danio rerio). *Mechanisms of Development*, *79*(1–2), 99–120. https://doi.org/10.1016/S0925-4773(98)00176-2

Grohar, P. J., Kim, S., Rangel Rivera, G. O., Sen, N., Haddock, S., Harlow, M. L., … Caplen, N. J. (2016). Functional Genomic Screening Reveals Splicing of the EWS-FLI1 Fusion Transcript as a Vulnerability in Ewing Sarcoma. *Cell Reports*, *14*(3), 598–610. https://doi.org/10.1016/j.celrep.2015.12.063

Gupta, P. B., Kuperwasser, C., Brunet, J. P., Ramaswamy, S., Kuo, W. L., Gray, J. W., … Weinberg, R. A. (2005). The melanocyte differentiation program predisposes to metastasis

after neoplastic transformation. *Nature Genetics*, *37*(10), 1047–1054. https://doi.org/10.1038/ng1634

Habeck, H., Odenthal, J., Walderich, B., Maischein, H., Schulte-Merker, S., & Tübingen 2000 screen consortium. (2002). Analysis of a zebrafish VEGF receptor mutant reveals specific disruption of angiogenesis. *Current Biology : CB*, *12*(16), 1405–1412. Retrieved from http://www.ncbi.nlm.nih.gov/pubmed/12194822

Hamada, H., Uemoto, T., Tanaka, Y., Honda, Y., Kitajima, K., Umeda, T., … Abe, G. (2019). Pattern of fin rays along the antero-posterior axis based on their connection to distal radials. *Zoological Letters*, *5*(1), 30. https://doi.org/10.1186/s40851-019-0145-z

Hernández-Vega, A., & Minguillón, C. (2011). The Prx1 limb enhancers: Targeted gene expression in developing zebrafish pectoral fins. *Developmental Dynamics*, *240*(8), 1977–1988. https://doi.org/10.1002/dvdy.22678

Huang, C. chen, Wang, T. C., Lin, B. H., Wang, Y. W., Johnson, S. L., & Yu, J. (2009). Collagen IX is required for the integrity of collagen II fibrils and the regulation of vascular plexus formation in Zebrafish caudal fins. *Developmental Biology*, *332*(2), 360–370. https://doi.org/10.1016/j.ydbio.2009.06.003

Jackson, R., Braubach, O. R., Bilkey, J., Zhang, J., Akimenko, M., Fine, A., … Jonz, M. G. (2013). Expression of sall4 in taste buds of zebrafish. *Developmental Neurobiology*, *73*(7), 543–558. https://doi.org/10.1002/DNEU.22079

Jerković, I., Ibrahim, D. M., Andrey, G., Haas, S., Hansen, P., Janetzki, C., … Mundlos, S. (2017). Genome-Wide Binding of Posterior HOXA/D Transcription Factors Reveals Subgrouping and Association with CTCF. *PLOS Genetics*, *13*(1), e1006567. https://doi.org/10.1371/journal.pgen.1006567

Jinawath, N., Morsberger, L., Norris-Kirby, A., Williams, L. M., Yonescu, R., Argani, P., … Murphy, K. M. (2010). Complex rearrangement of chromosomes 1, 7, 21, 22 in Ewing sarcoma. *Cancer Genetics and Cytogenetics*, *201*(1), 42–47. https://doi.org/10.1016/j.cancergencyto.2010.04.021

Kabrun, N., Bühring, H. J., Choi, K., Ullrich, A., Risau, W., & Keller, G. (1997). Flk-1 expression defines a population of early embryonic hematopoietic precursors. *Development (Cambridge, England)*, *124*(10), 2039–2048. Retrieved from http://www.ncbi.nlm.nih.gov/pubmed/9169850

Kherdjemil, Y., Lalonde, R. L., Sheth, R., Dumouchel, A., de Martino, G., Pineault, K. M., … Kmita, M. (2016). Evolution of Hoxa11 regulation in vertebrates is linked to the pentadactyl state. *Nature*, *539*(7627), 89–92. https://doi.org/10.1038/nature19813

Kikuchi, R., Murakami, M., Sobue, S., Iwasaki, T., Hagiwara, K., Takagi, A., … Murate, T. (2007). Ewing's sarcoma fusion protein, EWS/Fli-1 and Fli-1 protein induce PLD2 but not PLD1 gene expression by binding to an ETS domain of 5′ promoter. *Oncogene*, *26*(12), 1802–1810. https://doi.org/10.1038/sj.onc.1209973

Kimmel, C. B., Ballard, W. W., Kimmel, S. R., Ullmann, B., & Schilling, T. F. (1995). *Stages of Embryonic Development of the Zebrafish*. Retrieved from https://onlinelibrary.wiley.com/doi/pdf/10.1002/aja.1002030302

Krumlauf, R. (1994, July 29). Hox genes in vertebrate development. *Cell*, Vol. 78, pp. 191–201.

https://doi.org/10.1016/0092-8674(94)90290-9

Lalonde, R. L., & Akimenko, M.-A. (2018a). Contributions of 5'HoxA/D regulation to actinodin evolution and the fin-to-limb transition. *The International Journal of Developmental Biology*, *62*(11–12), 705–716. https://doi.org/10.1387/ijdb.180248rl

Lalonde, R. L., & Akimenko, M.-A. (2018b). Effects of fin fold mesenchyme ablation on fin development in zebrafish. *PLOS ONE*, *13*(2), e0192500. https://doi.org/10.1371/journal.pone.0192500

Lawson, N. D., & Weinstein, B. M. (2002). In vivo imaging of embryonic vascular development using transgenic zebrafish. *Developmental Biology*, *248*(2), 307–318. Retrieved from http://www.ncbi.nlm.nih.gov/pubmed/12167406

Leemann-Zakaryan, R. P., Pahlich, S., Sedda, M. J., Quero, L., Grossenbacher, D., & Gehring, H. (2009). Dynamic Subcellular Localization of the Ewing Sarcoma Proto-Oncoprotein and Its Association with and Stabilization of Microtubules. *Journal of Molecular Biology*, *386*(1), 1–13. https://doi.org/10.1016/J.JMB.2008.12.039

Li, Y., Luo, H., Liu, T., Zacksenhaus, E., & Ben-David, Y. (2015). The ets transcription factor Fli-1 in development, cancer and disease. *Oncogene*, *34*(16), 2022–2031. https://doi.org/10.1038/onc.2014.162

Loganathan, S. N., Tang, N., Fleming, J. T., Ma, Y., Guo, Y., Borinstein, S. C., … Wang, J. (2016). BET bromodomain inhibitors suppress EWS-FLI1-dependent transcription and the IGF1 autocrine mechanism in Ewing sarcoma. *Oncotarget*, *7*(28), 43504–43517. https://doi.org/10.18632/oncotarget.9762

Lu, P., Yu, Y., Perdue, Y., & Werb, Z. (2008). The apical ectodermal ridge is a timer for generating distal limb progenitors. *Development (Cambridge, England)*, *135*(8), 1395–1405. https://doi.org/10.1242/dev.018945

Mariani, F. V., Ahn, C. P., & Martin, G. R. (2008). Genetic evidence that FGFs have an instructive role in limb proximal–distal patterning. *Nature*, *453*(7193), 401–405. https://doi.org/10.1038/nature06876

Masselink, W., Cole, N. J., Fenyes, F., Berger, S., Sonntag, C., Wood, A., … Currie, P. D. (2016). A somitic contribution to the apical ectodermal ridge is essential for fin formation. *Nature*, *535*(7613), 542–546. https://doi.org/10.1038/nature18953

May, W. A., Lessnick, S. L., Braun, B. S., Klemsz, M., Lewis, B. C., Lunsford, L. B., … Denny, C. T. (1993). The Ewing's sarcoma EWS/FLI-1 fusion gene encodes a more potent transcriptional activator and is a more powerful transforming gene than FLI-1. *Molecular and Cellular Biology*, *13*(12), 7393–7398. Retrieved from http://www.ncbi.nlm.nih.gov/pubmed/8246959

McMillan, S. C., Zhang, J., Phan, H.-E., Jeradi, S., Probst, L., Hammerschmidt, M., & Akimenko, M.-A. (2018). A regulatory pathway involving retinoic acid and calcineurin demarcates and maintains joint cells and osteoblasts in regenerating fin. *Development (Cambridge, England)*, *145*(11), dev161158. https://doi.org/10.1242/dev.161158

Moore, J. C., Sheppard-Tindell, S., Shestopalov, I. A., Yamazoe, S., Chen, J. K., & Lawson, N. D. (2013). Post-transcriptional mechanisms contribute to Etv2 repression during vascular development. *Developmental Biology*, *384*(1), 128–140.

https://doi.org/10.1016/j.ydbio.2013.08.028

Nakamura, T., Gehrke, A. R., Lemberg, J., Szymaszek, J., & Shubin, N. H. (2016). Digits and fin rays share common developmental histories. *Nature*, *537*(7619), 225–228. https://doi.org/10.1038/nature19322

Nelson, C. E., Morgan, B. A., Burke, A. C., Laufer, E., DiMambro, E., Murtaugh, L. C., … Tabin, C. (1996). Analysis of Hox gene expression in the chick limb bud. *Development*, *122*(5), 1449–1466.

Parichy, D. M., Elizondo, M. R., Mills, M. G., Gordon, T. N., & Engeszer, R. E. (2009). Normal table of postembryonic zebrafish development: Staging by externally visible anatomy of the living fish. *Developmental Dynamics*, *238*(12), 2975–3015. https://doi.org/10.1002/dvdy.22113

Park, H. R., Jung, W. W., Kim, H. S., & Park, Y. K. (2014). Microarray-based DNA methylation study of Ewing's sarcoma of the bone. *Oncology Letters*, *8*(4), 1613–1617. https://doi.org/10.3892/ol.2014.2322

Patel, M., Simon, J. M., Iglesia, M. D., Wu, S. B., McFadden, A. W., Lieb, J. D., & Davis, I. J. (2012). Tumor-specific retargeting of an oncogenic transcription factor chimera results in dysregulation of chromatin and transcription. *Genome Research*, *22*(2), 259–270. https://doi.org/10.1101/gr.125666.111

Perez, W. D., Weller, C. R., Shou, S., & Stadler, H. S. (2010). Survival of Hoxa13 homozygous mutants reveals a novel role in digit patterning and appendicular skeletal development. *Developmental Dynamics : An Official Publication of the American Association of Anatomists*, *239*(2), 446–457. https://doi.org/10.1002/dvdy.22183

Pfaffl, M. W. (2001). A new mathematical model for relative quantification in real-time RT-PCR. *Nucleic Acids Research*, *29*(9), 45e – 45. https://doi.org/10.1093/nar/29.9.e45

Pfaltzgraff, E. R., Apfelbaum, A., Kassa, A. P., Song, J. Y., Jiang, W., Suhan, T. K., … Lawlor, E. R. (2019). Anatomic origin of osteochondrogenic progenitors impacts sensitivity to EWS-FLI1-Induced Transformation. *Cancers*, *11*(3). https://doi.org/10.3390/cancers11030313

Poss, K. D., Shen, J., Nechiporuk, A., McMahon, G., Thisse, B., Thisse, C., & Keating, M. T. (2000). Roles for Fgf Signaling during Zebrafish Fin Regeneration. *Developmental Biology*, *222*(2), 347–358. https://doi.org/10.1006/dbio.2000.9722

Radig, K., Schneider-Stock, R., Röse, I., Mittler, U., Oda, Y., & Roessner, A. (1998). p53 and ras Mutations in Ewing's Sarcoma. *Pathology - Research and Practice*, *194*(3), 157–162. https://doi.org/10.1016/S0344-0338(98)80016-2

Rajappa, S., Menon, P., & Sundaram, S. (2016). Ewings Sarcoma of the Hand–A Case Report. *Journal of Hand and Microsurgery*, *02*(02), 82–84. https://doi.org/10.1007/s12593-010-0016-5

Richter, G. H. S., Plehm, S., Fasan, A., Rossler, S., Unland, R., Bennani-Baiti, I. M., … Burdach, S. (2009). EZH2 is a mediator of EWS/FLI1 driven tumor growth and metastasis blocking endothelial and neuro-ectodermal differentiation. *Proceedings of the National Academy of Sciences*, *106*(13), 5324–5329. https://doi.org/10.1073/pnas.0810759106

Riggi, N., Knoechel, B., Gillespie, S. M., Rheinbay, E., Boulay, G., Suvà, M. L., … Rivera, M.

N. (2014). EWS-FLI1 utilizes divergent chromatin remodeling mechanisms to directly activate or repress enhancer elements in Ewing sarcoma. *Cancer Cell*, *26*(5), 668–681. https://doi.org/10.1016/j.ccell.2014.10.004

Rux, D. R., Song, J. Y., Swinehart, I. T., Pineault, K. M., Schlientz, A. J., Trulik, K. G., … Wellik, D. M. (2016). Regionally Restricted Hox Function in Adult Bone Marrow Multipotent Mesenchymal Stem/Stromal Cells. *Developmental Cell*, *39*(6), 653–666. https://doi.org/10.1016/j.devcel.2016.11.008

Rux, D. R., & Wellik, D. M. (2017, April 1). Hox genes in the adult skeleton: Novel functions beyond embryonic development. *Developmental Dynamics*, Vol. 246, pp. 310–317. https://doi.org/10.1002/dvdy.24482

Saiz-Lopez, P., Chinnaiya, K., Towers, M., & Ros, M. A. (2017). Intrinsic properties of limb bud cells can be differentially reset. *Development*, *144*(3), 479–486. https://doi.org/10.1242/dev.137661

Sambrook, J., & Russell, D. W. (David W. (2001). *Molecular Cloning : A Laboratory Manual* (3rd Ed). Cold Spring Harbor Laboratory Press.

Scheiber, M. N., Watson, P. M., Rumboldt, T., Stanley, C., Wilson, R. C., Findlay, V. J., … Watson, D. K. (2014). FLI1 Expression is Correlated with Breast Cancer Cellular Growth, Migration, and Invasion and Altered Gene Expression. *Neoplasia*, *16*(10), 801–813. https://doi.org/10.1016/j.neo.2014.08.007

Segarra, M., Kirchmaier, B. C., & Acker-Palmer, A. (2015). A vascular perspective on neuronal migration. *Mechanisms of Development*, *138*, 17–25. https://doi.org/10.1016/j.mod.2015.07.004

Shaut, C. A. E., Keene, D. R., Sorensen, L. K., Li, D. Y., & Stadler, H. S. (2008). HOXA13 Is essential for placental vascular patterning and labyrinth endothelial specification. *PLoS Genetics*, *4*(5), e1000073. https://doi.org/10.1371/journal.pgen.1000073

Shaut, C. A., Saneyoshi, C., Morgan, E. A., Knosp, W. M., Sexton, D. R., & Stadler, H. S. (2007). HOXA13 directly regulatesEphA6 andEphA7 expression in the genital tubercle vascular endothelia. *Developmental Dynamics*, *236*(4), 951–960. https://doi.org/10.1002/dvdy.21077

Shekhar, A., Korlhalli, S., & Murgod, G. (2015). Ewing's sarcoma of proximal phalanx of the hand with skip metastases to metacarpals. *Indian Journal of Orthopaedics*, *49*(3), 365–368. https://doi.org/10.4103/0019-5413.156229

Shi, Q., Shen, L., Dong, B., Fu, H., Kang, X., Dai, L., … Chen, K.-N. (2018). Downregulation of HOXA13 sensitizes human esophageal squamous cell carcinoma to chemotherapy. *Thoracic Cancer*, *9*(7), 836–846. https://doi.org/10.1111/1759-7714.12758

Smith, A., Avaron, F., Guay, D., Padhi, B. K., & Akimenko, M. A. (2006). Inhibition of BMP signaling during zebrafish fin regeneration disrupts fin growth and scleroblast differentiation and function. *Developmental Biology*, *299*(2), 438–454. https://doi.org/10.1016/J.YDBIO.2006.08.016

Sordino, P., van der Hoeven, F., & Duboule, D. (1995). Hox gene expression in teleost fins and the origin of vertebrate digits. *Nature*, Vol. 375, pp. 678–681. https://doi.org/10.1038/375678a0

Spence, R., Gerlach, G., Lawrence, C., & Smith, C. (2007). The behaviour and ecology of the zebrafish, Danio rerio. *Biological Reviews*, *83*(1), 13–34. https://doi.org/10.1111/j.1469-185X.2007.00030.x

Stadler, H. S., Higgins, K. M., & Capecchi, M. R. (2001). Loss of Eph-receptor expression correlates with loss of cell adhesion and chondrogenic capacity in Hoxa13 mutant limbs. *Development (Cambridge, England)*, *128*(21), 4177–4188. Retrieved from http://www.ncbi.nlm.nih.gov/pubmed/11684655

Stetsyuk, V., Peers, B., Mavropoulos, A., Verbruggen, V., Thisse, B., Thisse, C., … Scharfmann, R. (2007). Calsenilin is required for endocrine pancreas development in zebrafish. *Developmental Dynamics*, *236*(6), 1517–1525. https://doi.org/10.1002/dvdy.21149

Suzuki, T. (2013). How is digit identity determined during limb development? *Development, Growth & Differentiation*, *55*(1), 130–138. https://doi.org/10.1111/dgd.12022

Svoboda, L. K., Bailey, N., Van Noord, R. A., Krook, M. A., Harris, A., Cramer, C., … Lawlor, E. R. (2017). Tumorigenicity of Ewing sarcoma is critically dependent on the trithorax proteins MLL1 and menin. *Oncotarget*, *8*(1), 458–471. https://doi.org/10.18632/oncotarget.13444

Svoboda, L. K., Harris, A., Bailey, N. J., Schwentner, R., Tomazou, E., von Levetzow, C., … Lawlor, E. R. (2014). Overexpression of HOX genes is prevalent in Ewing sarcoma and is associated with altered epigenetic regulation of developmental transcription programs. *Epigenetics*, *9*(12), 1613–1625. https://doi.org/10.4161/15592294.2014.988048

Tanaka, M., Yamazaki, Y., Kanno, Y., Igarashi, K., Aisaki, K. I., Kanno, J., & Nakamura, T. (2014). Ewing's sarcoma precursors are highly enriched in embryonic osteochondrogenic progenitors. *Journal of Clinical Investigation*, *124*(7), 3061–3074. https://doi.org/10.1172/JCI72399

Teh, C., Chudakov, D. M., Poon, K. L., Mamedov, I. Z., Sek, J. Y., Shidlovsky, K., … Korzh, V. (2010). Optogenetic in vivo cell manipulation in KillerRed-expressing zebrafish transgenics. *BMC Developmental Biology*, *10*. https://doi.org/10.1186/1471-213X-10-110

Thorogood, P. (1991). The Development of the Teleost Fin and Implications for Our Understanding of Tetrapod Limb Evolution. In *Developmental Patterning of the Vertebrate Limb* (pp. 347–354). https://doi.org/10.1007/978-1-4615-3310-8_45

Toomey, E. C., Schiffman, J. D., & Lessnick, S. L. (2010). Recent advances in the molecular pathogenesis of Ewing's sarcoma. *Oncogene*, *29*(32), 4504–4516. https://doi.org/10.1038/onc.2010.205

Towers, M., Tickle, C., & Capecchi, M. R. (2009). Growing models of vertebrate limb development. *Development (Cambridge, England)*, *136*(2), 179–190. https://doi.org/10.1242/dev.024158

Truong, A. H. L., & Ben-David, Y. (2000, December 18). The role of Fli-1 in normal cell function and malignant transformation. *Oncogene*, Vol. 19, pp. 6482–6489. https://doi.org/10.1038/sj.onc.1204042

Ulrich, F., Ma, L. H., Baker, R. G., & Torres-Vázquez, J. (2011). Neurovascular development in the embryonic zebrafish hindbrain. *Developmental Biology*, *357*(1), 134–151. https://doi.org/10.1016/j.ydbio.2011.06.037

Uong, A., & Zon, L. I. (2010, January). Melanocytes in development and cancer. *Journal of Cellular Physiology*, Vol. 222, pp. 38–41. https://doi.org/10.1002/jcp.21935

van den Boogaart, J. G. M., Muller, M., & Osse, J. W. M. (2012). Structure and function of the median finfold in larval teleosts. *The Journal of Experimental Biology*, *215*(Pt 14), 2359–2368. https://doi.org/10.1242/jeb.065615

Vecchiarelli-Federico, L. M., Liu, T., Yao, Y., Gao, Y., Li, Y., Li, Y. J., & Ben-David, Y. (2017). Fli-1 overexpression in erythroleukemic cells promotes erythroid de-differentiation while Spi-1/PU.1 exerts the opposite effect. *International Journal of Oncology*, *51*(2), 456–466. https://doi.org/10.3892/ijo.2017.4027

Vlaeminck-Guillem, V., Carrere, S., Dewitte, F., Stehelin, D., Desbiens, X., & Duterque-Coquillaud, M. (2000). The Ets family member Erg gene is expressed in mesodermal tissues and neural crests at fundamental steps during mouse embryogenesis. *Mechanisms of Development*, *91*(1–2), 331–335. Retrieved from http://www.ncbi.nlm.nih.gov/pubmed/10704859

von Heyking, K., Roth, L., Ertl, M., Schmidt, O., Wack, J. C.-, Neff, F., … Richter, G. H. S. (2016). The posterior HOXD locus: Its contribution to phenotype and malignancy of Ewing sarcoma. *Oncotarget*, *7*(27). https://doi.org/10.18632/oncotarget.9702

Walker, M., & Kimmel, C. (2007). A two-color acid-free cartilage and bone stain for zebrafish larvae. *Biotechnic & Histochemistry*, *82*(1), 23–28. https://doi.org/10.1080/10520290701333558

Wang, B., Fallon, J. F., & Beachy, P. A. (2000). Hedgehog-regulated processing of Gli3 produces an anterior/posterior repressor gradient in the developing vertebrate limb. *Cell*, *100*(4), 423–434. Retrieved from http://www.ncbi.nlm.nih.gov/pubmed/10693759

Wang, H., Su, N., Wang, L. C., Wu, X., Bui, S., Chang, K. J., … Ma, X. J. (2015). Multiplex fluorescent RNA in situ hybridization via RNAscope. In *In Situ Hybridization Methods* (pp. 405–414). https://doi.org/10.1007/978-1-4939-2303-8_21

Welten, M. C. M., de Haan, S. B., van den Boogert, N., Noordermeer, J. N., Lamers, G. E. M., Spaink, H. P., … Verbeek, F. J. (2006). ZebraFISH: Fluorescent *In Situ* Hybridization Protocol and Three-Dimensional Imaging of Gene Expression Patterns. *Zebrafish*, *3*(4), 465–476. https://doi.org/10.1089/zeb.2006.3.465

Westerfield, M. (2007). *The zebrafish book : a guide for the laboratory use of zebrafish (Danio rerio)* (5th Edition). Retrieved from https://www.worldcat.org/title/zebrafish-book-a-guide-for-the-laboratory-use-of-zebrafish-danio-rerio/oclc/433076472

Wingert, R. A., & Zon, L. I. (2006). Genetic Dissection of Hematopoiesis Using the Zebrafish. In *Hematopoietic Stem Cell Development* (pp. 14–31). https://doi.org/10.1007/978-0-387-33535-3_2

Wolpert, L. 1929-, Tickle, C., & Martinez Arias, A. 1955-. (2015). *Principles of development*. Retrieved from https://global.oup.com/academic/product/principles-of-development-9780198800569?lang=en&cc=ca

Woltering, J. M., Noordermeer, D., Leleu, M., & Duboule, D. (2014). Conservation and Divergence of Regulatory Strategies at Hox Loci and the Origin of Tetrapod Digits. *PLoS Biology*, *12*(1), e1001773. https://doi.org/10.1371/journal.pbio.1001773

Wood, A., & Thorogood, P. (1984). An analysis of in vivo cell migration during teleost fin morphogenesis. *Journal of Cell Science*, *66*, 205–222. Retrieved from http://www.ncbi.nlm.nih.gov/pubmed/6746756

Wyngaarden, L. A., Vogeli, K. M., Ciruna, B. G., Wells, M., Hadjantonakis, A. K., & Hopyan, S. (2010). Oriented cell motility and division underlie early limb bud morphogenesis. *Development*, *137*(15), 2551–2558. https://doi.org/10.1242/dev.046987

Xi, Y., Chen, W. J., Deng, J. X., Cui, Z. J., Liu, H. L., Yan, M. C., … Wu, P. (2015). Vasculature-guided neural migration in mouse cerebellum. *Italian Journal of Zoology*, *82*(1), 15–24. https://doi.org/10.1080/11250003.2014.977359

Yano, T., Abe, G., Yokoyama, H., Kawakami, K., & Tamura, K. (2012). Mechanism of pectoral fin outgrowth in zebrafish development. *Development*, *139*(16), 2916–2925. https://doi.org/10.1242/dev.075572

Yano, Tohru, & Tamura, K. (2013). The making of differences between fins and limbs. *Journal of Anatomy*, *222*(1), 100–113. https://doi.org/10.1111/j.1469-7580.2012.01491.x

Yokouchi, Y., Nakazato, S., Yamamoto, M., Goto, Y., Kameda, T., Iba, H., & Kuroiwa, A. (1995). Misexpression of Hoxa-13 induces cartilage homeotic transformation and changes cell adhesiveness in chick limb buds. *Genes & Development*, *9*(20), 2509–2522. https://doi.org/10.1101/gad.9.20.2509

Zakany, J., & Duboule, D. (2007). The role of Hox genes during vertebrate limb development. *Current Opinion in Genetics & Development*, *17*(4), 359–366. https://doi.org/10.1016/j.gde.2007.05.011

Zhang, J., Gao, B., Zhang, W., Qian, Z., & Xiang, Y. (2018). Monitoring antiangiogenesis of bevacizumab in zebrafish. *Drug Design, Development and Therapy*, Vol. 12, pp. 2423–2430. https://doi.org/10.2147/DDDT.S166330

Zhang, J., Wagh, P., Guay, D., Sanchez-Pulido, L., Padhi, B. K., Korzh, V., … Akimenko, M.-A. (2010). Loss of fish actinotrichia proteins and the fin-to-limb transition. *Nature*, *466*(7303), 234–237. https://doi.org/10.1038/nature09137

Zhou, S., Shen, Y., Wang, L., & Li, P. (2015). Epithelial-mesenchymal transition and mesenchymal-epithelial transition response during differentiation of growth-plate chondrocytes in endochondral ossification. *International Journal of Clinical and Experimental Medicine*, *8*(8), 12076–12085. Retrieved from http://www.ncbi.nlm.nih.gov/pubmed/26550119

APPENDIX A

A.1 Construction of *m-Inta11:EWS-FLI1* and *m-Inta11:EWS-fli1a* plasmids

All cloning and subcloning of *m-Inta11:EWS-FLI1* and *m-Inta11:EWS-fli1a* were carried out according to the standard procedure described by Sambrook & Russell, 2001. The *pCDH-puro-EWS-FLI1* plasmid, previously created by Loganathan et al., 2016, was purchased from Addgene (Addgene plasmid # 102813; https://www.addgene.org/102813/). The human *EWS-FLI1* coding sequence was amplified using the FW *EWS* AgeI primer (5'-TCTAGAACCGGTACCATGGCGTCCACGGATTAC-3') and Rev *FLI1* NotI primer (5'-TAGCGCGGCCGCCTAGTAGTAGCTGCCTAAGT-3') and subsequently cloned into *pDrive* vector (QIAGEN). The *EWS-FLI1* coding sequence consisting of 1507 base-pairs (bp) was subcloned into the *m-Inta11-βG:eGFP* construct to replace the *eGFP* cDNA using AgeI and NotI restriction sites. The *m-Inta11: eGFP* plasmid was created and modified by Rob L. Lalonde as previously described in section 2.9 (Kherdjemil et al., 2016).

To create the *EWS-fli1a* chimeric construct, we aligned the *EWS-FLI1* (human) and *fli1a* (zebrafish) sequences using the standard nucleotide-BLAST tool provided by the National Center for Biotechnology Information (NCBI) website. The aligned sequence encoding the zebrafish C-terminal domain of *fli1a* was amplified from the *m-Inta11:fli1a* construct using the FW *fli1a* BamHI primer (5'- CAAACTGGATCCTACAGCCAAGCTCCATCTCACGCT-3') and Rev *fli1a* NotI primer (5'- GCTAGCGCGGCCGCTTAGTAGTAACTACCAAGG-3'). The non-aligned sequence, corresponding to the human N-terminal domain of *EWS* was amplified from the *pCDH-puro-EWS-FLI1* construct using the FW *EWS* AgeI primer (5'-TCTAGAACCGGTACCATGGCGTCCACGGATTAC-3') and the Rev *EWS* BamHI primer (5'-

GCTGTAGGATCCAGTTTGGGGTGGGTAACTAGTGGG-3'). Subsequently, the *EWS* and *fli1a* fragments were digested at the BamHI site, ligated, and accordingly cloned into the pDrive vector (QIAGEN). The *EWS-fli1a* chimeric construct, consisting of 1504 bp, was then subcloned in the *m-Inta11-βG:eGFP* construct using AgeI and NotI restriction sites, as described above. All primers were designed using SnapGene® software (from GSL Biotech; available at snapgene.com). Sequencing of *EWS-FLI1* and *EWS-fli1a* constructs was performed to verify that frame shift mutations did not occur during cloning and subcloning procedures. Once verified, *m-Inta11:EWS-FLI1* and *m-Inta11:EWS-fli1a* plasmids were each injected in a cohort of *Tg*(*m-Inta11:eGFP*) embryos. Microinjections were performed by Vishal Saxena as described in section 2.10.